Master's Theses and Capstones   Student Scholarship

Winter 2017

Rates and Drivers of Nitrate Uptake in Fluvial Wetlands in Urbanizing, Coastal Watersheds

Christopher Thomas Whitney
University of New Hampshire, Durham

Follow this and additional works at: https://scholars.unh.edu/thesis

RATES AND DRIVERS OF NITRATE UPTAKE IN FLUVIAL WETLANDS

IN URBANIZING, COASTAL WATERSHEDS

BY

CHRISTOPHER T. WHITNEY

B.S. Environmental Biology, Bridgewater State University, 2013

THESIS

Submitted to the University of New Hampshire

In Partial Fulfillment of

The Requirements for the Degree of

Master of Science

In

Natural Resources: Soil and Water Resource Management

December, 2017

This thesis/dissertation has been examined and approved in partial fulfillment of the requirements for the degree of Master of Science in Natural Resources: Soil and Water Resource Management by:

Thesis/Dissertation Director, Wilfred Wollheim

Associate Professor Natural Resourced and the Environment

Anne Lightbody

Associate Professor Earth Sciences

Gopal Mulukutla

Research Scientist Earth Systems Research Center

Original approval signatures are on file with the University of New Hampshire Graduate School

TABLE OF CONTENTS

ACKNOWLEDGEMENTS

LIST OF TABLES

LIST OF FIGURES

ABSTRACT

RATES AND DRIVERS OF NITRATE UPTAKE IN FLUVIAL WETLANDS

IN URBANIZING, COASTAL WATERSHEDS

by

Christopher T. Whitney

University of New Hampshire, December, 2017

Humans have had a substantial impact on the global nitrogen cycle, releasing large amounts of reactive nitrogen to the landscape. Watersheds have been found to remove substantial quantities of this anthropogenic nitrogen, with aquatic networks preventing much of it from reaching the coast. Within these aquatic networks, channelized streams have been studied extensively. However, in many coastal watersheds, fluvial wetlands are a large component of the aquatic network yet have not been studied as broadly as channelized reaches. As fluvial wetlands are also likely to have a sizeable impact on river network-scale nitrogen removal, a greater understanding of their effect on nitrogen cycling is necessary. We developed a new approach for quantifying fluvial wetland nitrate uptake measured at the whole ecosystem scale, using a method conceived in channelized reaches, in conjunction with new in situ sensor technology. Using this new approach, we found ambient uptake velocities in fluvial wetlands that ranged from -170.6 to 1220.0 m yr^{-1}. These uptake velocities were generally higher than those found for channelized reaches within the same watersheds and in a similar range as uptake velocities found for fluvial wetland surface transient storage patches. Neither gross primary productivity nor ecosystem respiration exerted strong control on uptake

rates, however, both discharge and detention time were significantly related to nitrate uptake. The effects of biology and hydrology on nitrate removal were then tested using a reach-scale numeric model. Hydrology was found to have a greater impact on nitrate removal compared to biology however, the cumulative effect of both hydrology and biology had the greatest impact. This is important because the watersheds draining suburban Boston, MA are experiencing ongoing urbanization, leading to greater inputs of anthropogenic nitrogen to the landscape. The beaver population is concurrently experiencing a resurgence, leading to an increase in the number of fluvial wetlands within these watersheds and with it, a greater potential for nitrogen removal. As such, fluvial wetlands may be able to offset the increase in nitrogen loading, preventing additional nitrogen from reaching the coast.

Introduction

The global nitrogen (N) cycle has been severely impacted by humans, leading to a multitude of environmental problems. Anthropogenic N makes its way to the landscape from a variety of sources including atmospheric deposition arising from agricultural emissions and the burning of fossil fuels, inputs from local fertilizer use, and human and animal waste (Galloway and Cowling 2002, Galloway et al. 2008, Schlesinger 2009). Anthropogenic N impacts water quality and leads to coastal eutrophication, resulting in harmful algal blooms and anoxic or hypoxic dead zones (Davidson et al. 2012). Freshwater systems can experience effects similar to those observed in coastal areas with impacts on drinking water also occurring (Smith et al. 1999). An understanding of what controls N fluxes from source to receiving waters is critical to fully comprehend the impacts of N on the environment.

Much of the anthropogenic N that is added to the landscape does not reach the coast. Watersheds in the northeastern United States have been found to remove about 80% of the total anthropogenic N inputs (Howarth et al. 1996, Van Breeman et al. 2002). While much of this N removal takes place on the terrestrial landscape, aquatic ecosystems can remove up to 50% of the N loads transferred from land via runoff and subsurface flow (Wollheim et al. 2008). Channelized streams and rivers have been studied considerably to evaluate the rates at which N removal takes place (Williams et al. 2004, Mulholland et al. 2008, Thouin et al. 2009) and these rates have been used to parameterize N reaction rates in river network-scale models that assume all rivers are channelized (Stewart et al. 2011). However, in many watersheds, fluvial wetlands (e.g. floodplains, backwaters, mill ponds, and beaver ponds) are an important component of the aquatic network. This is especially true in flat, coastal plain watersheds.

Although these wetlands can be abundant in river networks, they have been much less studied compared to channelized systems.

Fluvial wetlands have conditions that are conducive to enhanced N removal and may play a vital role in aquatic N removal at the watershed scale (Wollheim et al. 2008). N removal refers to the proportion of N inputs that are removed from downstream fluxes, taking into account both biological activity as well as residence time. This is compared to uptake rates which refer only to the amount of N processed via biological activity. Fluvial wetlands have hydrological and geomorphological traits intermediate between channelized reaches and lentic water bodies. These traits include connectivity to advective flow, reducing N source limitation (Wollheim et al. 2014), large surface areas providing increased contact with benthic surfaces (Johnston et al. 1997), and patches of low dissolved oxygen (DO) facilitating enhanced denitrification (Thouin et al. 2009). These intermediate characteristics result in more complex features that potentially intensify biogeochemical processing while also increasing residence time of water compared to channels (Johnston et al 1997). Recent studies have estimated N uptake in non-channelized reaches, finding them to be higher than in channelized reaches (Forshay and Stanley 2005, O'Brien et al. 2012, Powers et al. 2012, Wollheim et al. 2014).

Wetlands exhibit several mechanisms through which they can remove nitrogen including sedimentation, biotic uptake, and denitrification (Johnston et al. 1997, Seitzinger et al. 2006). Fluvial wetlands have a complex hydrology and geomorphology that affects these mechanisms including continuous upstream inputs, long residence times, variable water velocities, increased contact with riparian soils, large surface areas, high light inputs, and low hydraulic loads (Cirmo and Driscoll 1993, Johnston et al. 1997, Lightbody et al. 2008). In

addition to unique physical characteristics, fluvial wetlands also have chemical conditions that are favorable to N removal such as higher water temperatures, increased accumulation of organic matter, and patches with very low DO concentrations (Cirmo and Driscoll 1993, Fisher and Acreman 2004). These conditions make fluvial wetlands potential hotspots for nitrogen removal (McClain et al. 2003). With separately described N removal rates, fluvial wetlands can be explicitly incorporated into river network-scale models to improve estimates of N fluxes to the coast.

The same features that make fluvial wetlands potential hotspots for N removal also make N reaction rates in these systems inherently difficult to quantify. In channelized streams with short residence times and constrained flow paths, solute additions employed to discern N removal rates, including both plateau (e.g. Tank et al. 2008) and breakthrough curve (BTC) approaches (e.g. Covino et al. 2010), are straightforward to perform and interpret results. Plateau approaches are not feasible in high volume and long residence time fluvial wetlands due to the sheer mass of solute required to elevate concentrations to a steady state above ambient (Trentman et al. 2015). However, BTC approaches are a realistic option as the mass of solute required is relatively small and the experiment duration is reduced relative to plateau approaches. BTC solute addition experiments used to estimate nutrient spiraling metrics (uptake length, areal uptake, and uptake velocity) (Stream Solute Workshop 1990) in channelized reaches require discrete grab samples collected throughout the entire BTC as the solutes pass a fixed point (Ruggiero et al. 2006, Tank et al. 2008, Covino et al. 2010). In systems with abundant surface transient storage (STS), where residence times can exceed several hours, the collection of discrete grab samples is inefficient and may not fully characterize temporal

variability through the entire BTC. New ultraviolet-visual spectrophotometers have the ability to measure nitrate (NO_3^-) and bromide (Br^-), a conservative solute, concentrations continuously and simultaneously with a single instrument, allowing for a more accurate representation of the BTC and associated dynamics (Pellerin et al. 2013, Etheridge et al. 2014). These in situ sensors can also be deployed to autonomously collect high temporal resolution data throughout the entire BTC, thereby providing a better picture of the unique hydrological, geomorphological, and chemical attributes that control N removal in fluvial wetlands.

Before undertaking questions at the river network scale, an understanding at the reach, or whole ecosystem scale, must first be realized. This study askes the question: What are the whole-ecosystem estimates of NO_3-N removal in fluvial wetlands and how do they compare to removal estimates found for channelized streams or wetland patches? It is hypothesized that N removal in fluvial wetlands is greater than removal in channelized reaches due to both increased residence times and higher biological reaction rates. Increased residence times and reaction rates occur because fluvial wetlands have characteristics that are a combination of those found in both lotic and lentic aquatic systems. To test this hypothesis, we applied the "Tracer Additions for Spiraling Curve Characterization" (TASCC, Covino et al. 2010) approach in whole reaches dominated by fluvial wetlands using both traditional grab sampling as well as advanced in situ NO_3-N sensor technology to provide a more complete record of the BTC over longer periods of time than typical in channelized reaches. As the TASCC approach was developed and previously used primarily in channelized reaches, we evaluated the efficacy of this approach in fluvial wetlands by comparing estimates from high frequency sensor data to less frequent grab sample data.

4

Methods

Study Area

This study took place in fluvial wetlands located predominantly in the watersheds of the Parker and Ipswich Rivers, draining a combined 450 km^2 of suburban Boston in northeastern Massachusetts (Figure 1). Three wetland sites within the Parker and Ipswich River watersheds were studied in 2014 and 2015, each draining different land use types, with different amounts of NO_3-N loading (Table 1). These sites included a fluvial wetland periodically connected to its channel on upper Fish Brook in Boxford, MA (BOX); an active beaver pond on Cart Creek in Byfield, MA (CC); and a permanently inundated fluvial wetland on Sawmill Brook in Wilmington, MA (CH). Experimental solute additions were performed at these sites once in the early part of the growing season (June/July) and once again later in the year (November/December). Solute additions were also performed in the BOX and CH wetlands in the spring of 2015 (June/July). In addition to the sites in the Parker and Ipswich River watersheds, one natural fluvial wetland on an unnamed tributary to the Little River in Barrington, NH (BAR), within the Lamprey River watershed, was also studied in the spring of 2015 (Figure 1, Table 1). Wetlands were vegetated to varying degrees with the CC beaver pond being less than 50% vegetated and the wetland at CH consistently greater than 50% vegetated. The major emergent macrophytes consisted of cattails (*Typha* spp.), reeds (*Phragmites* spp.), and pickerelweed (*Pontedaria cordata*) while various grasses and submerged macrophytes were also abundant in each wetland.

5
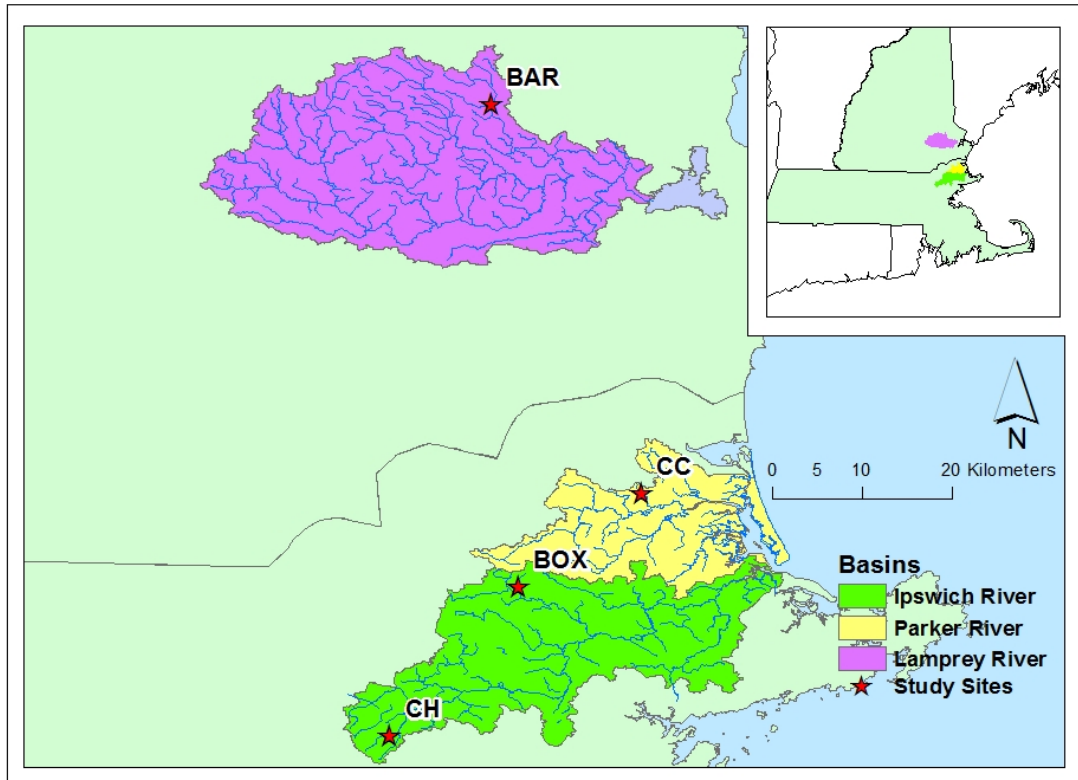
Figure 1. Map of the Parker, Ipswich, and Lamprey River watersheds with study fluvial wetlands denoted with stars.

Table 1. Physical attributes of the study wetlands for each solute addition.

Addition	Date	Reach Length (m)	Discharge (L s^{-1})	Average Width (m)	Average Depth (m)	Wetland Area (m)	Catchment Area (km^{-2})	Hydraulic Load (m yr^{-1})	Detention Time (hr)
BOX-1	6/11/14	170	2.64	1.83	0.14	311.1	1.76	299.49	4.10
BOX-2	11/11/14	170	7.3	9.66	0.154	1642.2	1.76	457.65	2.95
BOX-3	6/25/15	170	15.1	17.16	0.184	2917.2	1.76	854.77	1.89
CC-1	7/2/14	70	3.3	8.81	0.316	616.7	4.01	236.32	11.71
CC-2	11/19/14	70	22.1	8.21	0.247	574.7	4.01	536.59	4.03
BAR	6/11/15	140	2	3.09	0.094	432.6	0.75	197.94	4.16
CH-1	7/17/14	130	51.8	6.01	0.251	781.3	4.79	930.33	2.36
CH-2	12/5/14	130	70.53	11.45	0.271	1488.5	4.79	1870.53	1.27
CH-3	7/10/15	130	57	10.29	0.268	1337.7	4.79	1322.07	1.78

Overarching Approach

The overarching experimental design used to quantify N removal consisted of instantaneous solute slug additions sensu Covino et al. (2010) with BTC solute concentrations determined using traditional discrete grab sample as well as with an in situ nitrate sensor. BTC data were used to estimate continuous dynamic nutrient spiraling metrics over the range of experienced nitrate concentrations with the dynamic TASCC approach (Covino et al. 2010) as well as a single integrated uptake metric for the entire BTC (BTC-integrated approach, Covino et al. 2010, Tank et al. 2008). Ambient uptake metrics were derived from the dynamic uptake metrics by back-extrapolation to ambient nitrate concentrations. In addition to the experimental nutrient slug addition method, net nitrogen removal was also determined with a mass balance approach, using grab samples collected at the inflow and outflow of each wetland over the course of the sensor deployment.

Ancillary measurements, consisting of continuous monitoring of DO, water temperature, and photosynthetically active radiation (PAR), were also collected over the course of the nitrate sensor deployment at four locations at each wetland – inflow, a sidepool area representative of STS within the wetland, outflow, and downstream of the outflow after the stream rechannelized. Nutrient grab samples were collected at each of these four locations several times throughout the sensor deployments. Discharge measurements were made at the inflow and outflow of each wetland several times. Deployments typically lasted between one and two weeks with the nitrate sensor and dataloggers deployed several days prior to the solute addition to capture ambient data. Additions were targeted for periods with stable stream flow

which was predominantly the case apart from the fall 2014 addition at CH that took place in a brief window between high flow events.

Nutrient spiraling metrics for each measurement point calculated from the dynamic TASCC method as well as the BTC-integrated method included uptake length (S_w, m), the average distance a nutrient molecule travels while in suspended form before being immobilized; areal uptake (U, mg m^{-2} min^{-1}), the nutrient demand per unit area of stream bed per time; and uptake velocity (V_f, m yr^{-1}), a mass transfer coefficient from the water column to the benthos (Stream Solute Workshop, 1990). These nutrient spiraling metrics were calculated using the discrete grab samples as well as data from the in situ NO_3-N sensor for each point along the BTC. Ambient uptake metrics were then estimated from the dynamic TASCC results by back extrapolating S_w to ambient NO_3-N concentrations. Integrated spiraling metrics and total bulk removal were also calculated for all solute additions using the BTC-integrated approach outlined in Covino et al. (2010). Uptake metrics calculated from the discrete grab samples and in situ sensor were compared to one another to validate the sensor data as a means for estimating NO_3-N uptake using the sensor with the TASCC method. Uptake metrics were compared to wetland physical attributes, aquatic metabolism (gross primary productivity [GPP] and ecosystem respiration [ER]), concentrations of other constituents in the matrix (i.e. dissolved organic carbon (DOC), ammonium (NH_4)), and hydrological parameters including indices of the proportion of flow in the advective/dispersive and transient storage zones, to evaluate controls of N biological uptake and removal at the whole ecosystem scale.

A Submersible Ultraviolet Nitrate Analyzer (SUNA, Satlantic, LLC.) was used to continuously monitor at the wetland outflow concentrations of NO_3-N and Br, the reactive and conservative solutes used in the nutrient slug additions. The SUNA measures the amount of UV light absorbed in the range of wavelengths between 190 and 370 nm and uses proprietary algorithms to relate that absorbed light to concentrations of NO_3-N and Br. Sensor data must be calibrated to grab samples to maximize the accuracy of the NO_3-N and Br traces. However, the accuracy and precision of the SUNA Br trace has not been thoroughly assessed by the manufacturer.

The SUNA was deployed at the outflow of each wetland several days prior to the solute addition to collect data on ambient concentrations and diurnal variability of both NO_3-N and Br at a sampling interval of 15 minutes. On the day of the solute addition, prior to the slug being added to the wetland inflow, the SUNA sampling interval was changed to one minute to achieve a higher temporal resolution trace of both solutes through the BTC. Slug additions of NO_3-N and Br, as $NaNO_3$ and NaBr, took place by combining both salts in measured amounts in a 5 gallon bucket with stream water and thoroughly mixing until they were completely dissolved before dumping the entire slug mixture into the center of a well-mixed channel flowing into the wetland at the top of the reach. Simultaneous additions of Rhodamine WT (RWT) took place during the spring 2014 and 2015 nutrient additions (BOX-1, BOX-3, CC-1, BAR, CH-1, CH-3) as part of a concurrent project aiming to understand transient storage parameters (Wilderotter 2015). As the excitation and emission spectra of RWT are above the range of wavelengths monitored by the SUNA, no interference was expected to occur. Outflow RWT concentrations were measured with a C3 Submersible Fluorometer (Turner Designs). NO_3-N and

Br were added at a ratio of 1 with the exception for the BOX-1 addition where the added ratio was 0.78.

Grab samples were collected throughout the BTC at the sensor location at the constricted outflow of each fluvial wetland reach. Samples were collected at intervals of 5 to 30 minutes with samples collected more frequently on the rising limb and spaced further apart on the falling limb. Typically, in channelized streams, electrical conductivity monitored at the sampling location is used to dictate the frequency and duration of BTC grab sample collection. However, in fluvial wetlands where Br was used as a conservative solute, any increase in electrical conductivity was negligible, making the arrival of the slug more difficult to detect. Therefore, experiments where RWT was not added simultaneously, there was no visual indicator of the slug's arrival leading to grab samples not always capturing all of the rising limb. Grab samples were filtered in the field using Whatman GF/F filters with a 0.7 μm nominal pore size and kept cold and then stored frozen until analysis. Ambient and BTC NO_3-N, Br, and chloride (Cl) were analyzed on a Dionex ICS-1100 Ion Chromatograph, while ambient DOC and total dissolved nitrogen (TDN) were analyzed on a Shimadzu TOC-V, and ambient ammonium and phosphate (PO_4) were analyzed on a SmartChem 200.

Wetland Surveying

Wetlands were surveyed typically either the day of a solute addition prior to each experiment or within a day or two of the conclusion of the experiment. Transects were marked along the length of the reach of each wetland the first time surveying took place beginning at the outflow and moving upstream in 10 meter increments. In the case of the CH wetland, the

final 60 meters were surveyed at 20 m intervals as this section had a consistent width and

depth. At each transect, the wetted width of the wetland was measured. Depth was measured

at no less than 10 places equidistant along the transect to derive an average depth per transect.

Wetlands were not surveyed for the BOX-2 and BOX-3 additions or for the CH-3 addition so

average widths and depths were estimated from relationships between stage and measured

average width and depth. These relationships were determined by finding the best fit between

stage height and the measured average widths and depths, resulting in either an exponential,

logarithmic, or linear fit (Equations 1-4):

$$\overline{z}_{BOX} = 0.1181e^{2.8013*h} \qquad \text{Equation 1}$$

$$\overline{w}_{BOX} = 14.799 \ln h + 43.439 \qquad \text{Equation 2}$$

$$\overline{z}_{CH} = 0.1697 * h + 0.188 \qquad \text{Equation 3}$$

$$\overline{w}_{CH} = 45.247 * h - 10.705 \qquad \text{Equation 4}$$

where $\overline{z}$ is average depth at each site (m), $\overline{w}$ is average width for each site (m), and h is depth

from the outflow stage logger (m). The relationship between average width and average depth

with stage height at BOX were based on three measurements which were statistically

significant and had high r^2 values ($p < 0.001$, $r^2 = 0.99$). The relationships at CH were based upon

only two measurements so a simple linear fit was used and no p value was calculable. However,

for the experiment at CH where mean width and depth were not measured, stage height fell

within the range of measurements from which the relationships were derived, providing

confidence in the estimates of mean width and depth.

Discharge Measurements

Discharge was typically measured the day of a solute addition at the outflow of the wetland, prior to the addition taking place. For experiments where discharge was not measured the day of the addition, either a measurement collected the day before or after, or discharge estimated from the stage-discharge relationship was used. Measurements were made either using a FlowTracker Handheld Acoustic Doppler Velocimeter (SonTek/Xylem Inc.) with the area – velocity method or via dilution gaging using a slug of NaCl with dissolved Cl concentrations determined from electrical conductivity data collected with a HOBO U-24 Conductivity Logger (Kilpatrick and Cobb 1985).

Stage height was measured continuously at each wetland outflow with a HOBO U-20 Water Level Logger except at CH where stage height was continuously monitored using a Solinst Levelogger (Solinst Canada Ltd). Logger stage height was compensated for atmospheric pressure using barometric pressure data collected at the Plum Island Ecosystems LTER (PIE LTER) field station located in Newbury, MA using a HOBO U-20 Water Level Logger. For stage data collected with the HOBO loggers, the HOBOware Barometric Compensation Assistant was used for this correction while Solinst data were compensated by manually subtracting barometric pressure (m H_2O) from the stage logger data. Rating curves were developed using the logger stage height and measured discharge to develop a continuous record of discharge at the outflow of each wetland (Table 2). Stage-discharge relationships were fit to either linear, power, or exponential functions, depending on which function provided the best fit, following the formats of Equations 5-7, respectively. The rating curve at the CH wetland also had an offset of -0.06356 m applied to the logger stage height.

$$Q = a * h + b \qquad\qquad \text{Equation 5}$$

$$Q = a * h^b \qquad\qquad \text{Equation 6}$$

$$Q = a * \exp(b * h) \qquad\qquad \text{Equation 7}$$

where Q is discharge (L s^{-1}), h is the stage height from the logger (m), and a is the slope and b is the constant or exponent for each relationship.

Table 2. Rating curves for wetland outflow stage-discharge relationships where a is the slope and b is either the constant or exponent of the relationships and n is the number of discharge measurements used to develop the rating curve.

Site	Type	a	b	n
BAR	Power	16.25	2.747	4
BOX	Exponential	1.7348	12.914	9
CC	Linear	97.7877	-3.9705	5
CH	Power	2235	4.051	3

Sensor Data Calibration

SUNA Br data contained high-frequency variability that was smoothed using a moving average with a window of 5 sampling intervals (i.e. 5 minutes) to reduce this noise. Smoothing was performed using the 'rollapply' function in the 'zoo' package for R (R Core Team 2017, Zeileis and Grothendieck 2005). High-frequency variability was not present in the SUNA NO_3-N data, therefore, smoothing was only performed on the Br data. Instrument bias in the SUNA NO_3-N and Br traces from differences between sensor data and laboratory-analyzed grab

samples was corrected using either linear or polynomial regressions derived for each individual solute addition. The regression type used was determined by fitting both linear and polynomial models to the data and choosing the model that best fit the data. In cases where the r^2 values were nearly identical between models, a linear model was chosen as it was more parsimonious. For the BOX-1 addition, the peak of the Br BTC broke down, potentially due to exceeding the upper range of the instrument's detection limit. As such, RWT data collected simultaneously were used as the conservative tracer in the TASCC analysis for that experiment with uptake metrics derived from the added NO_3-N:RWT ratios rather than the NO_3-N:Br ratios.

Dynamic Uptake Metrics

For calculating the dynamic uptake metrics of the added NO_3-N through the BTCs with the TASCC method, the variable travel time (TT) approach was used for estimating U and V_f ($U_{add-dyn-TT}$, $V_{f-add-dyn-TT}$, Covino et al. 2010) for each sample along the BTC. The TT approach was used rather than the standard approach, which does not take into consideration variable travel times of each sample, as residence times in the wetlands were longer than those of a channelized reach of the same length. These longer residence times allow for a greater exposure of the added NO_3-N to biota and the TT approach takes into account the amount of time that the solutes have spent in the reach for each grab sample or sensor interval.

Samples in both SUNA and grab sample data for which the background-corrected NO_3-N:Br ratio was within 5% of the NO_3-N:Br ratio of the injectate solution were removed from each dataset, as indicative of uptake below detection. Samples where the NO_3-N:Br ratio was close to or greater than the NO_3-N:Br ratio of the injectate solution can occur due to errors or

trends in baseline concentrations used for background correction of either constituent and can result in artificially high or negative uptake lengths. Variation in baseline concentrations is potentially a larger problem in long residence time systems where diel variability can occur in nutrient concentrations.

Dynamic longitudinal uptake rates, often referred to as a rate constant, ($k_{w-add-dyn}$, m^{-1}), were calculated as the slope of the relationship between the natural log of the injectate NO_3-N:Br ratio and sample NO_3-N:Br ratio against reach length for each grab sample or sensor interval. Dynamic uptake length of the added NO_3-N ($S_{w-add-dyn}$, m) for each time point was then calculated as the negative inverse of the dynamic longitudinal uptake rates. $S_{w-add-dyn}$ was then used to calculate $U_{add-dyn-TT}$ and $V_{f-add-dyn-TT}$ for each sample/interval using Equations 8 and 9 (Covino et al. 2010):

$$U_{add-dyn-TT} = z * \left(\frac{L}{TT}\right) * [NO_3-N_{add-dyn}]/S_{w-add-dyn} \qquad \text{Equation 8}$$

$$V_{f-add-dyn-TT} = U_{add-dyn-TT}/[NO_3-N_{add-dyn}] \qquad \text{Equation 9}$$

where $U_{add-dyn-TT}$ (mg m^{-2} min^{-1}) and $V_{f-add-dyn-TT}$ (m yr^{-1}) are the added NO_3-N areal uptake rate and uptake velocity calculated using the travel time approach, respectively, z is the average depth, L is fluvial wetland reach length, TT is the travel time for each sample/interval calculated as the difference between the sample collection time and injection time, and [NO_3-$N_{add-dyn}$] is the geometric mean of observed and conservative NO_3-N concentration calculated as Equation 10 (Covino et al. 2010):

$$[NO_3-N_{add-dyn}] = \sqrt{[NO_3-N_{add-obs}] * [NO_3-N_{cons}]} \qquad \text{Equation 10}$$

where [NO$_3$-N$_{add-obs}$] is the observed, background-corrected NO$_3$-N concentration for each

sample or sensor interval and [NO$_3$-N$_{cons}$] is the conservative NO$_3$-N concentration for each

sample or sensor interval calculated as the observed, background-corrected Br concentrations

multiplied by the NO$_3$-N:Br ratio of the injectate solution.

Ambient Uptake Metrics

       In addition to dynamic uptake metrics that estimate uptake at experimentally elevated

nutrient concentrations, ambient uptake, or uptake at ambient nutrient concentrations, was

also estimated using the TASCC method from the relationship between dynamic uptake length

and NO$_3$-N concentrations. Ambient outflow NO$_3$-N concentrations in the study wetlands were

variable between sites but were generally relatively high compared to reaches studied by

Covino et al. (2010) (Table 3). Therefore, ambient uptake metrics were estimated following the

method employed by Gibson et al. (2015), calculating ambient uptake length (S$_{w-amb}$) by back

extrapolating the relationship between S$_{w-add-dyn}$ and total NO$_3$-N (NO$_3$-N$_{tot-dyn}$) to the ambient

NO$_3$-N concentration (zero added N), rather than to zero total N as in Payn et al. (2005) and

Covino et al. (2010). Back extrapolating to ambient NO$_3$-N instead of zero total NO$_3$-N allows for

estimation of ambient biotic uptake in streams where ambient NO$_3$-N concentrations are high

as well as reduces the error associated with those estimates (Gibson et al. 2015). This back

extrapolation provides an estimate of uptake length at ambient N concentrations which was

then used to estimate the ambient areal uptake rate (U$_{amb}$) and ambient uptake velocity (V$_{f-amb}$)

(Equations 11 and 12). If the resulting ambient uptake was negative, these rates were assumed to be zero.

$$U_{amb} = Q * [NO_3 - N_{amb}]/S_{w-amb} * w \qquad \text{Equation 11}$$

$$V_{f-amb} = U_{amb}/[NO_3 - N_{amb}] \qquad \text{Equation 12}$$

Table 3. Ambient nutrient concentrations during the day of each solute addition obtained from grab samples collected at the wetland outflow prior to the addition taking place. Also included are the injected masses of added NO_3-N and Br as well as the ambient and injected NO_3-N:Br ratios for each addition.

Addition	Date	Time of Addition (EST)	Duration of BTC (hr)	Ambient NO_3-N (mg L^{-1})	Ambient Br (mg L^{-1})	Ambient N:Br	Injected NO_3-N (g)	Injected Br (g)	Injected N:Br
BOX-1	6/11/14	11:43	7.78	0.2	0.075	2.667	28.85	36.19	0.797
BOX-2	11/11/14	8:15	6.75	0.086	0.035	2.457	55.83	55.91	0.999
BOX-3	6/25/15	9:30	4.5	0.021	0.036	0.583	41.2	41.2	1.000
CC-1	7/2/14	7:34	28.1	0.157	0.059	2.661	25.94	25.67	1.011
CC-2	11/19/14	9:27	6.55	0.057	0.025	2.280	10.81	10.8	1.001
BAR	6/11/15	8:45	8.75	0.026	0.015	1.733	32.96	32.96	1.000
CH-1	7/17/14	11:02	1.97	0.373	0.061	6.115	72.04	71.99	1.001
CH-2	12/5/14	12:23	2.62	1.094	0.057	19.193	65.99	66.07	0.999
CH-3	7/10/15	11:05	1.92	0.219	0.035	6.257	70.04	70.04	1.000

Error surrounding ambient uptake metrics was derived from the standard error of the intercept of the $S_{w-add-dyn}$ vs. NO_3-$N_{add-dyn}$ relationship. This standard error was used to calculate a minimum and maximum S_{w-amb} for each solute addition which was in turn used to estimate a minimum and maximum U_{amb} and V_{f-amb} using Equations 11 and 12 by substituting the minimum and maximum S_{w-amb} in Equation 11 and minimum and maximum U_{amb} in Equation 12.

For experiments where there were less than three viable data points, error around the intercept of the $S_{w\text{-add-dyn}}$ vs. NO_3-$N_{tot\text{-dyn}}$ relationship was not calculable (CH-1 and CC-2 grab sample data), therefore no error was calculated for either U_{amb} or $V_{f\text{-amb}}$.

NO_3-N removal was also calculated from TASCC ambient uptake to compare to removal estimates made using other methods. Removal determined from TASCC ambient uptake (R_{calc}, %) was calculated using Equation 13 with the ambient areal uptake rates for each experiment along with wetland surface area, discharge, and the ambient outflow NO_3-N concentration:

$$R_{calc} = 1 - \exp\left(-\frac{U*L*w}{C*Q}\right) * 100 \qquad \text{Equation 13}$$

where R_{calc} is removal calculated from TASCC ambient uptake (%), U is the ambient areal uptake rate (mg m^{-2} min^{-1}), L is reach length (m), w is mean wetland width (m), C is the ambient outflow NO_3-N concentration (mg L^{-1}), and Q is discharge (m^3 sec^{-1}).

Total Dynamic Uptake Metrics

Dynamic uptake calculated using the TT approach accounts for uptake of the added nutrient only. This does not account for the ambient uptake so total dynamic uptake metrics ($U_{tot\text{-dyn-TT}}$, $V_{f\text{-tot-dyn-TT}}$) were also calculated. These uptake metrics were calculated as the sum of the dynamic uptake rates of the added nutrient ($U_{add\text{-dyn-TT}}$, $V_{f\text{-add-dyn-TT}}$) and the ambient uptake rates (U_{amb}, $V_{f\text{-amb}}$). For cases where ambient uptake was zero, the total uptake metric is equal to uptake of the added nutrient only.

BTC-Integrated Uptake Metrics

The TASCC BTC-integrated approach results in a single uptake value for each experiment as opposed to the dynamic TASCC approach that estimates a separate uptake value for each data point. This approach, similar to approaches used by Ruggiero et al. (2006) and Tank et al. (2008), used the total recovered masses of NO_3-N and Br to calculate a longitudinal uptake rate as the slope of the relationship between the natural log of the injectate NO_3-N:Br and recovered NO_3-N:Br ratios against stream distance. BTC-integrated uptake length ($S_{w\text{-}add\text{-}int}$, m) was then calculated as the negative inverse of the longitudinal uptake rate. $U_{add\text{-}int}$ and $V_{f\text{-}add\text{-}int}$ were the calculated in a similar manner as U_{amb} and $V_{f\text{-}amb}$, modifying Equations 11 and 12 by substituting $S_{w\text{-}add\text{-}int}$ for $S_{w\text{-}amb}$ and [NO_3-$N_{add\text{-}int}$], the geometric mean of observed and conservative BTC-integrated NO_3-N, calculated using Equation 14, for [NO_3-$N_{add\text{-}obs}$].

$$[NO_3-N_{add-int}] = \sqrt{\frac{Q\int_0^t[NO_3-N_{add-obs}](t)dt}{\int_0^t Q(t)dt} * \frac{Q\int_0^t[NO_3-N_{cons}](t)dt}{\int_0^t Q(t)dt}} \qquad \text{Equation 14}$$

where [NO_3-$N_{add\text{-}int}$] is the geometric mean of observed and conservative BTC-integrated NO_3-N (mg L^{-1}), Q is discharge (m^3 sec^{-1}), [NO_3-$N_{add\text{-}obs}$] is the observed, background-corrected NO_3-N concentration at time t (mg L^{-1}), [NO_3-N_{cons}] is the conservative NO_3-N concentration at time t (mg L^{-1}), and dt is the sampling interval (sec). Removal of the added NO_3-N was also determined from the TASCC BTC-integrated approach. BTC-integrated removal (R_{add}, %) was calculated from the recovered NO_3-N:Br ratio and injected NO_3-N:Br ratio (Equation 15):

$$R_{add} = 1 - \left(\frac{NO_3\text{-}N_{rec}}{Br_{rec}}\right) \Big/ \left(\frac{NO_3\text{-}N_{inj}}{Br_{inj}}\right) * 100 \qquad \text{Equation 15}$$

where R_{add} is removal determined from the TASCC BTC-integrated approach (%), $NO_3\text{-}N_{rec}$ is the recovered mass of $NO_3\text{-}N$ (mg), Br_{rec} is the recovered mass of Br (mg), $NO_3\text{-}N_{inj}$ is the injected mass of $NO_3\text{-}N$ (mg) and Br_{inj} is the injected mass of Br (mg). This removal metric was compared to removal calculated from TASCC ambient uptake (R_{calc}) as well as a third and final removal metric.

Ambient Mass Balance Approach

The final removal metric calculated for each study wetland was determined using ambient $NO_3\text{-}N$ data from grab samples collected at the inflow and outflow at each wetland. Ambient mass balance removal estimates (R_{MB}, %) were made at least three times during each sensor deployment with one estimate made during the day of the solute addition and estimates made when the sensors were both deployed and collected. This approach estimates net $NO_3\text{-}N$ removal at ambient stream concentrations as the difference between inputs and outputs at each wetland and attributing the differences to internal wetland processing, calculated using Equation 16:

$$R_{MB} = \frac{(C_{in} - C_{out})}{C_{in}} \qquad \text{Equation 16}$$

where C_{in} is the inflowing NO_3-N concentration (mg L^{-1}) and C_{out} is the outflow NO_3-N

concentration (mg L^{-1}). This method assumes discharge is equal at the inflow and outflow of

each wetland and storage is constant. A hydrological mass balance was used to remove the

effects of lateral or groundwater inputs or losses and problems with sample collection or

storage on R_{MB}. These effects resulted in R_{MB} estimates that were potentially tainted by

dilution, the introduction of nutrients from unmonitored inflowing waters, or from time-varying

storage. This hydrological mass balance was performed using chloride data from the input and

output grab samples with the chloride R_{MB} calculated using Equation 16. If chloride R_{MB} was

greater than ± 15%, there was assumed to be a problem with one or both of the samples used

to make that R_{MB} estimate and that estimate was not included in further analyses.

Stream Metabolism

Aquatic metabolism was estimated using the single station method and the

'streamMetabolizer' package for R (Appling et al. 2017). Continuous data used in the calculation

of gross primary productivity (GPP) and ecosystem respiration (ER) included wetland outflow

DO concentrations and water temperature collected using HOBO U-26 Dissolved Oxygen

Loggers (Onset Computer Corp.) as well as wetland sidepool photosynthetically active radiation

(PAR) collected with Odyssey PAR Loggers (Dataflow Systems, Ltd.). DO loggers were calibrated

prior to deployment at both 100% and 0% saturation and checked for drift following each

deployment. Sidepool PAR was used as it was most representative of light conditions

experienced throughout the entire wetland compared to outflow PAR which was typically more

shaded than the entirety of the wetland. Barometric pressure data used for calculating DO

percent saturation were collected via a HOBO U-20 Water Level Logger centrally located at the

PIE LTER field station in Newbury, MA. Salinity data used in calculating DO percent saturation

was estimated from conductivity data collected with a HOBO U-24 Fresh Water Conductivity

Logger for all 2014 experiments following an approach from Grace and Imberger (2006). A

conductivity logger was not deployed during the 2015 solute additions, therefore salinity was

assumed to be zero in those metabolism calculations. Salinity does not play a large role in

determining DO percent saturation in freshwater so the assumption that salinity was zero did

not make a substantial difference in the DO percent saturation calculation (Grace et al. 2015).

The 'streamMetabolizer' package uses an inverse modeling technique to estimate

metabolism from the DO, PAR, and water temperature data collected continuously as well as

water depth. A Bayesian model was used to estimate GPP (g O_2 m^{-2} day^{-1}), ER (g O_2 m^{-2} day^{-1}),

and the reaeration coefficient K (day^{-1}). With this model, GPP varied within each day as a linear

function of light with an intercept of 0 and a slope that was allowed to vary by day. ER was

assumed to be constant over each 24-hour period, regardless of day and night or changes in

temperature. The ordinary differential equation relating dissolved oxygen to GPP, ER, and K was

solved with trapezoidal integration in which the change in DO between timesteps is a function

of the mean values of GPP and ER across timesteps. The model was run for a total of 50,000

iterations while it searched for the optimal parameter values with 5,000 burn-in steps and

45,000 saved steps. During the experiment at BAR, outflow DO logger data suggested a fault

with the logger between midnight and 4 AM on 2015-06-11. As the 'streamMetabolizer'

package requires complete data for a full day, defined as a 24 hour period beginning at 4 AM, in

order to calculate daily GPP, ER, and K estimates, this faulty data was backfilled using DO data

from the logger located 75 m downstream of the outflow. As this occurred during the early

morning hours with very little to no GPP, this backfilling was assumed to make little difference

in the overall daily estimates for that particular day.

Residence Time and Transient Storage

Residence times and transient storage parameters were both estimated from the

continuous conservative solute data collected during the solute additions. Detention time (T_{det},

hr) was estimated as the first moment of mass in the BTC (Equation 17):

$$T_{det} = \frac{\int t * C_t * Q * dt}{\int C_t * Q * dt}$$

Equation 17

where t is the time since addition (sec), C_t is the conservative solute concentration at time t (mg

L^{-1}), Q is discharge (L sec^{-1}), and dt is the sampling interval (sec). The denominator of this

equation is equal to the recovered mass of the conservative solute (M_{rec}).

Transient storage calculations were based on the "Stream tracer breakthrough curve

decomposition into mass fractions" method described by Wlostowski et al. (2016). The

advection/dispersion (A/D) fraction of the BTC is determined using an analytical solution

(Beltaos and Day 1978) to the advection dispersion equation (Taylor 1921). This fit the

conservative solute mass and dispersion coefficient to the observed concentration data by

means of a nonlinear least-squares fitting procedure implemented in R using the 'nls' function

(R Core Team 2017). This fitted dispersion coefficient was then input into the analytical solution

with the total mass recovered (M_{rec}) to simulate a hypothetical BTC where M_{rec} is transported

by advection and dispersion only (Wlostowski et al. 2016). The A/D component of the BTC is then defined as the simulated BTC concentration of the conservative solute until the time at which it crosses the observed BTC. The transient storage (TS) component is then defined as the difference between the A/D component and the observed BTC conservative solute concentration. See Wlostowski et al. (2016) for complete details. Mass fractions of A/D and TS were then calculated as the mass of conservative solute in each component relative to M_{rec}.

Mass fractions were generally calculated relative to the mass of conservative solute recovered (M_{rec}) despite recoveries being largely smaller than those found by Wlostowski et al. (2016). These recoveries were lower than expected potentially due to errors in sensor calibration or detection limits, errors in discharge measurements or drift during the BTC, or due to inherent wetland processes that retard the release of the conservative solute from transient storage (Whitmer et al. 2000). SUNA conservative solute data collected during the BOX-1 experiment were faulty at the peak of the BTC while no SUNA data were collected during the BAR experiment, therefore RWT data were used in those instances for both residence time and transient storage calculations.

Results

SUNA and Grab Sample Breakthrough Curves

Raw NO_3-N and Br concentrations measured with the SUNA were calibrated to the laboratory-analyzed grab samples collected throughout the BTC as well as to background samples collected during the sensor deployment. Separate calibrations were made for each individual solute addition. Global linear calibrations for both NO_3-N and Br were possible as

relationships between SUNA and grab sample data using all points from all deployments were closely correlated (r^2 = 0.95, p<0.001; r^2 = 0.9, p<0.001l for both NO_3-N and Br, respectively) (Table 4). However, experiment-specific calibrations provided better fits to the observed grab sample data due to site-specific and seasonal differences in the water matrix (e.g. DOC concentrations), which can affect the absorbance of NO_3-N – absorbing wavelengths (Pellerin et al. 2013). Experiment-specific calibrations were used to ensure the highest level of accuracy for each TASCC analysis.

After calibration of the SUNA data, NO_3-N and Br grab sample data fell along the continuous sensor trace apart from outliers that were not included in the calibration regressions (Figures 2 and 3). Outliers were determined by visually examining the SUNA NO_3-N and Br vs. grab sample NO_3-N and Br relationship and excluding points that obviously strayed too far from the relationship. These outliers were then omitted from the calibrations because they were not consistent with the breakthrough curve in terms of either the continuous sensor data or the discrete grab samples and were presumed to have resulted from sampling error. The SUNA provided an accurate trace for both NO_3-N and Br concentrations throughout the entire BTCs with a much higher temporal resolution compared to the discrete grab samples.

For the BOX-1 solute addition, the SUNA Br BTC showed a sharp drop near the peak, possibly due to reaching the upper limit of the detection range of the SUNA for Br as uncalibrated concentrations exceeded 9 mg L^{-1} (Figure 3). This experiment also had the highest Br concentrations experienced during any of the fluvial wetland solute additions. Multiple flowpaths were not believed to be the cause of the drop in the Br concentration at the peak as this trend was not evident in the NO_3-N or RWT BTCs, which would have exhibited similar

responses to multiple flowpaths. Due to the breakdown in the BOX-1 Br BTC, RWT data were

used as the conservative tracer for the TASCC calculations as well as for the estimation of

transient storage parameters and the calculation of detention time. There was also no SUNA

data collected for the BOX-3 addition due to a deployment error. All uptake metrics for this

solute addition were calculated from discrete grab sample data only while RWT data were used

to estimate transient storage parameters and residence time.

Comparison of Uptake Metrics During BTC Using SUNA and Grab Sample Data

Dynamic uptake lengths for all experiments based on grab sample data generally fall

within the range of uptake values estimated from SUNA data where both data types were

viable (Figure 4). Grab sample uptake lengths were typically in the lower range of the SUNA

data results but exhibit similar scatter during some experiments (e.g. CC-1, BAR). Uptake

lengths ranged from 20.1 to 3295.9 m in the SUNA dataset however, uptake lengths calculated

using grab sample data ranged from 44.5 to 2108.3 m. These fluvial wetland uptake lengths

were reasonable compared to values found for the Snake River in Wyoming as well as its

smaller channelized tributaries (108 – 2500 m) (Hall and Tank 2003, Tank et al. 2008), however

the shorter uptake lengths in fluvial wetlands suggest that uptake may be greater. During the

BOX-1 experiment, too few BTC grab samples were collected to calculate uptake metrics so only

SUNA results were considered. Also, dynamic NO_3-N:Br ratios for the grab samples collected

during the CH-3 solute addition were all within 5% of the injectate NO_3-N:Br ratio, therefore,

uptake was not calculable for that experiment using grab sample data.

Table 4. Regression coefficients used for calibration of SUNA data for each separate solute addition as well as a global calibration for each solute fit using all available data. x^2 is the coefficient associated with the leading term of a second order polynomial and has a value only if a polynomial was used for the calibration. N_{max} is the maximum observed NO_3-N concentration in the grab sample data for each addition so any SUNA value above that value has less certainty associated with it. n refers to the number of observations used to fit each relationship.

Addition	Date	Solute	N_{max}	Equation Type	x^2	Slope	Intercept	r^2	n
BOX-1	6/11/14	NO_3	1.509	Linear	NA	1.2997	-0.0401	0.92	3
BOX-1	6/11/14	Br		Linear	NA	0.2627	-0.4401	0.9	3
BOX-2	11/11/14	NO_3	1.048	Polynomial	-0.3333	1.2357	-0.0591	0.99	15
BOX-2	11/11/14	Br		Polynomial	-0.0451	0.4923	-0.1867	0.99	15
BOX-3	6/25/15	NO_3	NA	NA	NA	NA	NA	NA	NA
BOX-3	6/25/15	Br		NA	NA	NA	NA	NA	NA
CC-1	7/2/14	NO_3	0.27	Linear	NA	0.8135	0.0255	0.99	8
CC-1	7/2/14	Br		Linear	NA	0.3718	-0.3648	0.97	8
CC-2	11/19/14	NO_3	0.164	Linear	NA	0.7156	-0.0105	0.97	17
CC-2	11/19/14	Br		Polynomial	-0.0104	0.4048	-0.096	0.93	15
BAR	6/11/15	NO_3	1.127	Linear	NA	0.8559	0.0066	0.99	13
BAR	6/11/15	Br		Polynomial	-0.0384	0.4895	-0.4257	0.99	12
CH-1	7/17/14	NO_3	0.925	Linear	NA	0.5427	0.1656	0.93	14
CH-1	7/17/14	Br		Linear	NA	0.2522	-0.095	0.98	13
CH-2	12/5/14	NO_3	1.187	Linear	NA	0.3638	0.673	0.72	13
CH-2	12/5/14	Br		Polynomial	-1.3699	1.4027	-0.0565	0.93	14
CH-3	7/10/15	NO_3	0.685	Linear	NA	0.8928	0.0026	0.99	8
CH-3	7/10/15	Br		Linear	NA	0.2733	-0.1038	0.99	8
Global	-	NO_3	1.509	Linear	NA	0.8774	-0.0013	0.95	95
Global	-	Br		Linear	NA	0.216	-0.021	0.9	91
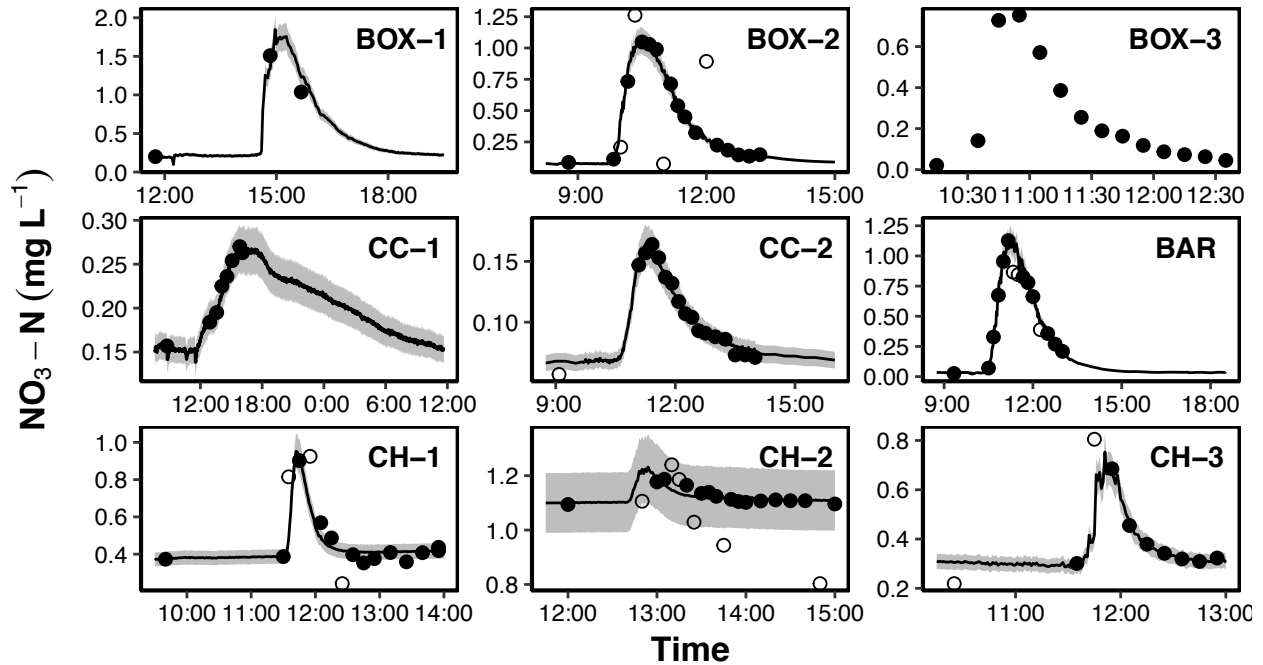
Figure 2. NO$_3$-N BTCs for each separate fluvial wetland solute addition in 2014 and 2015. Lines represent the continuous SUNA NO$_3$-N trace while points are grab sample concentrations. Closed points are grab samples that were included in the SUNA calibration regressions while open points are grab samples that were not included in the calibration regressions. The shaded ribbon around the SUNA NO$_3$-N trace represents the manufacturer-specified constant 10% error associated with each measurement.
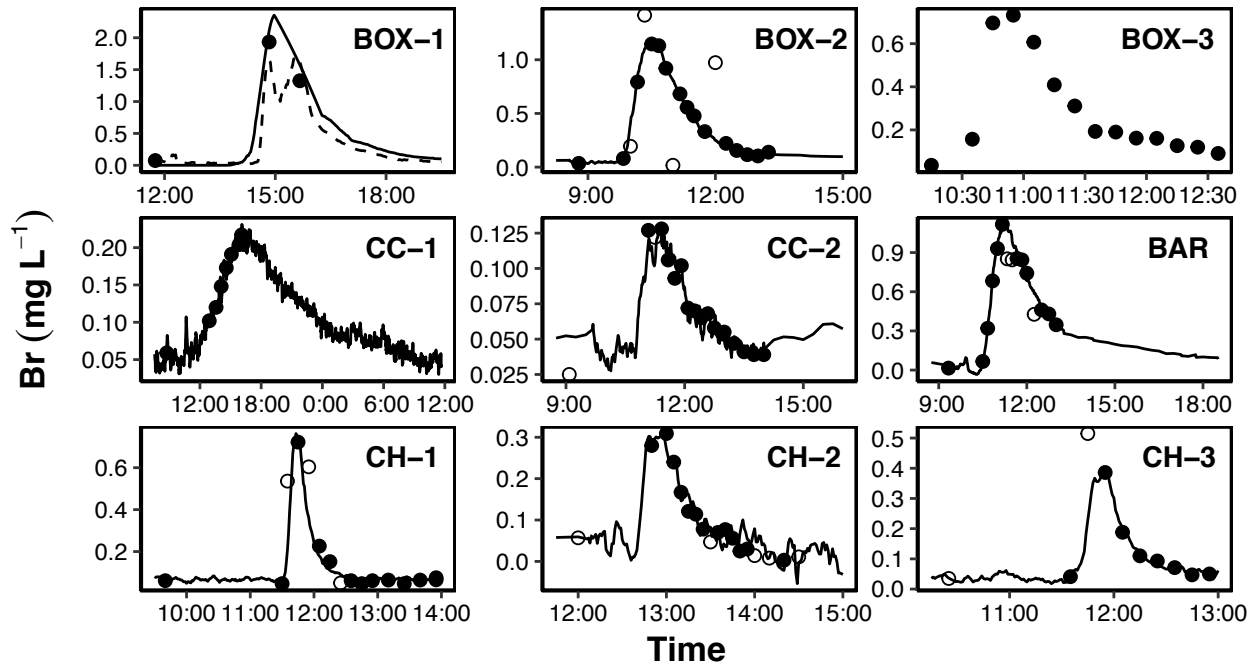
Figure 3. Br BTCs for each separate wetland solute addition in 2014 and 2015. Lines represent the moving average-smoothed continuous Br trace while points are discrete grab sample concentrations. Closed points represent grab samples that were included in the SUNA Br calibration regressions while open points are grab samples that were not included in the regressions. No error is associated with the SUNA Br trace as none was specified by the manufacturer. The BOX-1 panel shows the SUNA Br trace with a dashed line as well as the RWT trace, downscaled by a factor of 10 for visualization purposes, with a solid line.
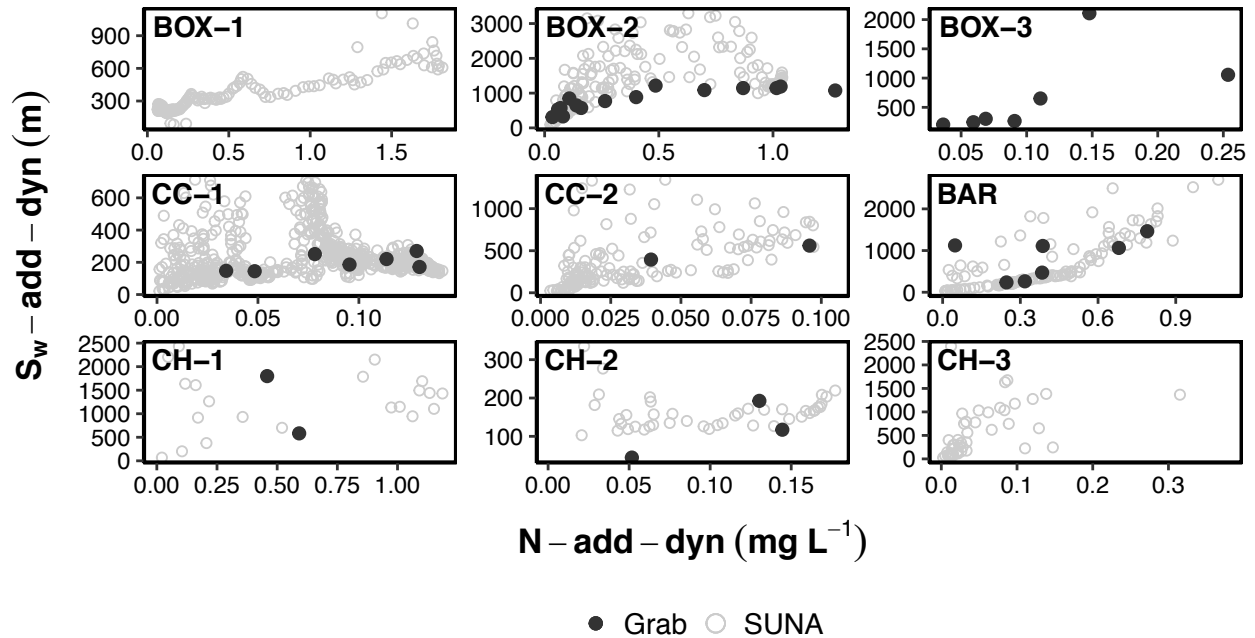
Figure 4. Dynamic uptake length for all solute additions plotted against added (i.e. background-corrected) NO_3-N concentrations using both SUNA data (open circles) and grab sample data (closed circles). Grab sample uptake metrics were not calculable for the BOX-1 and CH-3 experiments while SUNA-calculated uptake was not calculable for the BOX-3 experiment.

Uptake metrics calculated using both SUNA data as well as grab sample data were compared statistically to assess whether the novel SUNA-based approach provided results similar to the commonly used discrete grab sample method. Three experiments with greater than three grab sample results corresponding with SUNA results (BOX-2, CC-1, BAR) were used to make these comparisons. Experiments with three or fewer overlapping samples were omitted as these were not sufficient to assess agreeability between data types.

Uptake lengths from the two approaches using only paired samples indicated little bias for the BAR and CC-1 experiments while during the BOX-2 experiment, the SUNA tended to

show longer uptake lengths than grab samples (Figure 5). SUNA and grab sample-calculated

uptake lengths were positively related with slopes ranging from 0.34 to 0.63 and intercepts

ranging from 84 to 412 m. Dynamic uptake length estimates made using SUNA data were

significantly correlated with grab sample-estimated uptake lengths for the BOX-2 experiment

(r^2 = 0.43, p = 0.01) while the BAR and CC-1 experiments did not yield statistically significant

relationships (r^2 = 0.47, p = 0.09; r^2 = 0.38, p = 0.1, for BAR and CC-1, respectively). Unpaired t-

tests indicate that there was a significant difference in the dynamic uptake length estimates

made using SUNA and grab sample data for the BOX-2 experiment (p = 0.04) however,

differences for the BAR and CC-1 experiments were not statistically significant (p = 0.58 for both

BAR and CC-1).
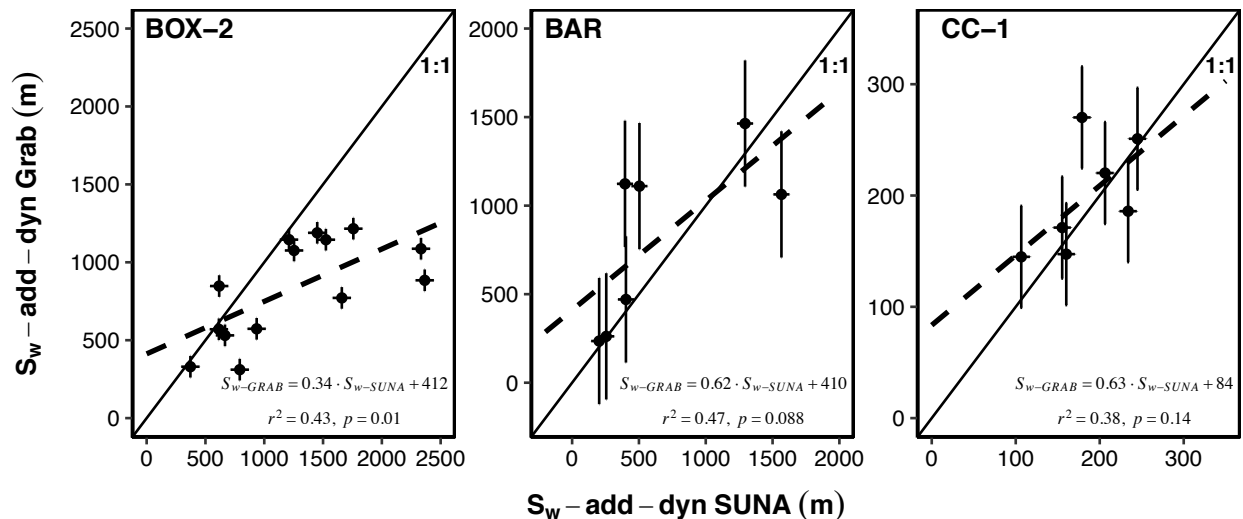
Figure 5. Comparison of uptake lengths estimated using SUNA and grab sample data where

sample timestamps matched. The dashed line represents the linear relationship between the

SUNA and grab sample uptake lengths while the solid line is 1:1.

Despite slopes being less than 1, error bars on each point representing the standard error of the intercept derived from the $S_{w\text{-add-dyn}}$ vs. $N_{add\text{-}dyn}$ relationships overlap the 1:1 line for a majority of the points in the BAR and CC-1 comparisons. This indicates that many of these points fall within the margin of error associated with the TASCC method. This reveals little bias for the BAR and CC-1 experiments as a whole but, while there is little bias for the BOX-2 experiment at low uptake lengths, SUNA uptake lengths increase more rapidly than grab sample uptake lengths.

Analysis of covariance (ANCOVA) was performed on the dynamic $S_{w\text{-add-dyn}}$ vs. $N_{add\text{-}dyn}$ relationships for SUNA and grab sample data for each of the three experiments, controlling for the interaction between data type and NO_3-N concentration. There were no statistically significant differences between the slopes or intercepts of the $S_{w\text{-add-dyn}}$ vs. $N_{add\text{-}dyn}$ relationships when using only SUNA data collected at the time of grab samples for the three experiments (Table 5). When using the full SUNA data, there were no statistically significant differences except for the BAR experiment where the intercept was higher (p=0.05). However, because grab samples were often sparse or not collected on one of the limbs (e.g. CC-1, CC-2, CH-1; Figures 2 and 3), the SUNA approach provides a more complete picture.

Table 5. ANCOVA p values for the comparison between the $S_{w\text{-}add\text{-}dyn}$ vs. $N_{add\text{-}dyn}$ relationships for SUNA and grab sample data using a subset of the SUNA data at grab sample intervals as well as the full SUNA data.

Experiment	SUNA (Subset) - Grab Intercept ANCOVA p	SUNA (Subset) - Grab Slope ANCOVA p	SUNA (All) - Grab Intercept ANCOVA p	SUNA (All) - Grab Slope ANCOVA p
BOX - 2	0.19	0.3	0.13	0.44
BAR	0.54	0.57	0.05	0.08
CC - 1	0.66	0.48	0.49	0.64

Total areal uptake rates ($U_{tot\text{-}dyn\text{-}TT}$, mg m^{-2} min^{-1}) increased with increasing NO_3-N concentrations with SUNA data-calculated areal uptake ranging from 0.01 to 4.17 mg m^{-2} min^{-1} while areal uptake rates calculated using grab sample data ranged from 0.01 to 1.52 mg m^{-2} min^{-1} (Figure 6). These fluvial wetland areal uptake rates were generally greater than those found for the Snake River and its channelized tributaries (0.002 to 0.12 mg m^{-2} min^{-1}) (Hall and Tank 2003, Tank et al. 2008). Like uptake length, estimates of areal uptake calculated from grab sample data follow a similar trend as the SUNA-calculated results and fall within the range of SUNA-derived values for the BOX-2, CC-1, BAR, and CH-1 experiments, but not for the CC-2 and CH-2 experiments. This difference in SUNA and grab sample-calculated total areal uptake rates for the CC-2 and CH-2 experiments was due to differences in U_{amb} as $U_{tot\text{-}dyn\text{-}TT}$ is the sum of U_{amb} and $U_{add\text{-}dyn\text{-}TT}$. The differences in ambient uptake were likely a result of too few samples to derive an accurate estimation of the ambient areal uptake rates.
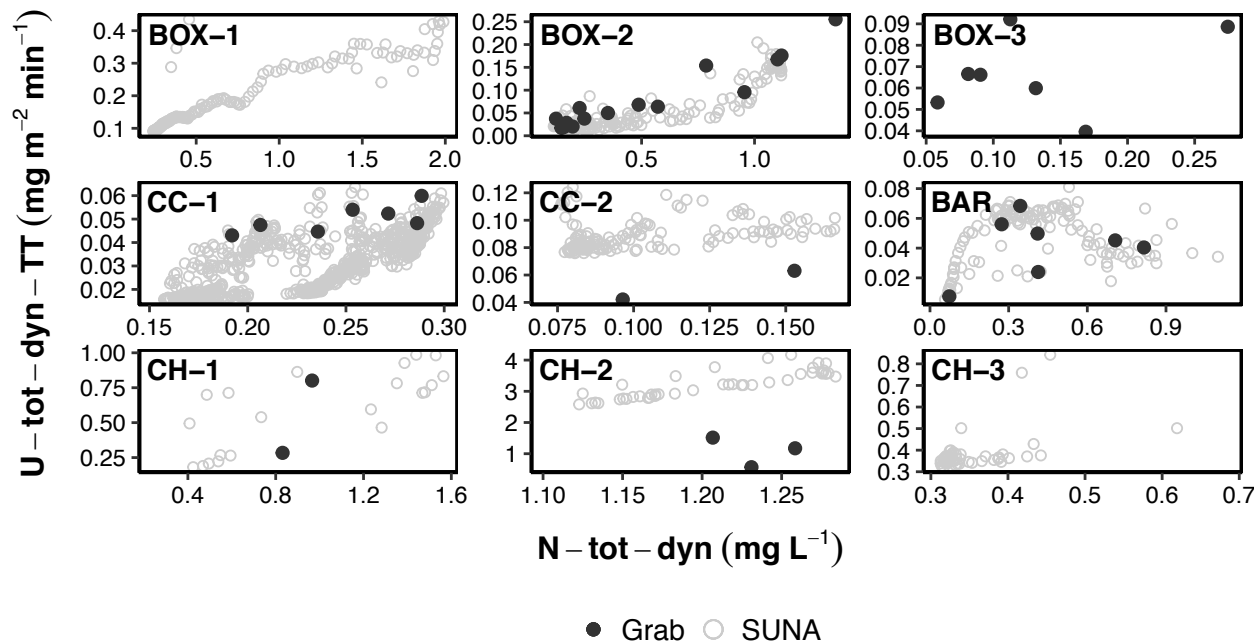
Figure 6. Total areal uptake rates ($U_{tot\text{-}dyn\text{-}TT}$, mg m^{-2} min^{-1}) for all wetland solute additions with useable data, plotted against total NO$_3$-N concentrations using both SUNA data (open circles) and grab sample data (closed circles).

SUNA data-calculated total areal uptake rates were also highly correlated with grab sample-calculated rates when comparing the three experiments with a sufficient number of points to make such a comparison (Figure 7). Like uptake length, the BOX-2 experiment was the only one to have a statistically significant relationship between SUNA and grab sample-calculated areal uptake (r^2 = 0.87, p<0.001), while BAR and CC-1 did not exhibit significant relationships (r^2 = 0.41, p = 0.12; r^2 = 0.45, p = 0.1, for BAR and CC-1, respectively). BOX-2 also has a slope of 1.2 and an intercept of 0.018 mg m^{-2} min^{-1} while BAR and CC-1 both had slopes less than 1 and CC-1 had an intercept greater than both BOX-2 and BAR. Unpaired t-tests indicate that differences between the SUNA and grab sample-calculated areal uptake rates

were not statistically significant for any of these three experiments (p = 0.25, p = 0.7, p = 0.08, for BOX-2, BAR, and CC-1, respectively). This indicates that the differences within sites using the two methods are smaller than the differences across sites, suggesting that either data type (SUNA or grab sample) provides a reasonable estimate when it comes to comparing sites.
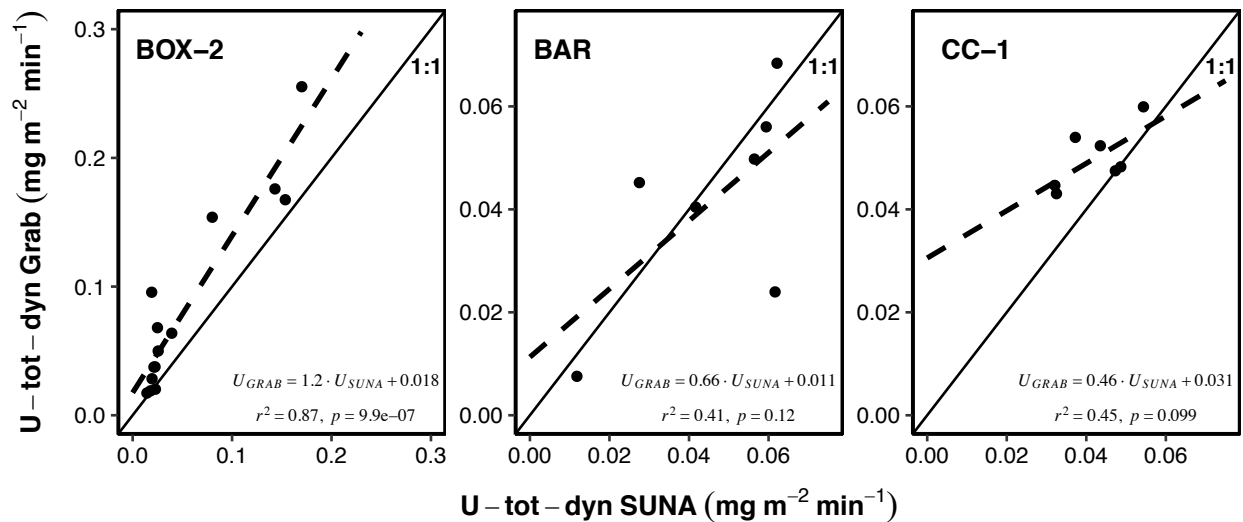
Figure 7. Relationships between fluvial wetland areal uptake rates calculated using SUNA and grab sample data at matching sampling times. Slopes and intercepts for each relationship as well as the r^2 and p-values of those relationships are also shown. The dashed lines represent these linear relationships while the solid line is 1:1.

Total uptake velocity ($V_{f\text{-tot-dyn-TT}}$, m yr^{-1}) generally declined with increasing nutrient concentrations through the BTC, indicating a higher demand at lower NO_3-N concentrations (Figure 8). Similar to both uptake length and areal uptake, grab sample-calculated uptake velocity fell within the scatter of the SUNA data-calculated results with SUNA estimates ranging from 14.2 to 10,700 m yr^{-1} and grab sample results ranging from 71 to 15,413.1 m yr^{-1}. This range in fluvial wetland uptake velocities is greater than the range found for the Snake River

and its channelized tributaries (210.24 to 4730.4 m yr^{-1}) (Hall and Tank 2003, Tank et al. 2008).

The CH-1 and CH-2 experiments did not yield statistically significant relationships between

uptake velocity and total NO_3-N using SUNA data (p = 0.26 & p = 0.36, respectively). However,

those two experiments had average uptake velocities of 1067.4 and 4642.6 m yr^{-1}, respectively.

CH also showed the highest NO_3-N demand among all sites.
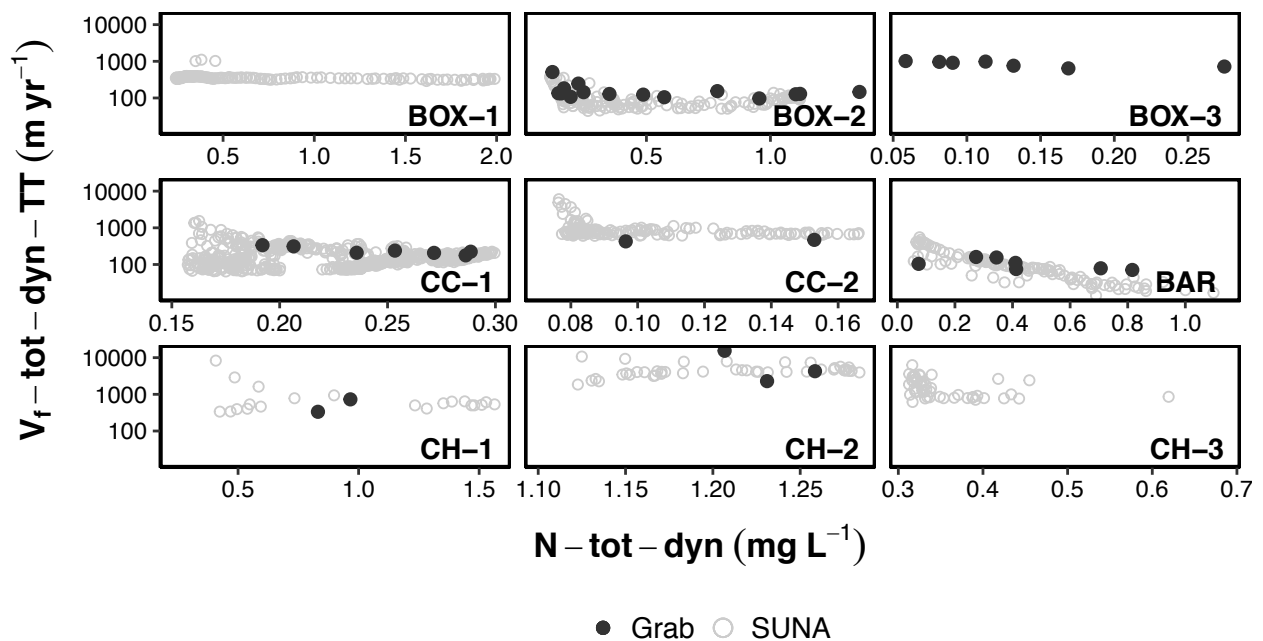
Figure 8. Total dynamic uptake velocities ($V_{f\text{-tot-dyn-TT}}$, m yr^{-1}) for all solute additions vs. total NO_3-N concentrations (mg L^{-1}) using both SUNA data (open circles) and grab sample data (closed circles). The y-axes were log-transformed and standardized for all plots.

SUNA and grab sample-calculated uptake velocities were generally correlated with

positive relationships exhibited for all three experiments with enough points to make a

meaningful comparison (Figure 9). These relationships were statistically significant for BOX-2

and CC-1 while the BAR comparison was not statistically significant (p < 0.001, p = 0.1, p = 0.02, for BOX-2, BAR, and CC-1, respectively). Similar to the comparison of dynamic areal uptake, the BOX-2 experiment had a slope greater than one while the other two relationships had slopes less than one. The BOX-2 relationship also had a negative intercept while BAR and CC-1 had comparable, positive intercepts. Ignoring the outlier in the upper range of uptake velocity calculated using grab sample data for BOX-2, the slope and intercept become 0.51 and 84.4 m yr^{-1}, more similar to the coefficients for the relationships at BAR and CC-1. Unpaired t-tests indicated that there were no statistically significant differences between SUNA and grab sample-calculated uptake velocities for any of the three experiments (p = 0.07, p = 0.4, p = 0.5, for BOX-2, BAR, and CC-1, respectively).

Figure 9. Comparison of uptake velocities calculated using SUNA and grab sample data at matching sampling times. Dashed lines represent the linear relationships between variables while the solid line is 1:1.

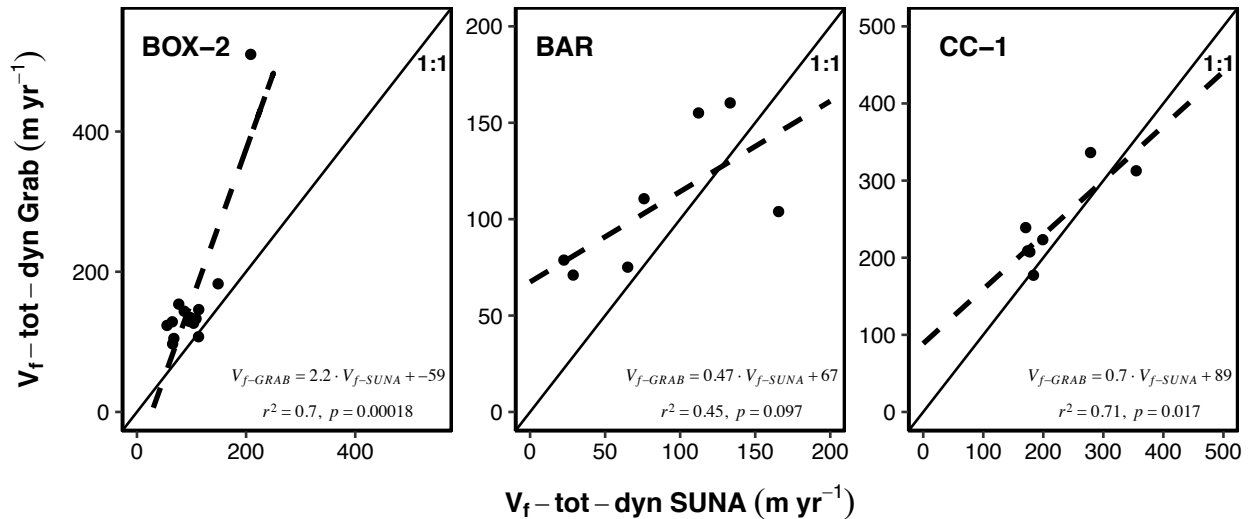SUNA and grab sample-calculated uptake metrics from the three experiments with greater than three paired points were pooled to explore generalities in uptake metric relationships calculated using either data type. Pooling data from all three experiments reduced site-specific trends and allowed for a greater range of values for each uptake metric. Using the pooled data, statistically significant relationships and relatively high r^2 values between the SUNA and grab sample-calculated uptake metrics indicated a large degree of agreement between the two approaches (Figure 10). Relationships using pooled data also resulted in slopes close to one and intercepts approaching zero for both areal uptake and uptake velocity. However, the comparison of uptake length had a slope of 0.46, largely driven by results from BOX-2 where SUNA-calculated uptake length increased more rapidly than grab sample-calculated estimates. Unpaired t-tests for each uptake metric indicated that differences between SUNA and grab sample-calculated uptake length and areal uptake were not statistically significant (p = 0.06, p = 0.18, respectively) however, there was a significant difference between SUNA and grab sample-calculated uptake velocity (p = 0.02). This significant difference was driven by one point where grab sample uptake velocity was more than double SUNA-calculated uptake velocity and with that point excluded, the significance goes away. Because of this correspondence between methods, we believe that the SUNA data, including the greater scatter that is evident, reflects actual wetland dynamics (rather than noise in the instrument).

Throughout each experiments BTC, the high frequency SUNA data reveal a considerable amount of short term variability that is not detectable using infrequently collected grab samples. While grab samples may begin to hint at this variability, the infrequency with which

they were collected would make this variability appear to be noise. This is evident in the falling

limb of each BTC almost exclusively where different flowpaths and STS create long tails in the

BTC and grab samples are typically collected less frequently by design. Because of the ability to

capture variability driven by internal wetland processes, SUNA data will be the primary focus

for the remainder of the results with the exception of BOX-3 for which there was only grab

sample data collected.
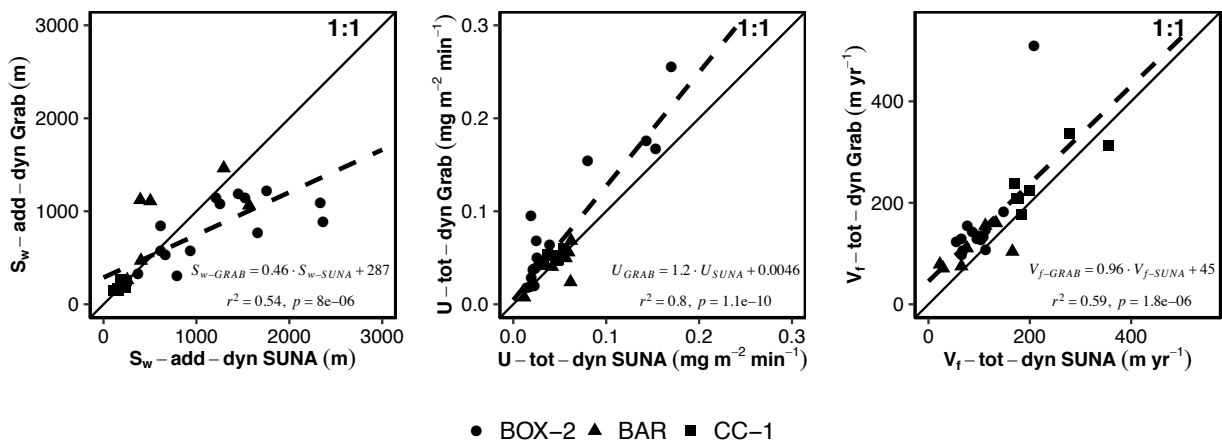
Figure 10. Comparison of uptake length, areal uptake, and uptake velocity estimates made

using both SUNA and grab sample data for all experiments with greater than three samples

collected at corresponding times. The dashed lines represent the linear relationships between

SUNA and grab sample-calculated uptake metrics while the solid line is 1:1.

Uptake Metrics on Rising and Falling Limbs

Hystereses were observed in uptake metric vs. NO_3-N concentration relationships during

the BTC at all sites. Hysteresis resulted in different intercepts and slopes for the uptake length

vs. NO_3-N relationships on the rising and falling limbs of the BTC. As a result, estimates of

uptake differed depending on whether the calculation used all data, rising limb only data, or falling limb only data. The calculation of ambient uptake parameters requires extrapolation of this uptake length vs. NO_3-N relationship back to ambient concentrations. Thus, hysteresis can influence this extrapolation and can therefore, result in different ambient uptake metrics for the rising and falling limbs (Figure 11). The difference in ambient uptake between limbs was the greatest for the CH-1 experiment ($S_{w-Rising}$ = 166.5 m, $S_{w-Falling}$ = 1775 m) while the BOX-2 experiment had the smallest difference ($S_{w-rising}$ = 962.5 m, $S_{w-Falling}$ = 911.5 m) (Figure 11, Table 6).

Figure 11. Dynamic uptake length vs. NO_3-N relationships for all solute additions using parameters calculated from SUNA data and differentiated by limb of the BTC. Dashed lines represent linear relationships for either limb with black showing rising limb data and the falling limb showed in grey. The solid black line uses combined rising and falling limb data.
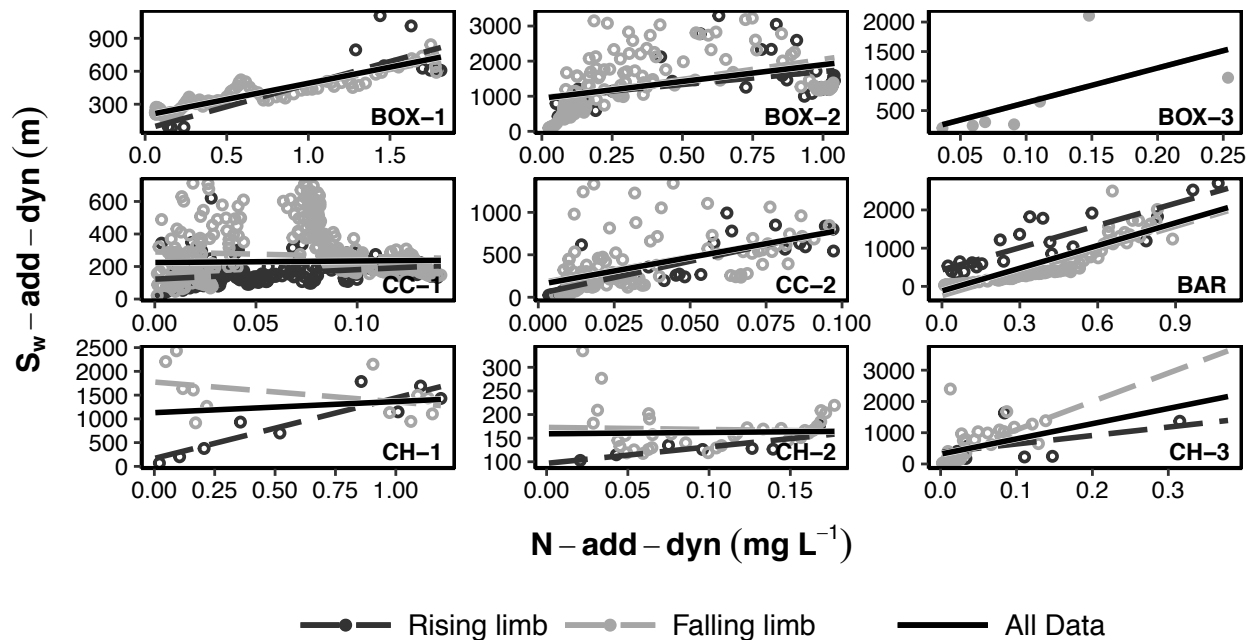
Table 6. Ambient uptake metrics for all experiments calculated using all data, rising limb data, and falling limb data. SUNA data was used for all experiments except BAR-3, where grab sample data were used. Asterisks indicate whether the intercept of the $S_{w-add-dyn}$ − $N_{add-dyn}$ relationships was statistically significant (p < 0.05). Standard error for each metric is in brackets where it was calculable.

Experiment	S_{w-amb} All (m)	S_{w-amb} Rising Limb (m)	S_{w-amb} Falling Limb (m)	U_{amb} All (mg m^{-2} min^{-1})	U_{amb} Rising Limb (mg m^{-2} min^{-1})	U_{amb} Falling Limb (mg m^{-2} min^{-1})	V_{f-amb} All (m yr^{-1})	V_{f-amb} Rising Limb (m yr^{-1})	V_{f-amb} Falling Limb (m yr^{-1})
BOX-1	197.7 * [9]	72.6 [142.1]	206.1 * [5.9]	0.08 [0]	0.21 [NA]	0.07 [0]	230.1 [10.5]	626.7 [NA]	220.7 [6.3]
BOX-2	943.8 * [78.3]	962.5 * [236.5]	911.5 * [84.6]	0.004 [0]	0.004 [0]	0.004 [0]	25.2 [2.1]	24.8 [6.5]	26.1 [2.4]
BOX-3	47.5 [431.6]	NA	47.5 [431.6]	0.02 [NA]	NA	0.02 [NA]	583.7 [NA]	NA	583.7 [NA]
CC-1	224.5 * [10.3]	122.3 * [7.5]	289.5 * [14.2]	0.02 [0]	0.03 [0]	0.01 [0]	52.6 [2.4]	96.5 [5.9]	40.8 [2]
CC-2	148.1 * [32.5]	41.2 [51.7]	166.6 * [38.7]	0.08 [0.02]	0.27 [NA]	0.07 [0.02]	573.1 [141.5]	2059.9 [NA]	509.6 [125.3]
BAR	-119.6 * [60.2]	431.9 * [123.7]	-243.9 * [47.5]	-0.01 [0]	0.003 [0]	-0.01 [0]	-170.6 [0]	47.3 [14.7]	-83.7 [0]
CH-1	1130.5 * [230.3]	166.5 [166.4]	1775 * [227.3]	0.17 [0.04]	1.17 [719.02]	0.11 [0.01]	240.4 [51.5]	1632.2 [1e+6]	153.1 [19.9]
CH-2	159.2 * [15]	96.7 * [12.5]	172.8 * [16.6]	2.55 [0.3]	4.21 [0.69]	2.35 [0.29]	1220 [144.6]	2009.9 [329.2]	1124.3 [136.6]
CH-3	316.4 * [92.3]	370 [326.4]	186.3 [99.1]	0.32 [0.1]	0.27 [1.09]	0.54 [0.4]	552.3 [176.2]	472.4 [1879.1]	938 [695.8]

ANCOVA was performed on the uptake length vs. NO_3-N relationships controlling for the effect of uptake on either limb of the BTC to test for differences in ambient uptake rates on the rising and falling limbs. Slopes were significantly different between rising and falling limbs for the BOX-1, CC-1, CH-1, and CH-3 experiments ($p < 0.001$, $p < 0.001$, $p < 0.001$, $p = 0.02$, respectively) (Table 7). Intercepts of these relationships, signifying S_{w-amb}, were significantly different for the BOX-1, CC-1, BAR, and CH-1 experiments ($p < 0.01$, $p < 0.001$, $p < 0.001$, $p < 0.001$, respectively). The difference between rising and falling limb intercepts at BAR were statistically significant despite a lack of significantly different slopes. ANCOVA was not performed on the BOX-3 data as grab samples only captured the rising limb of the BTC.

Table 7. ANCOVA p-values for the differences between slopes and intercepts calculated using rising and falling limb data from each BTC. There were no grab samples collected along the rising limb of the BOX-3 BTC, hence no comparison was made.

Experiment	$S_{w-add-dyn}$ - $N_{add-dyn}$ Intercept ANCOVA p	$S_{w-add-dyn}$ - $N_{add-dyn}$ Slope ANCOVA p
BOX-1	0.01	<0.001
BOX-2	0.84	0.27
BOX-3	NA	NA
CC-1	<0.001	<0.001
CC-2	0.16	0.42
BAR	<0.001	0.72
CH-1	<0.001	<0.001
CH-2	0.053	0.27
CH-3	0.51	0.02

Hysteresis was also evident in the $U_{tot\text{-}dyn\text{-}TT}$ and $V_{f\text{-}tot\text{-}dyn\text{-}TT}$ vs. NO_3-N concentration relationships. The greatest hystereses occurred during the BAR, CC-1, and CH experiments (Figures 12 and 13). The solute additions at BOX show less hysteresis while the BOX-3 experiment, with uptake metrics calculated using grab sample data only, was lacking data along the rising limb. For experiments with wide hysteresis loops, hystereses generally exhibited a clockwise pattern, indicating greater uptake on the rising limb compared to the falling limb (CC-1, CH-1, CH-2, CH-3). The experiment at BAR had a counter-clockwise hysteresis suggesting that uptake was greater on the falling limb of the BTC.
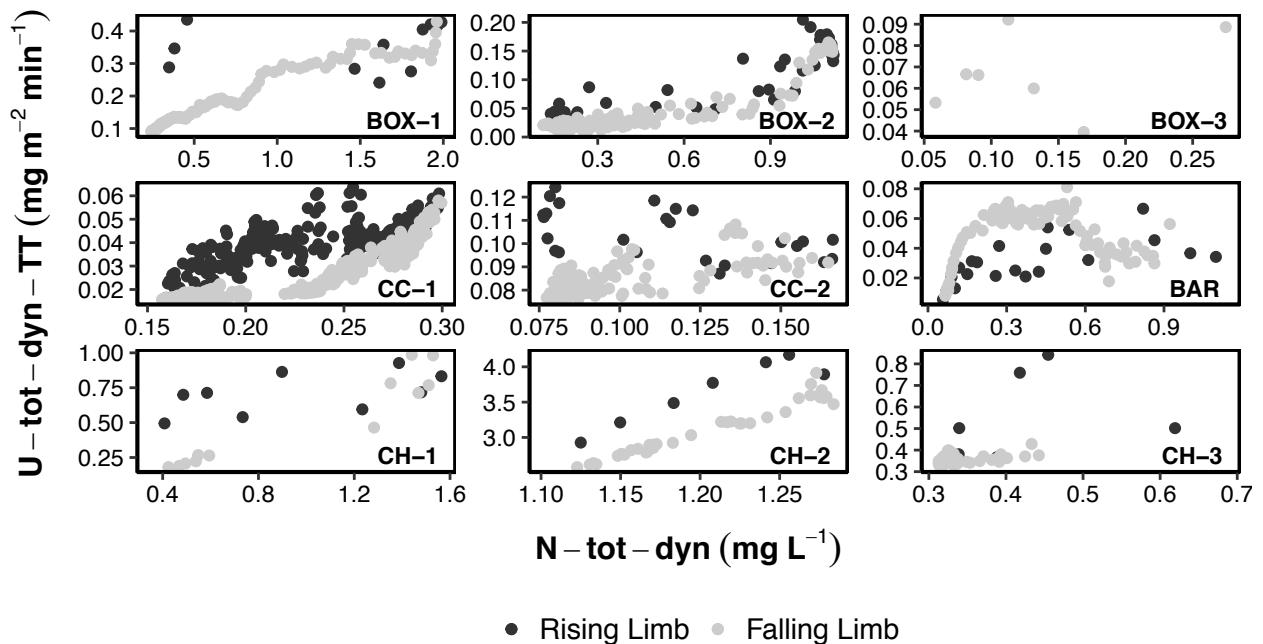

Figure 12. Areal uptake rate vs. total NO_3-N concentration on the rising and falling limbs of the BTC for all experiments with black points representing the rising limb of the BTC and grey points showing the falling limb. High frequency SUNA data are shown with the exception of the BOX-3 experiment which is showing grab sample results.
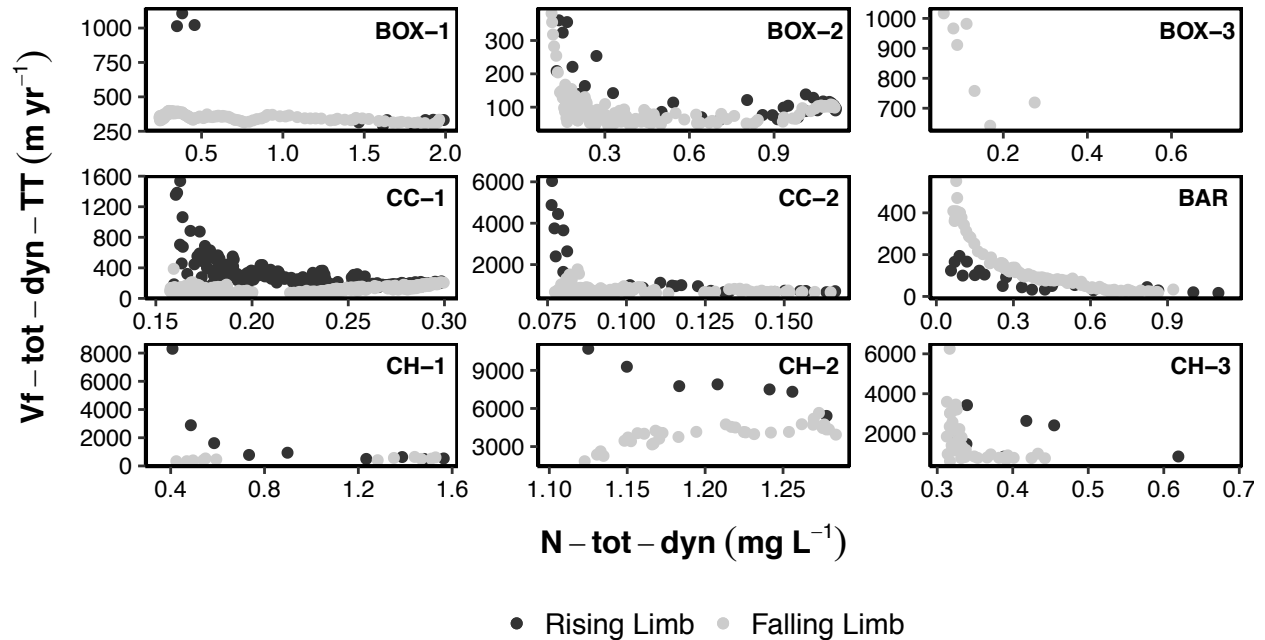
Figure 13. Relationships between uptake velocity and total NO_3-N concentrations on each limb of the BTC for all experiments with the black points representing rising limb data and grey points showing falling limb data in log-linear space. All plots are showing SUNA data with the exception of the BOX-3 experiment which used grab sample data for all calculations.

$S_{w\text{-amb}}$, estimated from the $S_{w\text{-add-dyn}}$ vs. $N_{add\text{-dyn}}$ relationships using both rising and falling limb data, ranged from -119.6 ± 60.2 m at BAR to 1130.5 ± 230.3 m for the CH-1 experiment (Table 6). Areal uptake rates for each experiment ranged from -0.01 ± 0 mg m^{-2} min^{-1} at BAR to 2.55 ± 0.3 mg m^{-2} min^{-1} for the CH-2 experiment. Ambient uptake velocities ranged from -170.6 ± 0 m yr^{-1} for the BAR experiment to 1220 ± 144.6 m yr^{-1} during the CH-2 experiment. The negative values for uptake metrics found for the BAR experiment were not theoretically possible however the negative ambient uptake length suggests high uptake for the amount of solute entering the wetland. As the ambient uptake length is an integral component for

calculating U_{amb} and V_{f-amb}, the negative sign is propagated to the other ambient uptake metrics but does not necessarily indicate low reactivity. For further analyses, ambient uptake metrics for the BAR experiment were assumed to be zero. Additionally, due to uptake metrics for the BOX-3 experiment being calculated from grab sample data and not the high frequency SUNA data, ambient uptake rates for this experiment should be viewed as minimum ambient uptake.

When considering data on the rising limb only, S_{w-amb} ranged from 41.2 ± 51.7 m for the CC-1 experiment to 962.5 ± 236.5 m for the BOX-2 experiment (Table 6). These ambient uptake lengths translated into ambient areal uptake rates spanning a range between 0.003 ± 0 mg m^{-2} min^{-1} at BAR to 4.21 ± 0.69 mg m^{-2} min^{-1} for CH-2. Finally, ambient uptake velocities estimated from rising limb data were found to extend from 24.8 ± 6.5 m yr^{-1} for BOX-2 to 2059.9 m yr^{-1} for CC-2. A meaningful standard error was not calculable for the CC-2 rising limb ambient uptake metrics as the error surrounding the estimate of S_{w-amb} was greater than the estimate of S_{w-amb} itself. This was also the case for the BOX-1 rising limb and the BOX-3 falling limb.

Falling limb uptake estimates were generally more similar to estimates made using the entire BTC with values for S_{w-amb} ranging from -243.9 ± 47.5 m at BAR to 1775 ± 227.3 m for CH-1. Falling limb ambient areal uptake rates were again lowest at BAR at -0.01 ± 0 mg m^{-2} min^{-1} but highest during the CH-2 experiment at 2.35 ± 0.29 mg m^{-2} min^{-1}. A similar pattern was found for falling limb V_{f-amb} where the BAR experiment had the lowest ambient uptake velocity and CH-2 had the highest at -83.7 ± 0 and 1124.3 ± 136.6 m yr^{-1}, respectively.

In general, uptake calculated using the falling limb data only was more similar to uptake calculated using all data, likely due to more points being sampled on the falling limb. Percentages of the BTCs sampled along the falling limb range from 64.6% for the BAR

experiment to 91.7% for the CH-2 experiment (Table 8). The $S_{w\text{-add-dyn}}$ vs. $N_{add\text{-}dyn}$ relationships using pooled data were determined to be sufficient to represent ambient uptake metrics, however it should be noted that these differences in ambient uptake between the rising and falling limbs do exist.

Table 8. Percentage of points sampled along either limb of the BTC for all experiments where n is the total number of samples for each experiment.

Experiment	n	Rising Limb %	Falling Limb %
BOX-1	150	12	88
BOX-2	203	20.2	79.8
BOX-3	13	23.1	76.9
BAR	198	35.4	64.6
CC-1	1441	18.6	81.4
CC-2	216	23.1	76.9
CH-1	91	15.4	84.6
CH-2	144	8.3	91.7
CH-3	82	22	78

Comparison of Fluvial Wetland Uptake to Channels and STS Patches

Fluvial wetland uptake velocities estimated using solute additions performed at the whole ecosystem scale were greater than uptake velocities for channelized reaches in the same geographic region and in several cases, higher than those found for fluvial wetland STS patches alone (i.e. not factoring in the channel). The response of uptake to changing NO_3-N concentrations followed an efficiency loss (EL) pattern, where areal uptake increases with increasing concentration but at a slower rate (Wollheim et al. 2014). Comparing uptake

velocities, seven of the nine experimental solute additions had statistically significant declines

in $V_{f\text{-tot-dyn-TT}}$ as NO_3-N concentrations increased, while two additions, both at the high nitrate

CH site (CH-1, CH-2) showed little change during the two additions ($p > 0.05$) (Figure 14). The

seven additions with significant declines showed that uptake velocities were greater than those

found for total NO_3-N gross uptake in channelized streams in the Parker and Ipswich River

watersheds (Mulholland et al. 2008) (Figure 14). Uptake velocities were also similar to fluvial

wetland STS patches also in the Parker and Ipswich River watersheds (Wollheim et al. 2014)

(Figure 14) with three experiments yielding uptake velocities less than STS patches (i.e. not

whole system) while four had greater uptake velocities. The two additions that did not have

statistically significant EL relationships (spring 2014 CH-1; fall 2014 CH-2) had average uptake

velocities that were greater than both channelized reaches and fluvial wetland STS patches over

the range of NO_3-N concentrations experienced during the additions. One of these additions

returned a mean V_f greater than all other additions (CH-2). This suggests that stream reaches

with linked channel and STS may be hotspots of nitrate removal.

Comparison of Ambient Uptake Across Sites and Seasons

Ambient uptake metrics varied more across seasons than among sites. Ambient areal

uptake rates (U_{amb}) varied from 0 to 2.55 mg m^{-2} min^{-1} over the course of the experiments. The

lowest U_{amb} was found for the BAR experiment while the highest U_{amb} was measured at CH

during the late fall addition in 2014. Similarly, $V_{f\text{-amb}}$ ranged from 0 to 1220 m yr^{-1} with the

lowest occurring at the addition at BAR while the highest was again found for the late fall 2014

addition at CH. There were no significant differences among sites (Kruskal-Wallis: H = 6.511, p =

0.09; H = 3.489, p = 0.32, for U_{amb} and $V_{f\text{-}amb}$, respectively) or seasons (Kruskal-Wallis: H = 2.667,

p = 0.61; H = 1.067, p = 0.3, for U_{amb} and $V_{f\text{-}amb}$, respectively) (Figure 15).
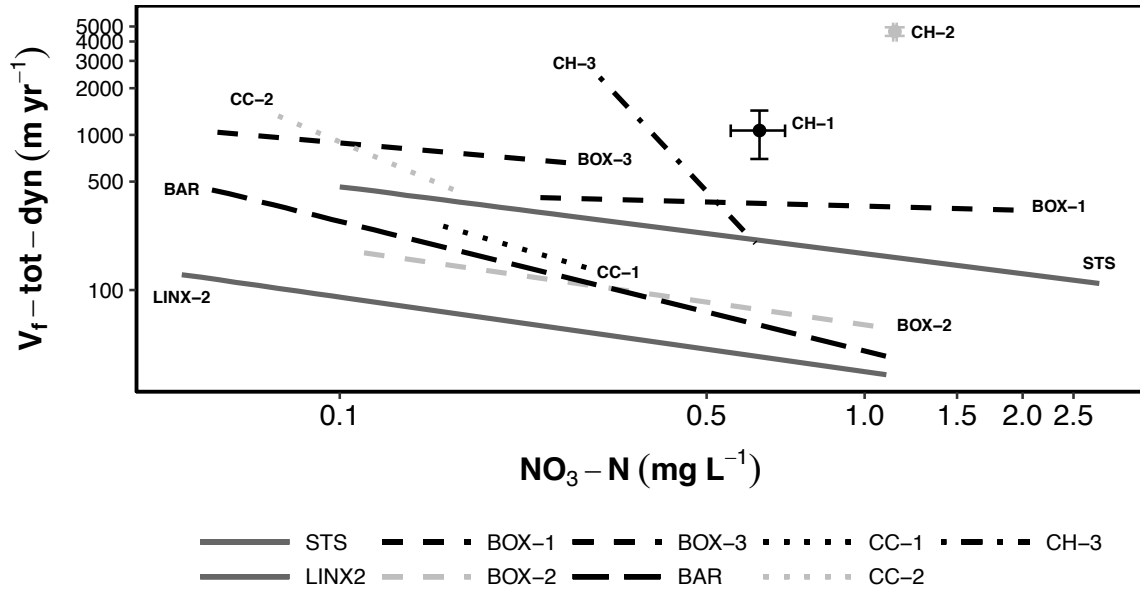
Figure 14. Uptake velocities estimated using data collected during whole-wetland reach solute additions across the range of experimentally elevated NO_3-N concentrations. Shown are the power functions derived from experimental data plotted in log-log space. Fluvial wetland results were calculated using high temporal resolution SUNA data with the exception of BOX-3 which was calculated from discrete grab sample data. Uptake velocity vs. NO_3-N relationships that were not statistically significant (CH-1, CH-2) are shown with points representing the mean uptake velocity and mean NO_3-N experienced for that addition with error bars indicating two standard errors for both uptake velocity and NO_3-N. Also shown are previously reported relationships for total uptake velocity for channelized headwater streams in the Parker and Ipswich River watersheds (LINX2, Mulholland et al. 2008) and fluvial wetland STS patches (Wollheim et al. 2014).
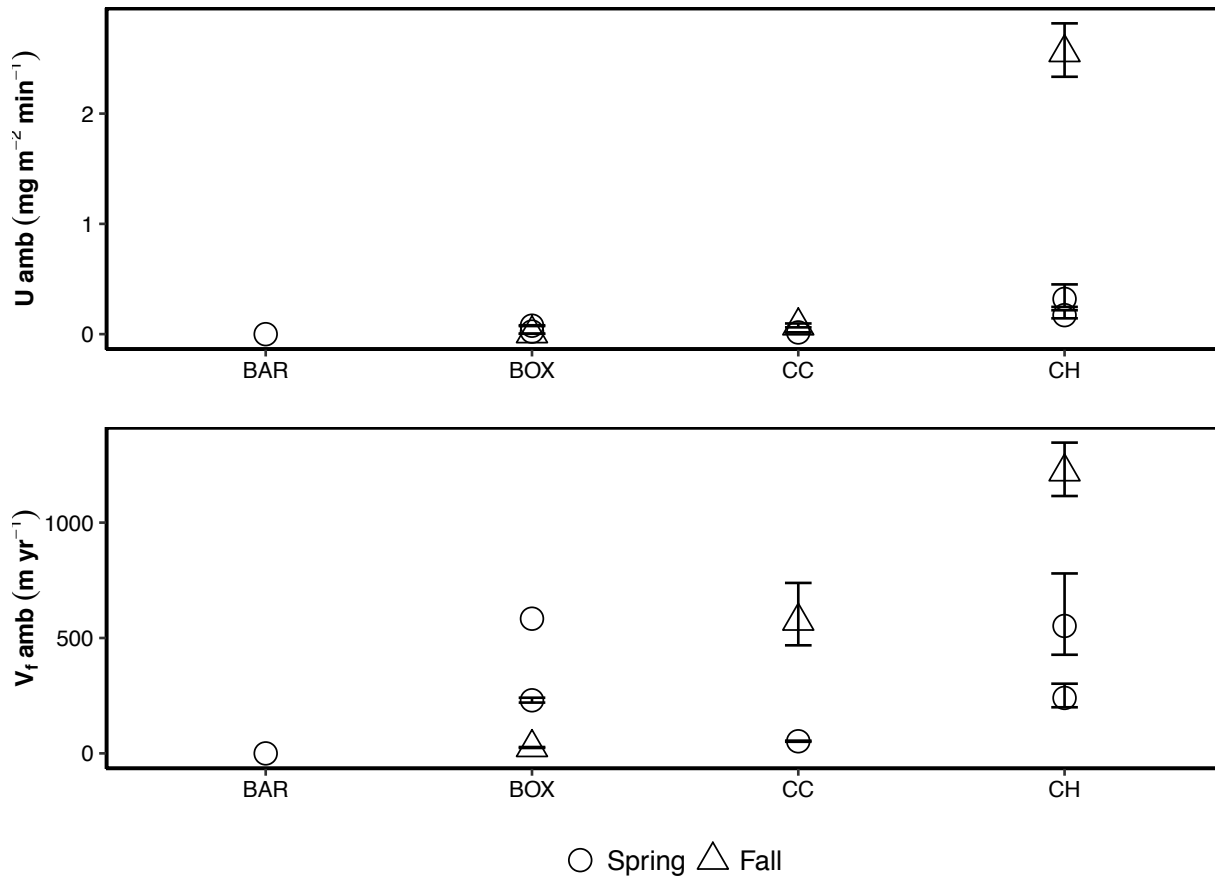
Figure 15. Ambient uptake metrics compared across sites, differentiated by the season in which the experiments were performed. Circles represent spring additions while triangles represent fall experiments.

Uptake Determined from TASCC BTC-Integrated Approach

BTC-integrated uptake metrics were variable across sites and seasons. BTC-integrated areal uptake rates (U_{add}) ranged from 0.002 to 0.09 mg m^{-2} min^{-1} with the lowest U_{add} occurring during the spring 2015 addition at CH while the greatest U_{add} was found for the fall 2014 addition at CH (Table 9). BTC-integrated uptake velocities ($V_{f\text{-}add}$) varied between 8.4 and 959.4 m yr^{-1} with the lowest found for the spring 2015 experiment at BOX while the highest occurred

during the fall 2014 experiment at CH. Percent removal of the added NO_3-N (R_{add}) spanned a range of 1 to 47% with the lowest removal found for the spring 2015 experiment at CH while the highest was found for the fall 2014 experiment at CH.

BTC-integrated uptake metrics differed more across seasons than among sites, similar to ambient uptake metrics summarized above. CH general exhibited greater demand for NO_3-N (e.g. CH mean V_{f-add} = 342.3 m yr^{-1} compared to 41.6 – 208.5 m yr^{-1} at the other three sites) but differences were not statistically significant (Kruskal-Wallis: H = 0.89, p = 0.83; H = 1.16, p = 0.76, for U_{add} and V_{f-add}, respectively). Experiments performed in the fall showed greater demand for NO_3-N than those performed during the summer (e.g. fall mean V_{f-add} = 454.5 m yr^{-1} compared to 44.9 m yr^{-1} during the spring) but again, the differences between seasons were not statistically significant (Kruskal-Wallis: H = 0.6, p = 0.44; H = 1.67, p = 0.2, for U_{add} and V_{f-add}, respectively).

Table 9. BTC-integrated uptake metrics for all wetland solute addition experiments. Metrics were calculated using SUNA data except for the BOX-3 experiment where grab sample data were used.

Experiment	Date	Br Recovery (%)	S_{w-add} (m)	U_{add} (mg m^{-2} min^{-1})	V_{f-add} (m yr^{-1})	R_{add} (%)
BOX-1	6/11/14	114.5	478.6	0.07	95.1	29.9
BOX-2	11/11/14	78.5	1112.5	0.01	21.4	14.2
BOX-3	6/25/15	74.8	3286.2	0	8.4	5
CC-1	7/2/14	66.4	342.6	0	34.5	18.5
CC-2	11/19/14	141.3	211.9	0.02	382.6	27.1
BAR	6/11/15	54.7	319.7	0.03	63.8	35.5
CH-1	7/17/14	100.2	4754.4	0.02	57.2	2.7
CH-2	12/5/14	45.1	202.5	0.09	959.4	47.4
CH-3	7/10/15	43	16775.3	0	10.4	0.8

Removal Determined Using Ambient Input-Output Mass Balance Approach

NO_3-N removal at the whole fluvial wetland scale estimated from the mass balance of

ambient NO_3-N (R_{MB}) ranged from -22% at CC to 70% at BOX with higher R_{MB} tending to occur in

the spring   (-7 – 70%) and lower in the fall (-22 – 14%) (Figure 16). Negative removal of NO_3-N

indicates greater NO_3-N coming out of the wetland compared to what is entering and is likely

due to nitrification, or the biological oxidation of ammonium to nitrate. Mean seasonal NO_3-N

R_{MB} across all sites was 22% in the spring and -1% in the fall (Figure 16). These differences in

removal between seasons were statistically significant (Kruskal-Wallis: H = 6.82, p = 0.009). On a

per site basis, average NO_3-N R_{MB} spanned a range between -7% at CC to 29% at BOX and,

similar to the seasonal comparison, the difference in NO_3-N R_{MB} between sites was statistically

significant (Kruskal-Wallis: H = 12.86, p = 0.005).

NO_3-N mass balance removal estimates over the course of each sensor deployment

were compared to removal determined from the TASCC BTC-integrated approach (R_{add}), as well

as removal calculated from the ambient uptake rates determined using the dynamic TASCC

approach (R_{calc}). NO_3-N R_{calc} was highly variable spanning a range between 0 and 97% for the

BAR and BOX-3 experiments, respectively (Figure 16). NO_3-N R_{MB} was consistently less than R_{calc}

for all experiments, resulting in a relationship between the two removal estimates with an

intercept of 2.4% and a slope of 0.32 (r^2 = 0.88, p = 0.06) (Figure 17 A). NO_3-N R_{add} estimates

were more similar to NO_3-N R_{MB} estimates with little bias and an intercept of 0.5% and a slope

of 0.76 (r^2 = 0.64, p = 0.1) (Figure 17 B). The NO_3-N R_{calc} and R_{add} estimates from the BOX-3

experiment were not included in these comparisons as they were made using grab sample data

only and are not a direct comparison to the other estimates made using the high frequency

SUNA data. Likewise, the NO_3-N R_{calc} estimates from the BAR experiment were also omitted as they were calculated from negative ambient uptake determined from the TASCC method. As estimates of NO_3-N R_{MB} from several experiments were excluded due to their ambient Cl mass balance suggesting wetlands were not behaving conservatively, R_{add} estimates were considered in further analyses due to their greater similarity to R_{MB} estimates compared to R_{calc}.
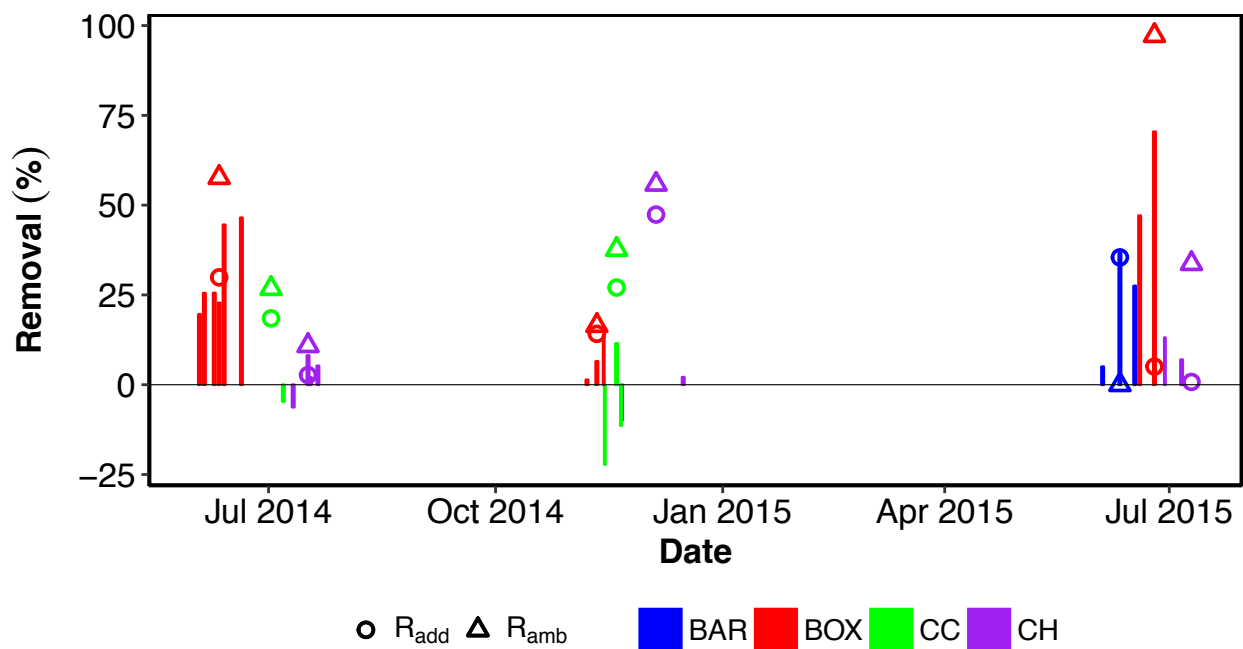

Figure 16. NO_3-N removal estimates made using the ambient mass balance approach (R_{MB}, bars), BTC-integrated removal (R_{add}, open circles), and removal calculated from ambient uptake rates derived from the dynamic TASCC method (R_{calc}, open triangles).
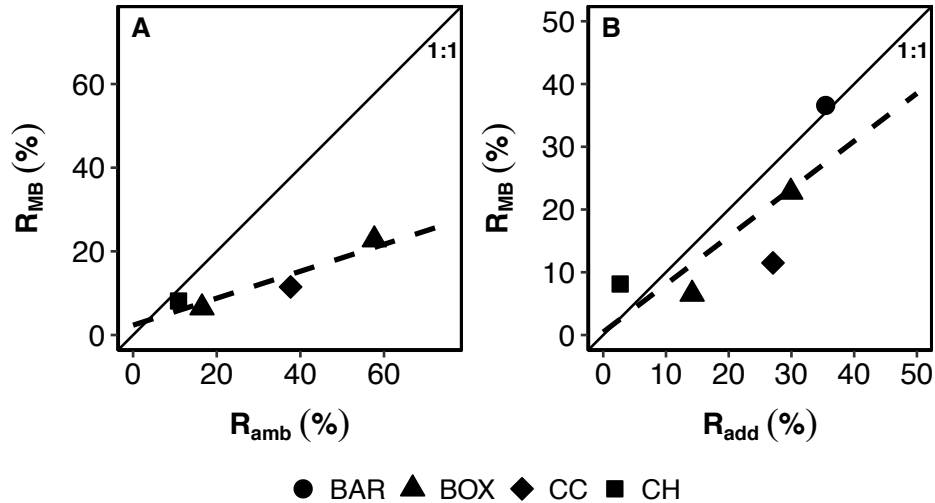
Figure 17. Comparisons of NO$_3$-N ambient mass balance removal (R$_{MB}$) and removal calculated from ambient uptake rates (R$_{calc}$) (A) as well as R$_{MB}$ and BTC-integrated removal (R$_{add}$). The dashed line represents the linear relationship between variables while the solid line is 1:1.

NO$_3$-N removal rates estimated from the ambient mass balance approach were significantly correlated with ambient mass balance removal of DOC, calculated in a manner similar to NO$_3$-N R$_{MB}$ (r^2 = 0.59, p = 0.006) (Figure 18). This relationship was largely driven by NO$_3$-N and DOC R$_{MB}$ from the BOX and CC sites. The highest rates of NO$_3$-N removal coincided with the highest rates of DOC production while NO$_3$-N production, resulting from nitrification, was likely to occur when DOC was removed. The greatest DOC removal (18.8%) and NO$_3$-N production (22.2%) occurred at the CC site while the greatest DOC production (16.8%) and NO$_3$-N removal (70.4%) was found to take place at the BOX site (note reporting of absolute values for production rather than the raw negative values). The two fall 2014 samples from the BOX site had very little change in either NO$_3$-N (1.4 – 6.5%) or DOC (-1.3 – 0.05%) while all samples from the CH site showed little change in both NO$_3$-N (-9.9 – 7%) and DOC (-3.4 – 1.4%).
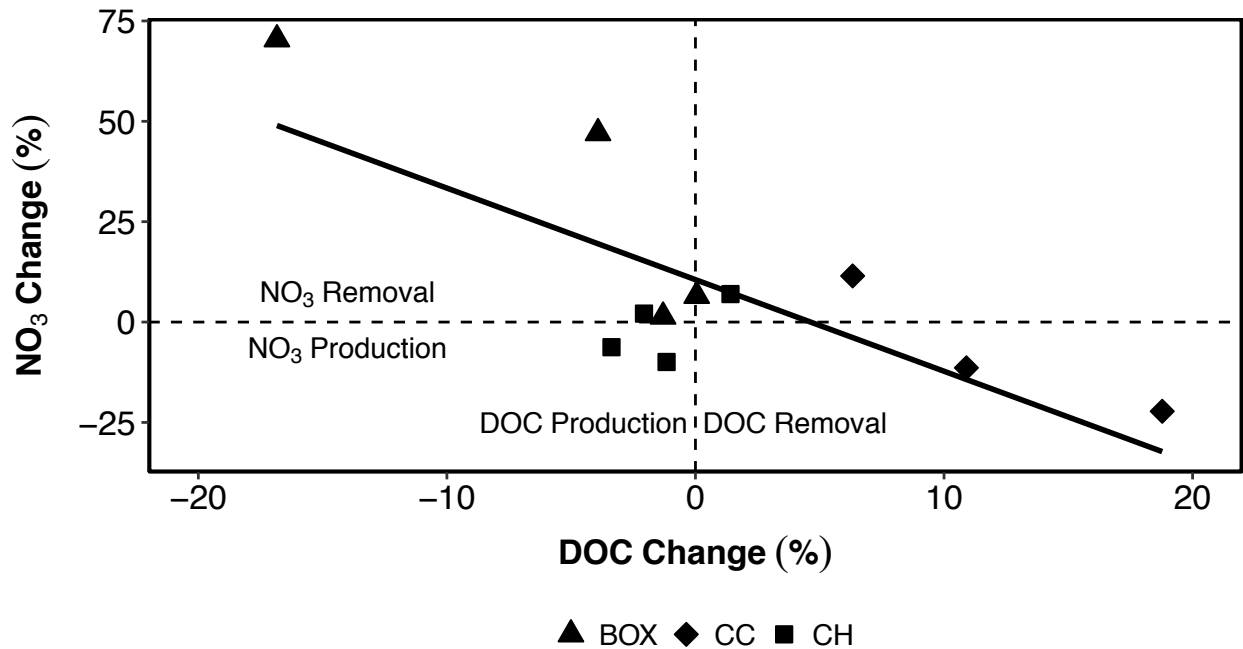
Figure 18. Relationship between ambient NO_3-N and DOC removal and production from the ambient mass balance approach. Dashed lines divide the plot area into quadrants signifying NO_3-N and DOC removal or production. The solid line represents the statistically significant linear relationship between change in NO_3-N and DOC.

Fluvial Wetland Metabolism

The Bayesian inverse modeling technique used for making metabolism estimates did a reasonable job of predicting the diel variation in observed DO concentrations with Nash-Sutcliffe Efficiency (E) values ranging from 0.69 for the BOX-1 experiment to 0.98 for the CH-2 experiment (Figure 19). This indicated that metabolism estimates from the model could be used to compare to NO_3-N uptake rates and removal. Estimates of daily average GPP and ER were made at each site for a total of 87 separate days, 86 of which had GPP:ER < 1, indicating that the fluvial wetlands were typically net heterotrophic.
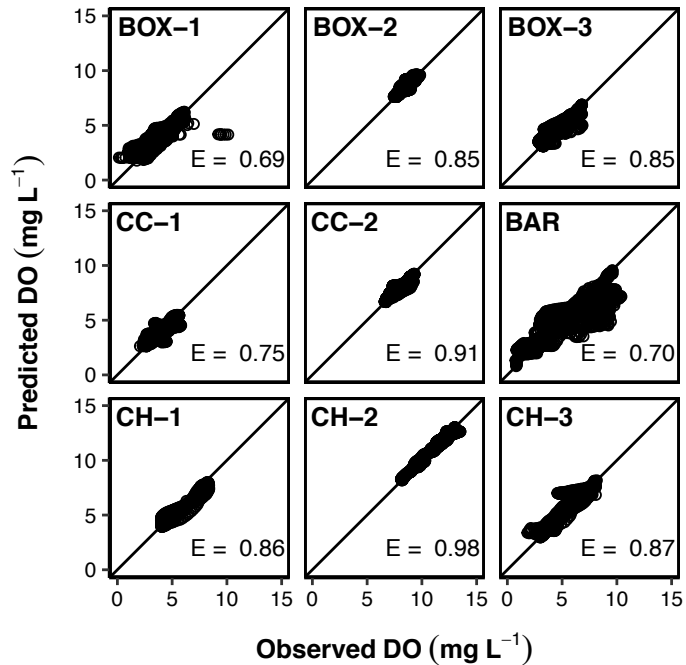
Figure 19. Predicted DO concentrations from the USGS 'streamMetabolizer' package for R plotted against observed DO concentrations. Nash-Sutcliffe Efficiencies (E) range from 0.69 to 0.98.

The variability in daily average metabolic rates within deployments was less than the variability between sites and seasons (Figure 20) so mean GPP and ER across each logger deployment was calculated to compare metabolism across sites and seasons (Table 10). Across all sites, metabolic rates were generally higher during the spring (mean GPP = 0.87 ± 0.1 g O_2 m^{-2} day^{-1}, mean ER = 5.33 ± 0.47 g O_2 m^{-2} day^{-1}) compared to the fall (mean GPP = 0.24 ± 0.03 g O_2 m^{-2} day^{-1}, mean ER = 2.90 ± 0.29 g O_2 m^{-2} day^{-1}). These seasonal differences in GPP and ER were statistically significant (Kruskal-Wallis: H = 27.815, p < 0.001; H = 12.73, p < 0.001, for GPP and ER, respectively). Reaeration rates were also significantly different across seasons (mean spring K = 4.70 ± 0.39 day^{-1}, mean fall K = 7.98 ± 1.02 day^{-1}) (Kruskal-Wallis: H = 6.38, p = 0.01).
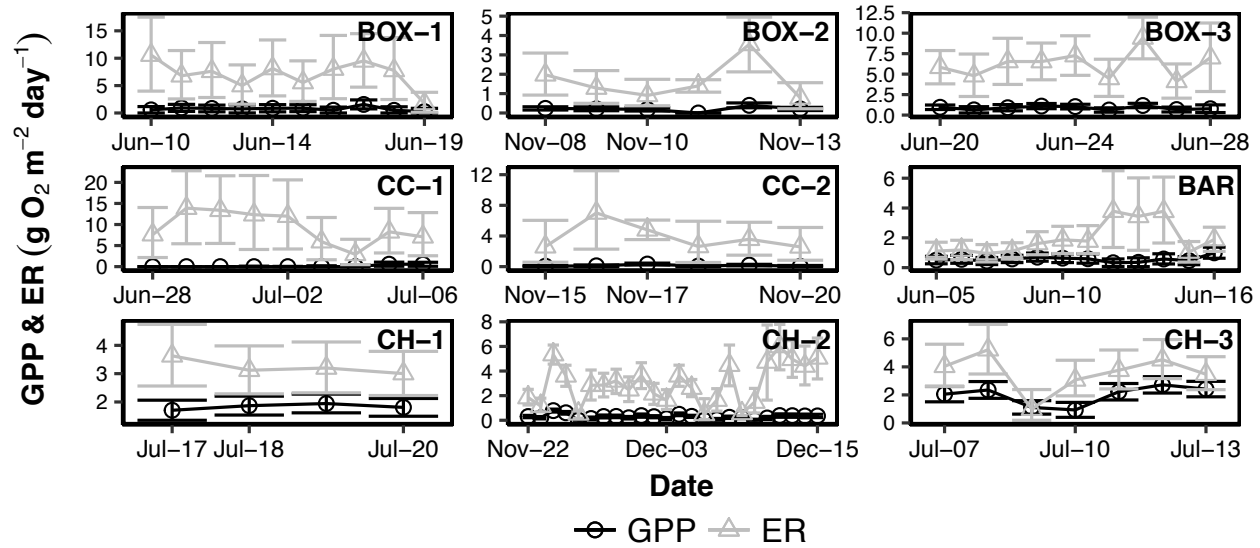
Figure 20. Metabolic rates (GPP & ER, g O_2 m^{-2} day^{-1}) for all complete days that DO and PAR loggers were deployed for each experiment.

Table 10. Metabolic rates (GPP, g O_2 m^{-2} day^{-1}; ER g O_2 m^{-2} day^{-1}) and mean reaeration rates (K, day^{-1}) across entire logger deployments associated with each experimental solute addition. Values for each deployment are the mean with the standard error in brackets.

Experiment	Deployment Dates	Mean GPP (g O_2 m^{-2} day^{-1})	Mean ER (g O_2 m^{-2} day^{-1})	Mean K (day^{-1})
BOX-1	6/10/14 - 6/19/14	0.76 [0.11]	7.07 [0.79]	7.81 [0.80]
BOX-2	11/8/14 - 11/13/14	0.21 [0.05]	1.65 [0.42]	3.43 [0.78]
BOX-3	6/20/15 - 6/28/15	0.87 [0.07]	6.22 [0.55]	6.08 [0.62]
CC-1	6/28/14 - 7/6/14	0.13 [0.08]	9.26 [1.27]	5.43 [0.64]
CC-2	11/15/14 - 11/20/14	0.14 [0.05]	3.86 [0.72]	4.33 [0.66]
BAR	6/5/15 - 6/16/15	0.56 [0.05]	1.96 [0.31]	3.31 [0.42]
CH-1	7/17/14 - 7/20/14	1.83 [0.05]	3.24 [0.14]	1.69 [0.17]
CH-2	11/22/14 - 12/15/14	0.28 [0.04]	2.96 [0.33]	10.02 [1.34]
CH-3	7/7/15 - 7/13/15	1.97 [0.26]	3.58 [0.51]	1.62 [0.20]

Across sites, mean GPP was lowest at CC (0.13 ± 0.05 g O_2 m^{-2} day^{-1}) and greatest at CH

(0.79 ± 0.14 g O_2 m^{-2} day^{-1}) while mean ER was lowest at BAR (1.96 ± 0.31 g O_2 m^{-2} day^{-1}) and

highest at CC (7.10 ± 1.06 g O_2 m^{-2} day^{-1}). These differences in metabolic rates were also

significantly different across sites (Kruskal-Wallis: H = 22.137, p < 0.001; H = 24.901, p < 0.001,

for GPP and ER, respectively). Site-wise differences in reaeration, however, were not

significantly different, with the lowest mean K occurring during the BAR deployment (3.31 ±

0.42 day^{-1}) and the highest mean K found for the CH deployment (7.39 ± 1.13 day^{-1}) (Kruskal-

Wallis: H = 6.757, p = 0.08).

Fluvial wetland metabolic rates from the days that solute additions were performed

were used to explore drivers of NO_3-N uptake and removal. Single-day rates were used rather

than means over the entire deployment for a more accurate representation of actual metabolic

conditions during the experiments (Figure 21). These single-day rates largely mirrored trends in

mean values over entire deployments with the lowest GPP occurring at both the CC-1 and BOX-

2 experiments (0 ± 0.03 and 0 ± 0 g O_2 m^{-2} day^{-1}, for CC-1 and BOX-2, respectively) and the

highest found for the CH-1 experiment (1.71 ± 0.35 g O_2 m^{-2} day^{-1}). ER was lowest during the

BAR experiment (1.78 ± 0.94 g O_2 m^{-2} day^{-1}) and highest for the CC-1 experiment (11.98 ± 8.20 g

O_2 m^{-2} day^{-1}). Daily average reaeration rates were found to be lowest during the CH-3

experiment 1.19 ± 1.05 day^{-1} while the highest reaeration was found for the CH-2 experiment

(8.8 ± 2.48 day^{-1}). Rates of GPP and ER were found to reside within the range of metabolic rates

found for channelized streams in Grand Teton National Park (GPP = 0.13 to 3.11 g O_2 m^{-2} day^{-1},

ER = 0.97 to 13.3 g O_2 m^{-2} day^{-1}) by Hall and Tank (2003). However, fluvial wetland reaeration

rates were lower than reaeration rates for these channelized reaches (K = 44.1 to 143.8 day^{-1}) (Hall and Tank 2003).
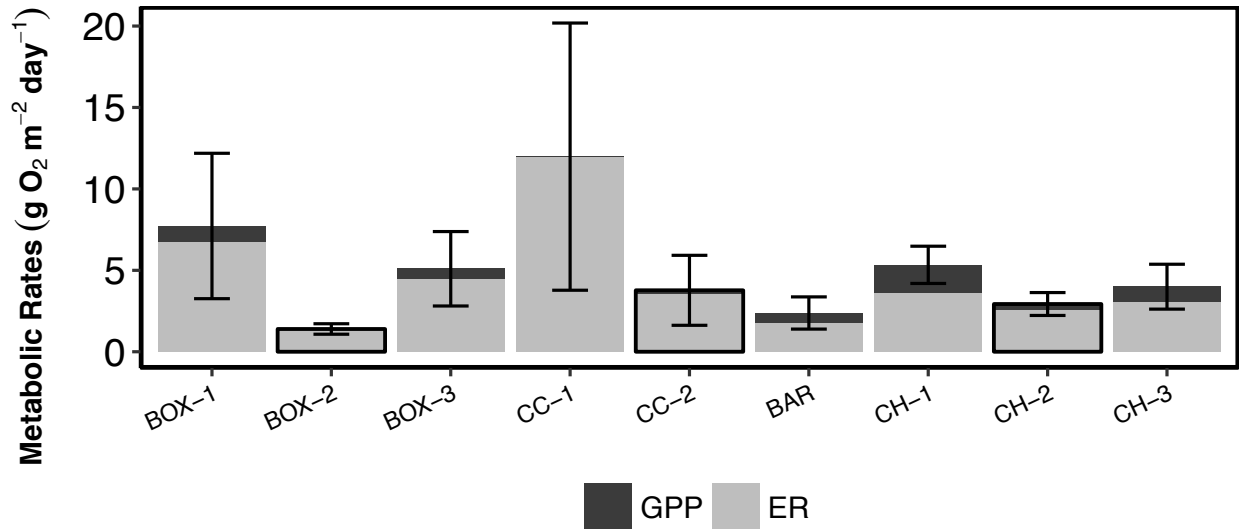
Figure 21. Total metabolic rates (GPP and ER, g O_2 m^{-2} day^{-1}) for all experiments. Dark grey bars represent GPP while light grey bars are ER. Error bars represent the fractional error associated with both GPP and ER. Fall deployments (BOX-2, CC-2. CH-2) are represented visually by bars with black borders while spring deployments lack borders.

BTC Decomposition

Fractions of added conservative solute in the advection/dispersion (AD) zones ranged from 0.16 for the CH-2 experiment to 0.85 for the CC-2 experiment while transient storage (TS) fractions ranged from 0.05 for CH-3 to 0.37 for BOX-3 (Figure 22). The BOX-3 experiment also exhibited the greatest proportion of conservative mass lost (0.97) while the lowest loss proportion was -0.07 for the CC-2 experiment. The negative mass loss value for the CC-2

experiment indicated greater recovery of the conservative solute than what was added and

may have been caused by uncertainties related to discharge measurements, sensor calibration,

or background correction of the conservative solute. The extremely high proportion of mass

lost for the BOX-3 experiment was likely due to an instrumentation error, therefore AD and TS

fractions for that experiment were calculated relative to the conservative mass recovered,

rather than mass injected. AD fractions were similar across seasons (Spring = 0.45, Fall = 0.50)

and differences were not statistically significant (Kruskal-Wallis: H = 0.067, p = 0.80) (Table 11).

Similarly, TS fractions were also alike between seasons (Spring = 0.22, Fall = 0.24) and were not

significantly different (Kruskal-Wallis: H = 0.267, p = 0.61). Proportions of mass lost were

greater in the spring, largely driven by the high-loss BOX-3 experiment (Spring = 0.49, Fall =

0.25) however, these differences were not statistically significant (Kruskal-Wallis: H = 1.067, p =

0.30).

Across sites, mean AD proportions ranged from 0.30 at BAR to 0.68 at CC while the

mean TS proportion was lowest at CC (0.19) and greatest at BOX (0.32) (Table 11). These

differences in TS and AD fractions, however, were not statistically significant (Kruskal-Wallis: H

= 6.489, p = 0.09; H = 4.622, p = 0.20, for the AD and TS fractions, respectively). Mean

proportions of mass lost at each site ranged from 0.13 at CC to 0.52 at CH (Table 11) and these

differences between sites were not statistically significant (Kruskal-Wallis: H = 5.389, p = 0.15).
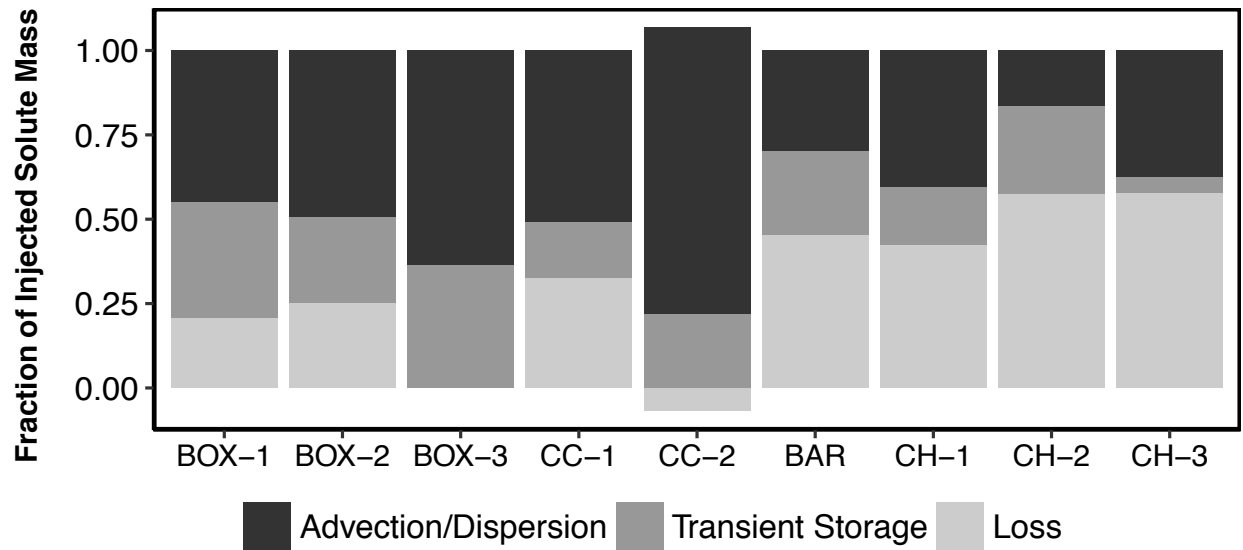
Figure 22. Proportions of recovered solute mass in either AD or TS components determined using the BTC-Decomposition method (Wlostowski et al. 2016). Light grey bars represent mass lost while dark grey and black bars represent the TS and AD fractions, respectively. No mass loss is shown for the BOX-3 experiment as recovered mass was only about 3%, necessitating the use of recovered mass in the calculation of the AD and TS fractions for that experiment.

Proportions of mass lost in fluvial wetlands were greater than the range of lost mass proportions for channelized reaches located on Alaska's North Slope (-0.11 to 0.14) (Wlostowski et al. 2016). The relatively high proportions of mass lost, while potentially affected by the aforementioned uncertainties, are possibly due to greater connectivity of the main channel to transient storage (TS). This increased connectivity to TS may retard the added conservative solute, with the resulting effect of outflow concentrations being below the detection limit of the sensor. As such, the proportions of mass lost may be indicative of the amount of connectivity between the main channel and transient storage. There was a weak negative

relationship between the fraction of mass lost with the TS fraction however this relationship was not statistically significant ($r^2 = 0.15$, $p = 0.35$) (Figure 23 A). Conversely, there was a strong significant negative relationship between the fraction lost and the AD fraction ($r^2 = 0.83$, $p < 0.01$), indicating that higher AD fractions coincided with less mass lost (Figure 23 B).

Table 11. Added conservative solute mass, recovered mass, and fractions of mass in AD and TS determined from the breakthrough curve decomposition method (Wlostowski et al. 2016). Also shown are Péclet numbers for each experiment and the Nash-Sutcliffe Efficiencies for the model fits used to determine AD and TS proportions. Due to the mass loss proportion for the BOX-3 experiment being extremely high, AD and TS proportions were calculated relative to mass recovered, rather than mass injected.

Experiment	Date	Mass Injected (g)	Mass Recovered (g)	Proportion AD [-]	Proportion TS [-]	Proportion Loss [-]	Pe [-]	Nash-Sutcliffe Efficiency
BOX-1	6/11/14	471.6	373.6	0.45	0.34	0.21	191.5	1.00
BOX-2	11/11/14	55.9	41.7	0.49	0.25	0.25	82.2	0.89
BOX-3	6/25/15	140.3	4.1	0.63	0.37	0.97	78.5	0.77
CC-1	7/2/14	25.7	17.3	0.51	0.16	0.33	25.0	0.93
CC-2	11/19/14	10.8	11.5	0.85	0.22	-0.07	31.4	0.84
BAR	6/11/15	33.0	18.0	0.30	0.25	0.45	65.6	0.90
CH-1	7/17/14	72.0	41.5	0.41	0.17	0.42	138.7	0.99
CH-2	12/5/14	66.1	28.1	0.17	0.26	0.57	105.7	0.99
CH-3	7/10/15	70.0	29.6	0.37	0.05	0.58	53.5	0.88
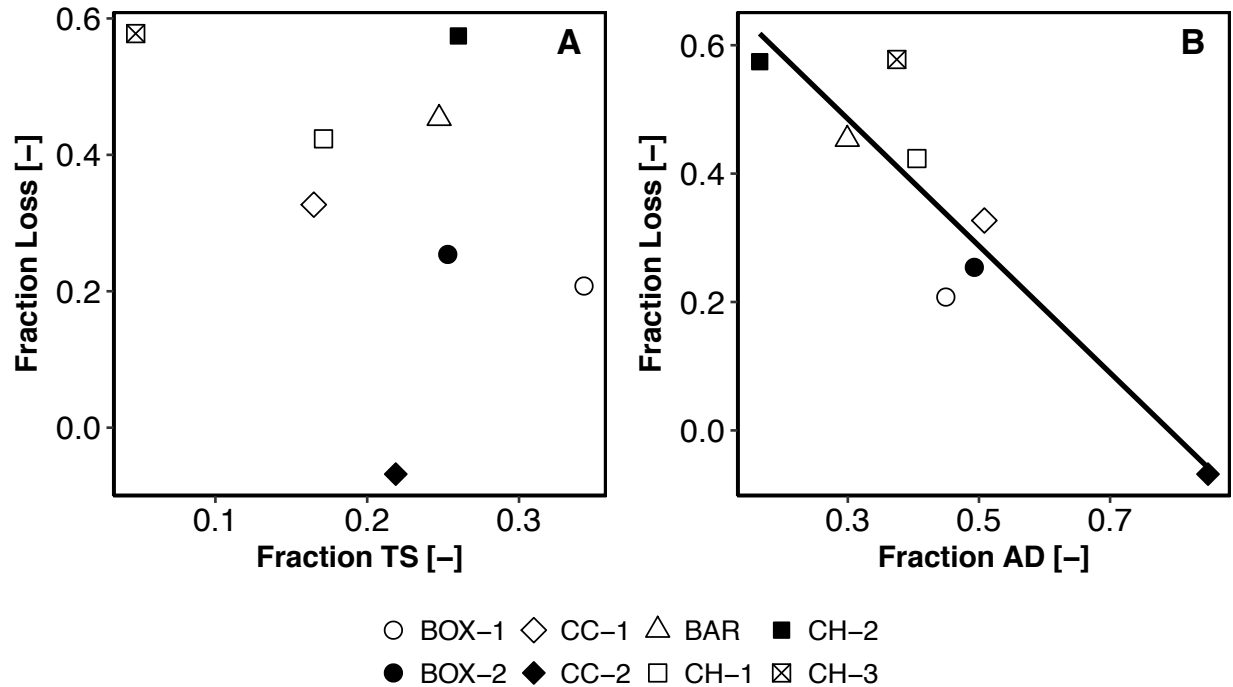
Figure 23. Fraction of mass lost vs. the TS fraction (A) and AD fraction (B). The relationship between the loss and AD fractions was statistically significant (p < 0.01).

Proportions of mass lost and mass in the TS and AD fractions were compared to discharge to evaluate whether discharge had any control on mass fractions. The TS fraction exhibited a generally negative relationship with discharge indicating that mass in the transient storage fractions decreased with increasing discharge (Figure 24 A). This relationship was not statistically significant (r^2 = 0.2, p = 0.22). When comparing the AD fraction to discharge, there were two different relationships with the BOX, BAR, and CC sites showing an increase in the AD fraction with increasing discharge while CH exhibited a decrease in the AD fraction with increasing discharge (Figure 24 B). The relationship for BOX, BAR, and CC was statistically significant (r^2 = 0.88, p < 0.01) while the relationship for CH alone was not significant (r^2 = 0.98,

p = 0.1). There was a similar, yet opposite division when comparing the fraction of mass lost to

discharge, with the lost fraction for BOX, BAR, and CC decreasing with increasing discharge and

CH showing an increase in the lost fraction relative to increasing discharge (Figure 24 C). Like

the AD fraction vs. discharge relationship, BOX, BAR, and CC had a significant relationship

between the lost fraction and discharge (r^2 = 0.82, p = 0.04) while the lost fraction at CH was

not significantly related to discharge (r^2 = 0.49, p = 0.51). The lack of a relationship between the

TS fraction and discharge notwithstanding, these results suggest that at BOX, BAR, and CC

higher discharges short circuited alternative flowpaths through the wetlands, resulting in less

conservative mass lost, while at the CH wetland, higher flows likely resulted in greater

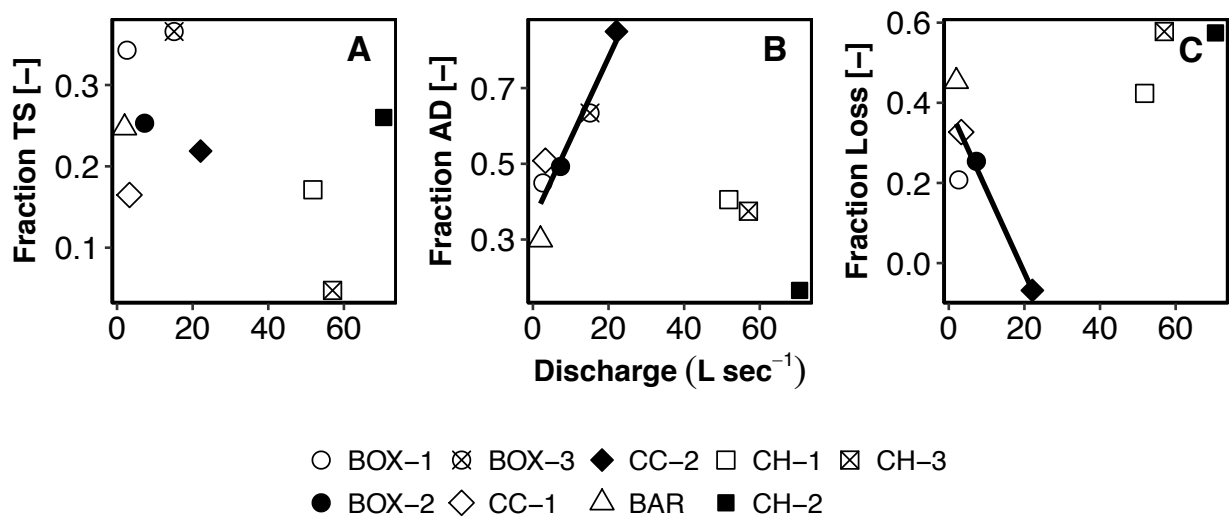connectivity with its floodplain and greater mass lost.

Figure 24. Conservative solute mass in TS (A), AD (B) and lost fractions (C) for each experiment

plotted against discharge. AD fractions for the BOX, BAR, and CC sites were significantly related

to discharge while mass lost fractions for BOX, BAR, and CC were significantly related to

discharge.

Hydrologic Parameters

Detention times (T_{det}) estimated from the conservative tracer BTC ranged from 1.27 to 11.71 hours with the BTC durations lasting from 1.92 to 28.1 hours (Tables 1 and 3). Mean T_{det} was shortest at CH (1.8 hours) and longest at CC (7.9 hours), but differences between sites were not statistically significant (Kruskal-Wallis: H = 5.711, p = 0.13). Mean T_{det} across all sites was generally higher in the spring (4.3 hours) compared to the fall additions (2.8 hours) however, similar to the site-wise comparison, seasonal differences were not statistically significant (Kruskal-Wallis: H = 0.6, p = 0.44). There was a negative relationship between T_{det} and discharge with the shortest detention times coinciding with the highest discharges (Figure 25). This relationship was not significant with the CC-1 experiment in the beaver pond included (r^2 = 0.3, p = 0.13), however, with that experiment omitted, the relationship becomes significant (r^2 = 0. 61, p = 0.02).

Hydraulic load, calculated as depth/T_{det}, ranged from 197.9 m yr^{-1} during the BAR experiment to 1869.3 m yr^{-1} for the CH-2 experiment. Mean spring hydraulic load was 639.5 m yr^{-1} while mean hydraulic load during the fall was 954.5 m yr^{-1}. Like T_{det}, there were no significant differences between hydraulic load across sites or seasons (Kruskal-Wallis: H = 6.511, p = 0.09; H = 0.6, p = 0.44, for the site-wise and seasonal comparisons, respectively). Hydraulic load was significantly related to discharge with hydraulic load increasing with increasing discharge (Figure 26). This suggests that an increase in depth or decrease in residence time resulted as discharge increased.
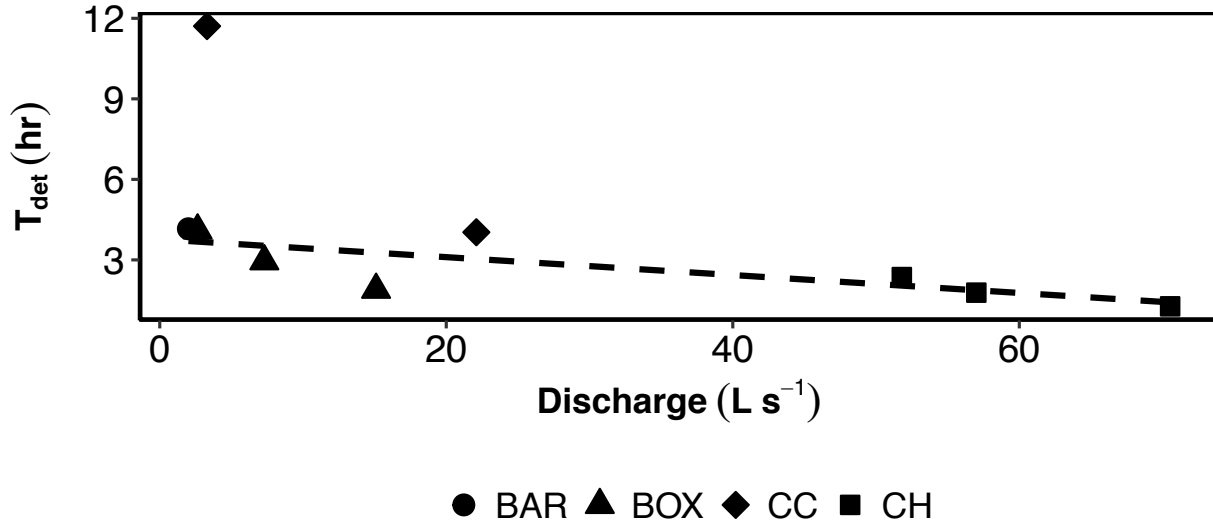
Figure 25. Relationship between detention time (T_{det}) and discharge for all nine solute addition experiments differentiated by site. Relationship was not significant with the inclusion of the CC-1 experiment however, with that experiment omitted, the relationship became significant.
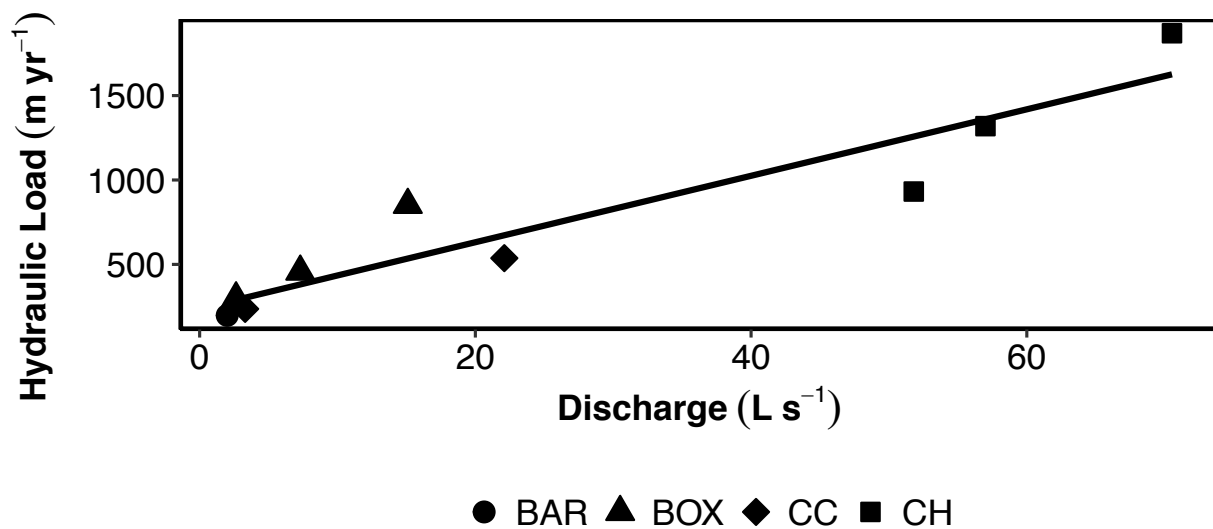
Figure 26. Relationship between hydraulic load, calculated as depth/T_{det}, and discharge for all nine solute addition experiments broken down by site. The solid line represents the significant linear relationship between the variables ($p < 0.001$).

Discharge was also found to have an effect on fluvial wetland dimensions. Wetted width had a weak relationship with discharge with widths generally increasing with increasing discharge (Figure 27 A). This relationship was not statistically significant (r^2 = 0.08, p = 0.45). Mean depth increased non-linearly with increasing discharge however this relationship, including the high-depth, low-discharge CC-2 experiment at the active beaver pond, was not significant (Figure 27 B). With the CC-2 experiment in the beaver-influenced reach omitted, this relationship between depth and discharge becomes significant (p < 0.001).

Figure 27. Mean wetted width (A) and mean depth (B) plotted against discharge measured the day of the solute addition. The relationship between mean wetted width and discharge was not significant and the mean depth vs. discharge relationship was significant with the CC-2 experiment at the active beaver pond omitted.

Controls of Ambient Nitrate Uptake and Removal

There was no clear relationship between $V_{f\text{-amb}}$ and either GPP or ER ($r^2 = 0$, $p = 0.95$; $r^2 = 0.06$, $p = 0.52$, for GPP and ER, respectively) (Figures 28 A, B). Similarly, BTC-integrated rem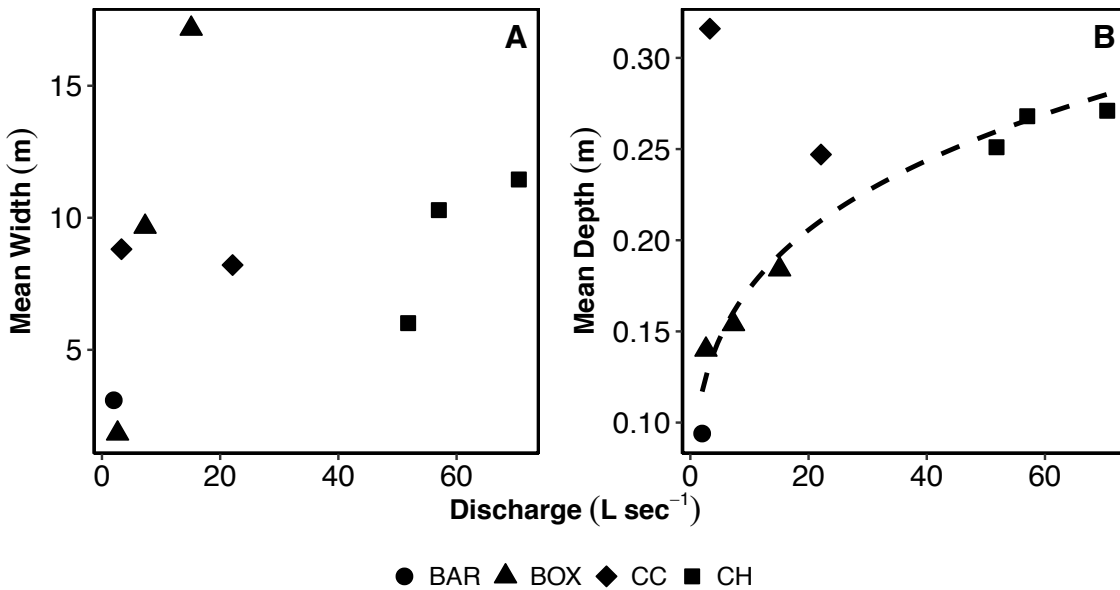oval (R_{add}) was not related to either GPP or ER either ($r^2 = 0.17$, $p = 0.28$; $r^2 = 0$, $p = 0.87$, for GPP and ER, respectively) (Figures 28 C, D). This suggests that metabolic activity was not the main driver of NO_3-N demand in these fluvial wetlands, contrary to findings for channelized reaches in Grand Teton National Park by Hall and Tank (2003).

There was a statistically significant positive relationship between $V_{f\text{-amb}}$ and ambient NO_3-N concentrations ($r^2 = 0.58$, $p = 0.02$) (Figure 29 A). This is counter to expectations that NO_3 uptake velocity declines with increasing concentrations in channelized streams (Mulholland et al. 2008), as well as during slug additions (Wollheim et al. 2014) (Figure 14). This relationship was driven by one point from the fall addition at CH (CH-2), suggesting that this pattern is not strong. With the CH-2 experiment omitted, the relationship becomes non-significant ($r^2 = 0$, $p = 0.85$), meeting expectations from literature and observations. There was no significant relationship between R_{add} and ambient NO_3-N, with or without the inclusion of the CH-2 experiment ($r^2 = 0.2$, $p = 0.23$; $r^2 = 0.3$, $p = 0.16$, with and without CH-2 included, respectively) (Figure 29 B).
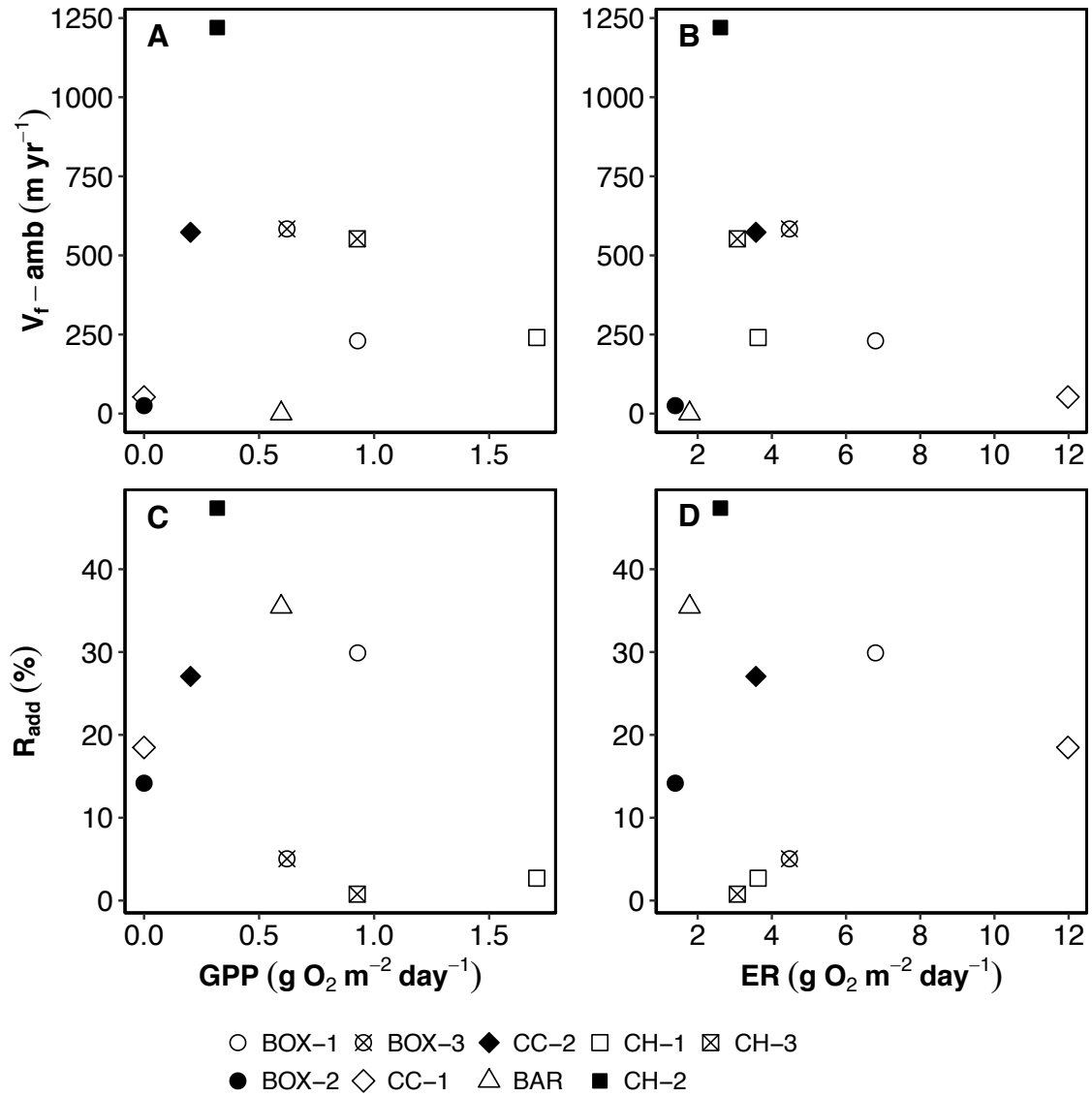
Figure 28. Ambient uptake velocity plotted against rates of GPP (A) and ER (B) as well as R_{add} vs. GPP (C) and ER (D).
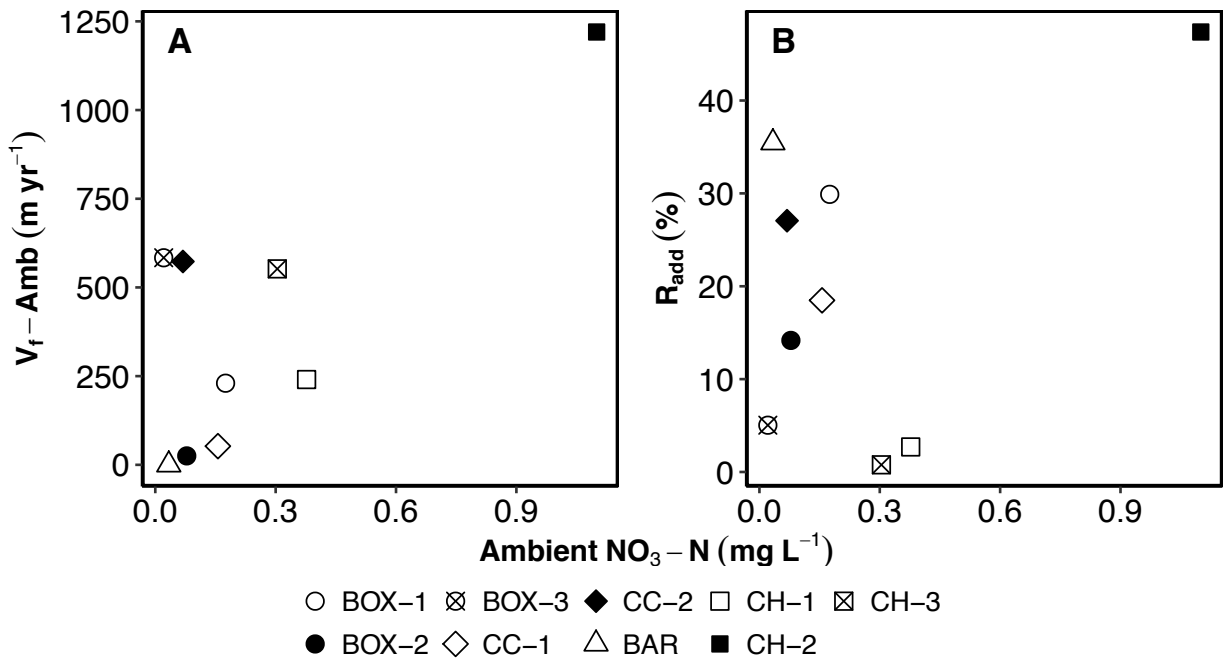
Figure 29. $V_{f\text{-amb}}$ (A) and R_{add} (B) plotted against ambient NO_3-N concentrations. $V_{f\text{-amb}}$ was significantly related to ambient NO_3-N using all data, however, with the CH-2 experiment excluded, the relationship became non-significant. There was no statistical significance between R_{add} and ambient NO_3-N with or without the inclusion of the CH-2 experiment.

Ambient uptake velocity declined with increasing detention time with the nonlinear relationship between $V_{f\text{-amb}}$ and T_{det} being statistically significant (p = 0.006) (Figure 30 A). The significance of this relationship was largely driven by two experiments, CC-1 (longest detention time with low $V_{f\text{-amb}}$) and CH-2 (shortest detention time and highest $V_{f\text{-amb}}$) with the remaining experiments falling in between. With the CC-1 and CH-2 experiments omitted, the relationship loses significance but the negative trend remains. R_{add} increased with increasing detention time (Figure 30 B) but this relationship was not significant (r^2 = 0, p = 0.87). With the CC-1 and CH-2

experiments excluded, the linear relationship between R_{add} and detention time becomes

significant (r^2 = 0.95, p < 0.001). Increasing detention times allowed for greater interaction

between inflowing waters with reactive surfaces within the wetlands, leading to lower ambient

uptake rates, however, due to the greater amount of time water spent within wetlands,

removal proportions were elevated.

Figure 30. Ambient uptake velocity (A) and removal (B) plotted against wetland detention time.

Solid lines represent the statistically significant relationships between V_{f-amb} and T_{det} including
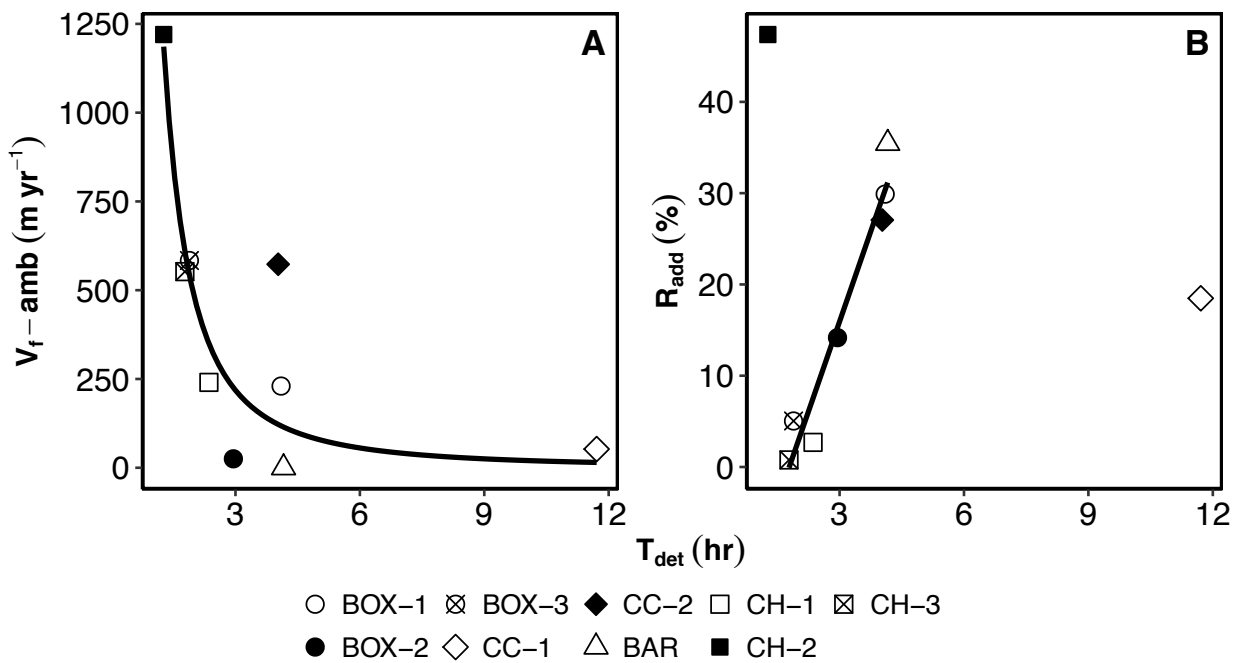
all experiments as well as between R_{add} and T_{det} with the CC-1 and CH-2 experiments omitted.

Similar to metabolic processing, there was no significant relationship between $V_{f\text{-amb}}$ and the TS fraction ($r^2 = 0$, $p = 0.88$) (Figure 31 A). There was, however, a statistically significant negative, nonlinear relationship between $V_{f\text{-amb}}$ and the AD fraction ($p = 0.04$), driven largely by the high ambient uptake velocity found for the CH-2 experiment (Figure 31 B), indicating that ambient uptake velocities declined with increasing AD fractions. With the CH-2 experiment omitted, however, this statistical significance disappears ($p = 0.14$). R_{add} was found to increase with increasing TS fraction but this relationship was not significant ($r^2 = 0.14$, $p = 0.33$) (Figure 31 C). There was a significant nonlinear relationship between R_{add} and the AD fraction ($p = 0.05$) with R_{add} decreasing with increasing AD fraction (Figure 31 D). These results indicate that, although the relationships between the TS and AD fractions and $V_{f\text{-amb}}$ were not strong, as the proportions of AD increase, reducing connectivity to the reactive surfaces in the TS zones, ambient uptake rates decline. The relative proportions of TS and AD had a greater effect on removal compared to uptake with more removal taking place during additions with higher TS and lower AD fractions. This suggests hydrology had a strong impact on fluvial wetland NO_3-N removal.

There was a statistically significant positive relationship between $V_{f\text{-amb}}$ and discharge ($r^2 = 0.56$, $p = 0.02$) (Figure 32 A). R_{add} tended to decline with increasing discharge but this relationship was not significant using all data points ($r^2 = 0$, $p = 0.91$) (Figure 32 B). However, with the CH-2 experiment omitted, the relationship gains significance ($r^2 = 0.54$, $p = 0.04$). Higher discharges led to greater wetted widths and mean depths (Figure 27), increasing connectivity with reactive zones and thus, potentially greater uptake rates. Detention times were lower at higher discharges (Figure 25), reducing the amount of time inflowing water spent

within fluvial wetlands. Despite the elevated uptake velocities, the net effect of increasing

discharge appears to be a reduction in the proportion of nitrate removed.
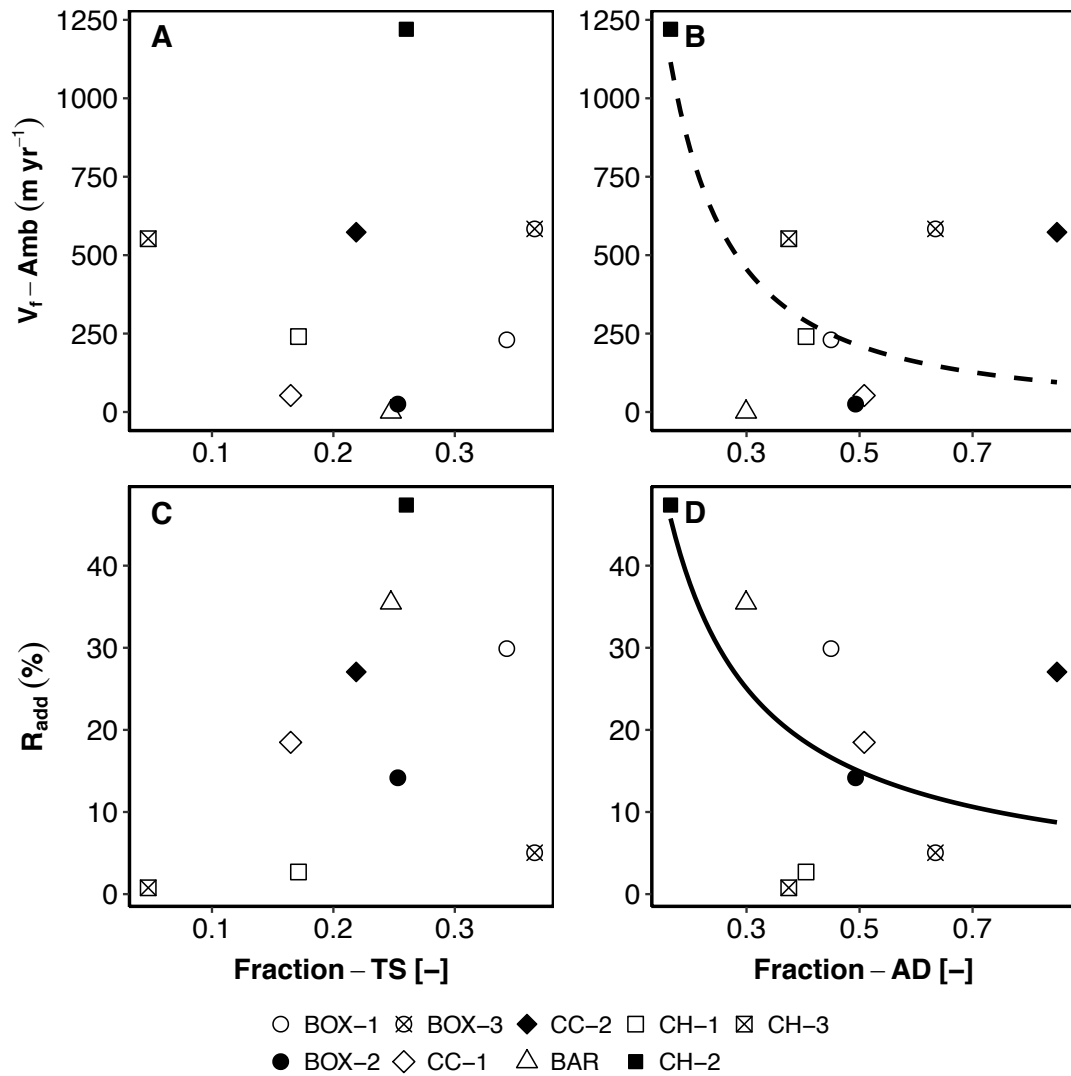
Figure 31. Ambient uptake velocity plotted against fractions of TS (A) and AD (B) as well as

removal plotted against fractions of TS (C) and AD (D) experienced during the solute additions.

The dashed line in Figure 31 B represents the conditionally significant relationship between $V_{f\text{-}amb}$ and the AD fraction with the CH-2 experiment included. The solid line in Figure 31 D

represents the significant relationship between R_{add} and the AD fraction.
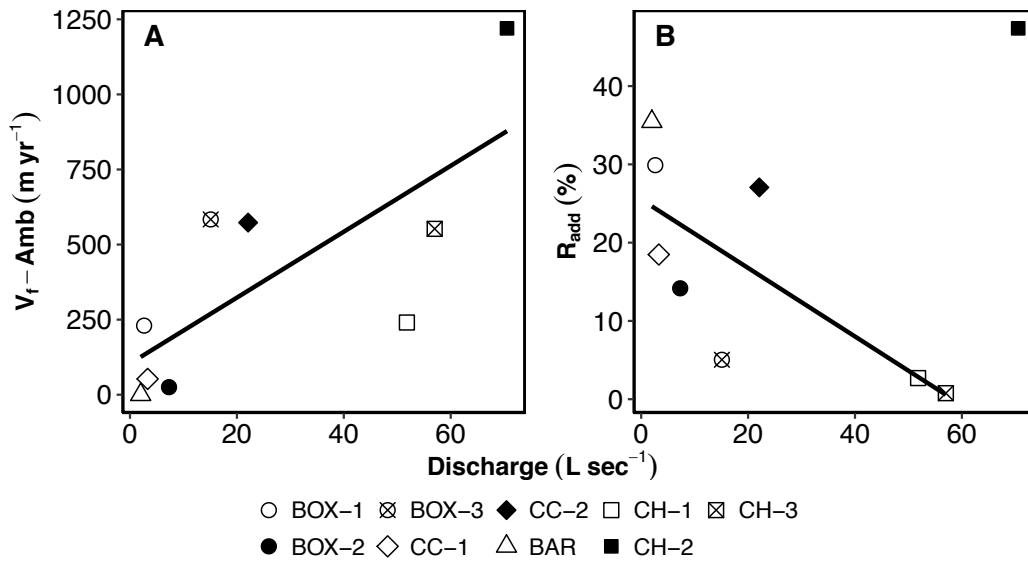
Figure 32. Ambient uptake velocity (A) and removal (B) plotted against discharge. The solid lines represent the statistically significant linear relationships between the independent variables and discharge. The relationship between R_{add} and discharge was only significant with the omission of the CH-2 experiment.

$V_{f\text{-amb}}$ increased with increasing mean wetted width, however, this relationship was not statistically significant (r^2 = 0.26, p = 0.16) (Figure 33 A). $V_{f\text{-amb}}$ also increased with increasing mean depth, however, this relationship also lacked significance (r^2 = 0.18, p = 0.26) (Figure 33 B). However, with the spring 2014 experiment at the beaver influenced CC reach excluded, the relationship becomes significant (r^2 = 0.52, p = 0.04). As wetted widths increase, inflowing water comes into greater contact with riparian soils, leading to elevated demand for NO_3-N. Greater depths may result in lower DO concentrations at the sediment-water interface, enhancing denitrification rates and therefore, increasing the demand for NO_3-N. There were negative relationships between R_{add} and both mean wetted width and mean depth and like $V_{f\text{-}}$

$_{amb}$, neither of these relationships were statistically significant ($r^2 = 0.11$, $p = 0.37$; $r^2 = 0.04$, $p =$ 0.62, for mean wetted width and mean depth, respectively) (Figure 33 C, D). While increases in mean wetted width and depth coincided with increasing discharge, detention times decreased with increasing discharge. This likely drove the decrease in NO_3-N removal, despite the increasing uptake velocities, as inflowing water spent less time within fluvial wetlands, reducing the likelihood that NO_3-N would be either assimilated or denitrified.
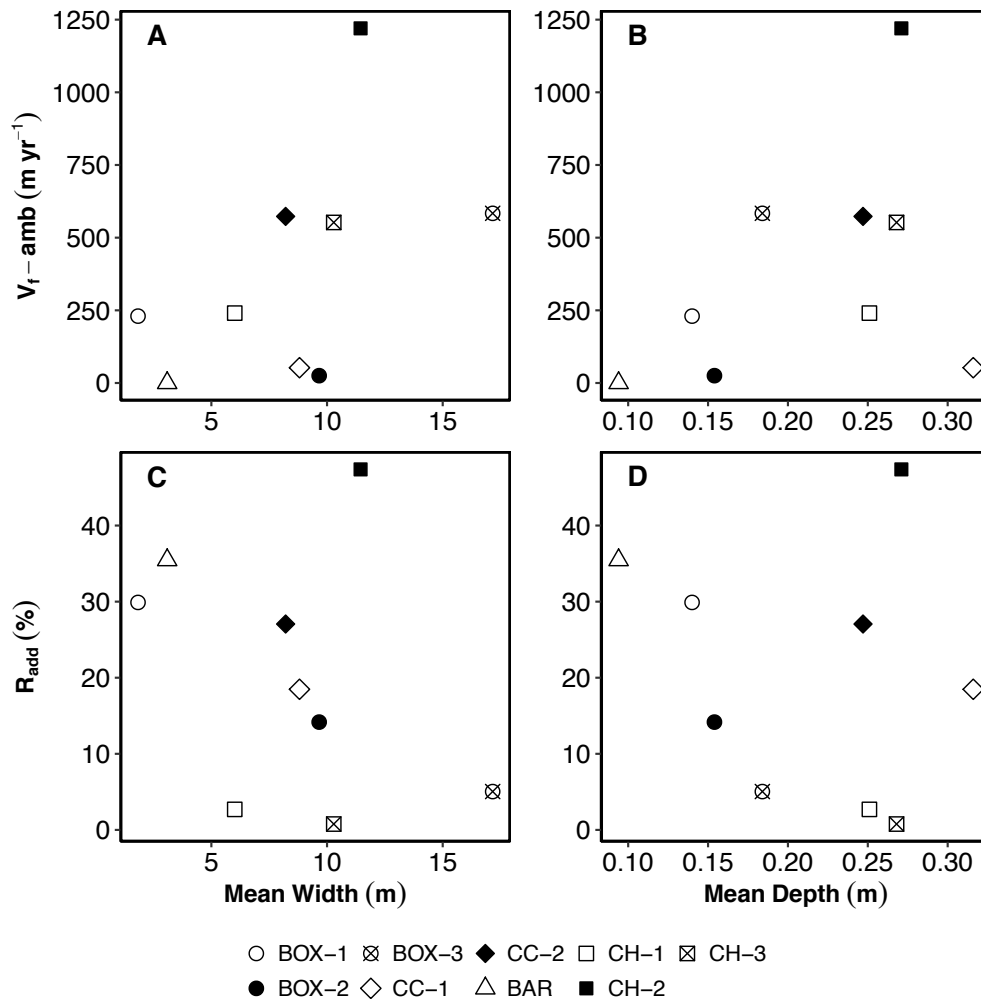
Figure 33. Ambient uptake velocity vs. mean wetted width (A) and mean depth (B) as well as R_{add} vs. mean wetted width (C) and mean depth (D). None of the relationships were significant.

There was a significant, positive relationship between V_{f-amb} and hydraulic load ($r^2 =$ 0.76, p = 0.002) (Figure 34 A). R_{add} declined with increasing hydraulic load but this relationship was not significant due to the high-removal, high-hydraulic load CH-2 experiment ($r^2 = 0$, p = 0.92). With the CH-2 experiment omitted, the linear relationship between R_{add} and hydraulic load becomes significant ($r^2 = 0.73$, p = 0.007) (Figure 34 B). The negative trend was similar to the relationship found by Seitzinger et al. (2006), with fluvial wetlands falling within the lower portion of the range that included estuaries, river reaches, lakes, and the continental shelf.
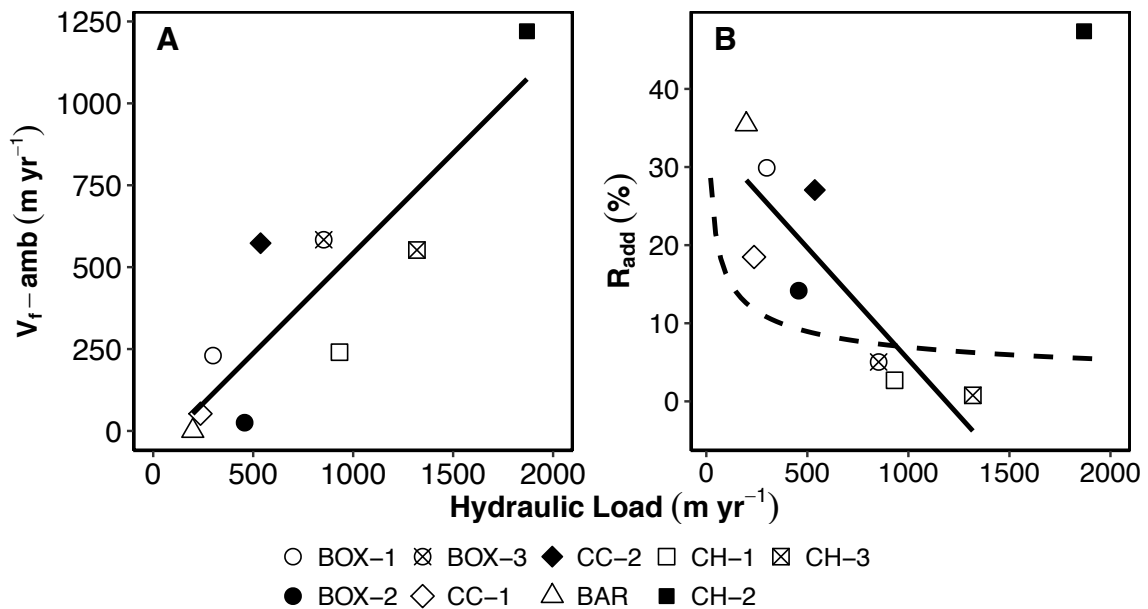
Figure 34. V_{f-amb} (A) and R_{add} (B) plotted against hydraulic load. The solid lines represent the significant, linear relationships between variables. The R_{add} vs. hydraulic load relationship was only significant with the omission of the CH-2 experiment. The dashed line in Figure 34 B represents the power function found by Seitzinger et al. (2006) relating nitrogen removal to hydraulic load.

Other univariate comparisons indicated that there were no clear relationships between either V_{f-amb} or R_{add} with mean daily fluvial wetland PAR, DO, or water temperature during the days that solute additions were performed. Similarly, there were also no discernable relationships between V_{f-amb} or R_{add} with other constituents in the matrix including phosphate, ammonium, sulfate, chloride, bromide, DOC, total dissolved nitrogen, or dissolved organic nitrogen.

Discussion

Sensor vs. Grab Sample Approach in Fluvial Wetlands

We applied a dynamic approach for estimating nutrient spiraling parameters, based on tracking a nutrient slug, to fluvial wetlands. This method, developed in channelized streams, was preferable over a plateau, or steady-state approach, which can be unfeasible in longer residence time and high-volume systems. The use of an in situ NO_3-N sensor in conjunction with the slug additions to estimate spiraling metrics had not been previously described before this study. Historically, laboratory analyzed grab samples were the only approach. However, grab samples are subject to uncertainty in laboratory analyses, sample collection and storage, as well as matrix effects (Hanafi et al. 2007). It is also more difficult to determine when to time the collection of grab samples during the BTC in fluvial wetlands. Increases in electrical conductivity that signal the arrival of the nutrient slug are less pronounced due to the dilution of the added salts by the large volume of water present, leading to the possibility that portions of the BTC may not be sampled. Grab samples are also collected less frequently than the sampling intervals possible with an in situ sensor. Advantages of using the sensor include high temporal

resolution data collected at intervals as small as one minute, continuous data collection throughout the entire BTC, and the benefit of greatly reducing uncertainty in sample collection and storage. The sensor data does, however, require calibration to laboratory analyzed grab samples in order to be accurate, introducing potential uncertainties. Sensors are also subject to unique circumstances such as biological fouling, mishaps during deployment that may hinder data collection, as well as similar matrix effects experienced by grab samples. Despite these caveats, the benefits of using the sensor far outweigh the disadvantages.

Slug additions have been reported to reveal hysteresis in uptake along the rising and falling limbs of the BTC (Covino et al. 2010, Gibson et al. 2015, Trentman et al. 2015). Hystereses were not always apparent during fluvial wetland solute additions in grab sample results but were exposed in the high frequency sensor data (e.g. Figure 12). These differences in uptake rates along the rising and falling limbs are believed to represent uptake occurring at the sediment-water interface in the main advective portion of the stream and within transient storage zones, respectively (Gibson et al. 2015). Unlike previously studies where greater uptake has been observed on the falling limb (i.e. Covino et al. 2010, Gibson et al. 2015, Trentman et al. 2015, Day and Hall 2017), the fluvial wetlands of this study generally show greater uptake on the rising limb of the BTC. This suggests that the main channel in fluvial wetlands may be more reactive than the transient storage zones.

Potential differences in reactivity on the rising and falling limbs were explored by comparing dynamic areal uptake rates (U) to changing light conditions in the wetland sidepools at matching timestamps. U was significantly, positively related to PAR for the spring 2014 additions at BOX and CC (r^2 = 0.94, p < 0.001; r^2 = 0.18, p = 0.002, for BOX-1 and CC-1,

respectively) as well as the spring 2015 addition at BAR (r^2 = 0.56, p < 0.001) (Figure 35). As PAR

data were collected at 15-minute intervals, compared to the uptake metrics which were

calculated from 1 minute interval data, this reduced the number of points for making a

meaningful comparison, particularly in the short duration experiments at CH. Similarly, as rising

limbs were shorter than falling limbs, there were fewer rising limb points to compare.

There was also a temporal pattern in the $U_{tot-dyn-TT}$ vs. PAR relationships with points

along the rising limb, at the beginning of the experiments, coinciding with the highest PAR for

the BOX-1 and CC-1 experiments (Figure 35). Conversely, at BAR, the rising limb points occur at

the low end of the range in PAR during the earlier part of the experiment. This suggests that for

the BOX-1 and CC-1 experiments, the rising limb of the BTCs experienced greater PAR, whereas

the BAR experiment encountered the greatest PAR during the falling limb of the BTC. As PAR is

the main driver of biological processes, reactivity was likely greater during the rising limbs for

the BOX-1 and CC-1 experiments while the falling limb of the BAR experiment experienced a

more reactive fluvial wetland. Thus, the observed hysteresis patterns were not necessarily the

result of less reactivity in the STS compared to the main channel, rather, the patterns arose

from the timing of the experiments, the orientation of the wetland relative to the path of the

sun, and shading from riparian vegetation, affecting when each wetland was most reactive.
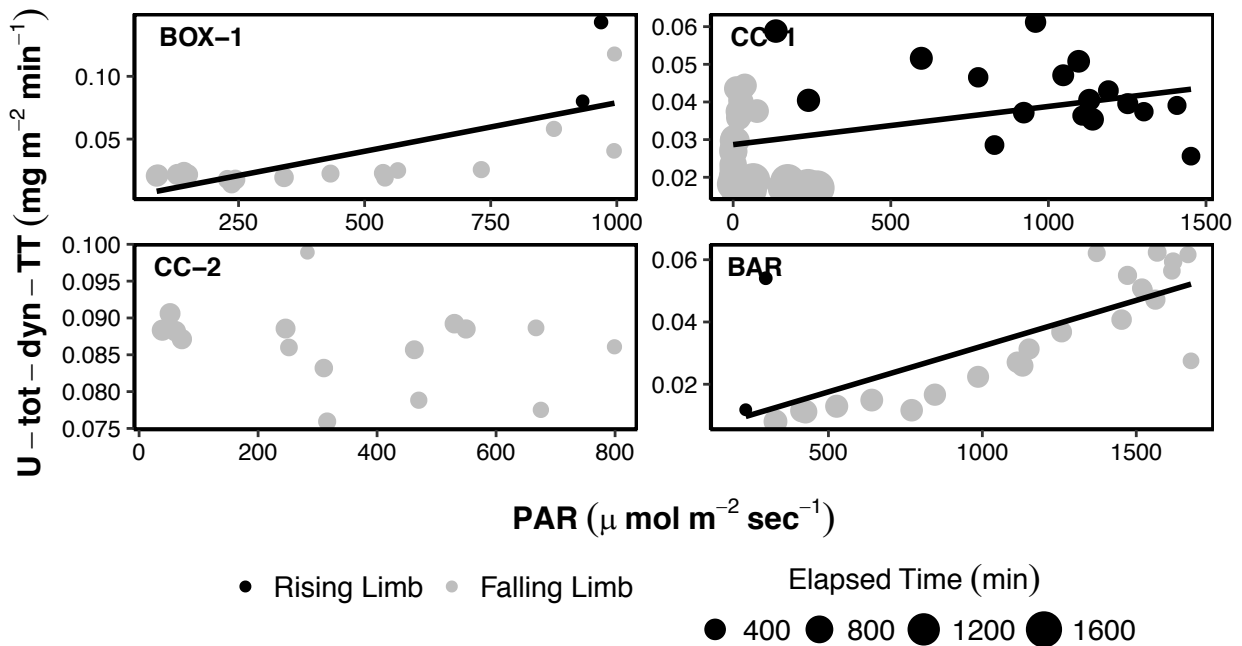
Figure 35. $U_{tot-dyn-TT}$ vs. PAR relationships for the four experiments with greater than four matching timestamps in both the sensor data-calculated uptake metrics and the 15-minute interval PAR data. Solid lines represent the statistically significant linear relationships between the variables.

Comparison of Channel and Fluvial Wetland Uptake and Removal

There are a number of studies that have examined nitrogen uptake and removal in streams as well as wetlands. Mulholland et al. (2008) found that across 72 channelized stream reaches in eight different biomes, total NO_3-N uptake velocities, measured using a stable isotope technique, ranged from no detectable uptake to 9381.1 m yr^{-1}. For the channelized streams in the Parker and Ipswich River watersheds only, Mulholland et al. (2008) found uptake velocities ranging from no detectable uptake to 437 m yr^{-1}, lower than the range of uptake velocities found for fluvial wetlands in northeastern Massachusetts (-170.6 to 1220 m yr^{-1}).

Rodríguez-Cardona et al. (2016) found ambient uptake velocities in the Lamprey River watershed in southeastern New Hampshire ranging from -904 to 51,829.4 m yr^{-1} across 18 solute addition experiments performed in 4 different forested headwater channelized stream reaches. The greatest ambient uptake velocities found by Rodríguez-Cardona et al. (2016) occurred in a channelized reach downstream of a fluvial wetland where ambient NO_3-N concentrations were low and DOC concentrations were relatively high, suggesting that the wetland impacted reach had greater demand for NO_3-N than the reaches lacking fluvial wetlands.

Rodríguez-Cardona et al. (2016) also found negative ambient uptake for one experiment from kinetics that indicated uptake, similar to the experiment at the BAR fluvial wetland. These negative uptake metrics can result from N saturation (O'Brien et al. 2007), not enough added solute to sufficiently increase background concentrations above ambient (Rodríguez-Cardona et al. 2016), or high discharge leading to infinitely high uptake metrics (Hall and Tank 2003). In long residence time systems such as fluvial wetlands, it is also possible that trending background concentrations in either the conservative or reactive solute can have an effect on uptake metrics.

In fluvial wetland STS patches, Wollheim et al. (2014) found NO_3-N uptake velocities estimated from an efficiency loss function that ranged from 171 to 7,862 m yr^{-1}. The upper end of the range in fluvial wetland STS patches found by Wollheim et al. (2014) is greater than ambient uptake velocities found for fluvial wetlands measured at the whole ecosystem scale, however the maximum uptake velocity experienced during the solute addition experiments in fluvial wetlands in this study was 10,700.6 m yr^{-1}, occurring at the beginning of the CH-2 BTC

when NO_3-N concentrations were closest to ambient. While uptake rates in fluvial wetlands

have been found to be, in some cases, higher than those in channelized reaches, hydrologic

connectivity between the main channel and STS can limit N sources, reducing net uptake.

Powers et al. (2012) found higher uptake velocities for channelized subreaches compared to

wetland subreaches and attributed this to a lack of connectivity between N sources and sinks.

Thus, the role of fluvial wetland reaches in terms of contributions to network-scale N retention

depends not only on uptake rates within the wetland, but also the delivery of high N water to

those wetlands.

Controls of V_f in Fluvial Wetlands

Measured independent biological variables (GPP, ER), were not found to drive ambient

uptake velocities in fluvial wetlands. In low ambient N channelized streams in Wyoming, GPP

was found to be a strong indicator of nitrate uptake velocity (Hall and Tank 2003), with GPP

explaining about 75% of variability in nitrate V_f. However, in fluvial wetlands, metabolic rates

were not found to be good predictors of nitrate V_f with 0% and 6% of variability in V_{f-amb}

explained by GPP and ER, respectively (Figure 28). Mulholland et al. (2001) did not find a strong

relationship between nitrate V_f and whole system metabolic parameters which Hall and Tank

(2003) attributed to low variability in nitrate V_f as well as the large distance between study

streams in 8 different biomes, resulting in latent variables exhibiting control on V_f. As the fluvial

wetlands in this study were all within the same region, latent variables resulting from the

distance between sites (e.g. differences in climate, elevation, geology, etc.), were not a factor in

explaining drivers of NO_3-N uptake velocity. Rather, low variability in the range of uptake

velocities may explain the lack of a relationship between metabolic parameters and V_f. The

NO_3-N V_f coefficient of variability (CV) in the Hall and Tank (2003) study was 1.41 while the CV

for NO_3-N V_f in fluvial wetlands was 1.02, closer to the NO_3-N V_f CV of 0.99 found by Mulholland

et al. (2001). This means that although we found that metabolic parameters were not good

predictors of NO_3-N V_f, the range in V_f was too small to definitively rule out metabolism as a

driver of uptake.

Rodríguez-Cardona et al. (2016) found no link between ambient NO_3-N uptake velocity

and the physiochemical parameters that control stream metabolism (PAR, water temperature,

DO). They concluded that, as forested streams are typically net heterotrophic, it was unlikely

that autotrophic processes would drive NO_3-N uptake and rather, stream chemistry, specifically

DOC concentrations, can possibly control NO_3-N uptake. Taylor and Townsend (2010) found a

consistent negative, non-linear relationship between organic carbon and NO_3-N concentrations

across a range of ecosystems from inland waters to open oceans, with the highest NO_3-N

concentrations coinciding with the lowest organic carbon concentrations. They found that

carbon limitation drove NO_3-N accrual across ecosystems, which could then be exacerbated by

nitrification. DOC concentrations in the fluvial wetlands included in this study ranged from 2.9

to 8.8 mg L^{-1}, with the highest DOC concentrations significantly corresponding with the lowest

NO_3-N concentrations ($p < 0.001$), lending support to this conclusion that high DOC may drive

NO_3-N uptake.

While neither metabolism nor the variables regulating metabolism were found to exert

control on biological uptake of NO_3-N in fluvial wetlands, hydrological variables were found to

affect ambient NO_3-N V_f. Uptake velocities in fluvial wetlands increased with both increasing

discharge and increasing hydraulic load but decreased with increasing detention time (Figures 32, 34, 30). Hydraulic load depends on both depth and residence time, therefore an increase in depth or a decrease in residence time (as detention time) resulted in an increase in $V_{f\text{-amb}}$ (Figures 30, 33). Discharge affected both depth and detention time with an increase in discharge resulting in increased depth but also a decrease in detention time (Figures 25, 27), driving the changes in hydraulic load (Figure 26). With increasing depth, benthic DO concentrations are likely to decrease, enhancing denitrification (Wollheim et al. 2014) and reach-scale NO_3-N uptake rates. Powers et al. (2012) found a decrease in uptake efficiency along the transition from lotic to lentic, (i.e. increasing residence time), resulting in a tradeoff between uptake efficiency and residence time. Increases in fluvial wetland residence time resulted in lower hydraulic loads and therefore, lower $V_{f\text{-amb}}$, consistent with this tradeoff suggested by Powers et al. (2012).

While biological controls were expected to drive biological NO_3-N uptake, neither GPP, ER, nor drivers of GPP and ER (PAR, water temperature) exhibited strong relationships with $V_{f\text{-amb}}$. Hydrological factors however, did relate to biological NO_3-N uptake. An increase in discharge, affecting both depth and detention time, was found to result in an increase in fluvial wetland NO_3-N demand. This was likely due to a larger hypoxic zone at the sediment-water interface leading to increased denitrification (Wollheim et al. 2014) despite increased residence times that resulted in lower NO_3-N uptake efficiency (Powers et al. 2012). In fluvial wetlands, hydrological factors drove biological uptake, however, it is likely that hydrology affected other latent biological variables that were not considered in this study, therefore controlling uptake rates.

Controls of Removal in Fluvial Wetlands

Control of fluvial wetland NO_3-N removal, like ambient uptake velocity, was dominated by hydrological factors including detention time, hydraulic load, and discharge. With the experiment with both the highest hydraulic load and greatest NO_3-N removal excluded (CH-2), hydraulic load was found to be a strong predictor of removal (r^2 = 0.73, p < 0.05) (Figure 34 B). Seitzinger et al. (2006) and Heffernan et al. (2010) found hydraulic load to be a good predictor of NO_3-N removal for a wide range of aquatic habitats including rivers, lakes, and estuaries. The fluvial wetlands in this study fall within the higher range of hydraulic loads considered by Seitzinger et al. (2006) (197.9 to 1869.3 m yr^{-1}) as well as within the lower half of the removal estimates (0.8 to 47.4%) but fall along the relationship between removal and hydraulic load described by Seitzinger et al. (2006) (Figure 34 B).

When the fluvial wetland experiments with the longest and shortest detention times were excluded, detention time was also found to be a strong predictor of NO_3-N removal (r^2 = 0.95, p < 0.001) (Figure 30 B), also similar to findings by Seitzinger et al. (2006). Detention time is a variable used in calculating hydraulic load so the similarly close relationships between residence time and hydraulic load with removal were expected to be present. Finally, discharge was also found to be a strong predictor of NO_3-N removal when the highest discharge experiment (CH-2) was omitted (Figure 32 B). Discharge was found to control both detention time and hydraulic load (Figures 25 and 26) as well as affected both fluvial wetland width and depth (Figure 27), therefore, changing discharge was likely to have a substantial impact on NO_3-N removal.

Comparison of Fluvial Wetland and Stream Channel Removal

As removal integrates the effects of biological uptake of NO_3-N as well as hydrological effects, specifically residence or detention time, we determined the relative importance of both biology and hydrology using a modeled hypothetical reach with different biological and hydrological parameters for both channelized stream reaches and fluvial wetland stream reaches. The model used the removal equation modified from Wollheim et al. (2006, Equation 1):

$$R = 1 - \exp\left(-\frac{V_f L w}{Q}\right) * 100 \qquad\qquad \text{Equation 18}$$

where R is removal (%), V_f is uptake velocity (m yr^{-1}), L is reach length (m), w is mean channel/wetland width (m), and Q is discharge (m^3 sec^{-1}). The Lw/Q component is equal to the inverse of hydraulic load and is the hydrological piece of the equation while V_f is the biological component. In the model, reach length and discharge were kept constant with only V_f and w being varied (Table 12). Uptake velocities for three channelized reaches included in the LINX 2 study were compared to uptake velocities from the three fluvial wetland dominated reaches along the same streams (Cart Creek [CC], Fish Brook [FB], and Sawmill Brook [SB]) as the biological component of the model. Arbitrary characteristic widths were selected to represent the hydrological difference between fluvial wetland and channelized reaches ($w_{channel}$ = 2 m, $w_{wetland}$ = 10 m).

Table 12. Parameters for the reach-scale NO_3-N removal model for comparing removal between channelized stream reaches and reaches dominated by fluvial wetlands. Stream channel V_f came from Mulholland et al. (2008) while fluvial wetland V_f were from this study. Also included are Damköhler numbers (Da) for each stream in each scenario.

	Scenario	Length (m)	Discharge (L s^{-1})	w (m)	V_f (m yr^{-1})	Removal %	Da [-]
A	Channel Hydrology Channel Biology	100	10	2	CC - 169.5 FB - 179.5 SB - 11.1	CC - 10.2 FB - 10.8 SB - 0.7	CC - 0.11 FB - 0.11 SB - 0.01
B	Channel Hydrology Wetland Biology	100	10	2	CC - 50.5 FB - 416.4 SB - 227.3	CC - 3.2 FB - 23.2 SB - 13.4	CC - 0.03 FB - 0.15 SB - 0.15
C	Wetland Hydrology Channel Biology	100	10	10	CC - 169.5 FB - 179.5 SB - 11.1	CC - 41.6 FB - 43.4 SB - 3.6	CC - 0.54 FB - 0.57 SB - 0.04
D	Wetland Hydrology Wetland Biology	100	10	10	CC - 50.5 FB - 416.4 SB - 227.3	CC - 14.8 FB = 73.3 SB - 51.4	CC - 0.17 FB - 0.73 SB - 0.76

Removal calculated for scenario A, using both width and uptake velocity representative of channelized stream reaches, ranged from 0.7 to 10.8% and yielded the lowest average removal across all three reaches (7.2 ± 3.3%) (Table 12, Figure 36). When fluvial wetland V_f was used in conjunction with stream channel width in scenario B, removal percentages ranged from 3.2 to 14.1% with a mean removal of 10.3 ± 3.5%. In scenario C, with width representative of fluvial wetlands and stream channel biological uptake rates, removal spanned a range of 3.6 to 43.4% with a mean value of 29.5 ± 13.0%. The greatest removal was found for the fluvial wetland width with fluvial wetland uptake rate scenario D, with removal for individual reaches extending from 15.4 to 53.3% and a mean removal for all three reaches of 40.2 ± 12.4%.
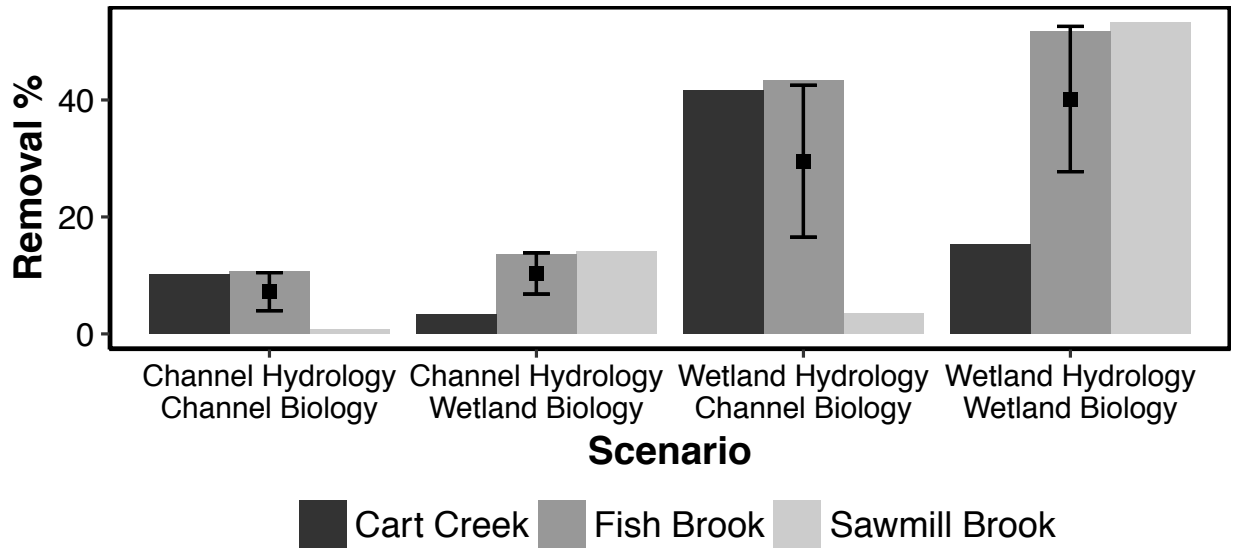
Figure 36. Removal determined using a reach-scale model and parameters representative of channelized stream reaches and fluvial wetland-dominated stream reaches. Bars represent removal for each stream for each scenario while points represent mean removal for each scenario across all three reaches with error bars indicating one standard error in either direction.

Damköhler numbers (Da, [-]) were lowest for the channel biology/channel hydrology scenario (scenario A) with a mean Da across all streams of 0.08 ± 0.03, indicating that reaction rates were generally much less than diffusion rates. Da was greater for scenario B, using fluvial wetland V_f with channel width (0.11 ± 0.04) and higher still for scenario C, with channel V_f and wetland width (0.38 ± 0.17). The greatest mean Da across streams was found for the final scenario, scenario D, with both wetland V_f and wetland width (0.55 ± 0.19), indicating that, while diffusion still occurs faster than the reaction in fluvial wetlands, it is less dominant in fluvial wetland reaches compared to channelized reaches.

Fluvial wetland V_f was generally greater than stream channel V_f, resulting in 3.1 ± 5.6% more removal in the scenario with the fluvial wetland uptake rates and channel width (scenario B) over the baseline with both channel uptake and width (scenario A) (Figure 37). The exception is the Cart Creek reach where the beaver pond had a lower ambient uptake rate than what was found for the channelized reach. This was potentially due to the beaver pond being recently established, containing a lower organic matter content and being heavily shaded. Fluvial wetland hydrology had a greater impact on removal with the scenario using the channel uptake rates and fluvial wetland width (scenario C) resulting in 22.3 ± 9.7% more removal over the baseline scenario. Finally, the scenario with both fluvial wetland uptake rates and width (scenario D) resulted in 32.9 ± 14.3% more removal compared to the baseline scenario. This suggests that the cumulative effect of both fluvial wetland hydrology and biology had the greatest impact on removal in comparable reaches.

Management Implications

Fluvial wetlands are likely to play a significant role in river network-scale nitrogen removal in shallow-sloped watersheds where they are likely to be numerous. This northeastern Massachusetts model may also be applied to other coastal watersheds with high anthropogenic nitrogen loading. Based on ambient areal uptake rates and wetland area, fluvial wetlands in this study were found to retain from -0.4 to 328.4 kg NO_3-N per day. As long as connectivity remains high and the fluvial wetlands do not become source limited, they may act as a substantial sink for anthropogenic nitrogen.
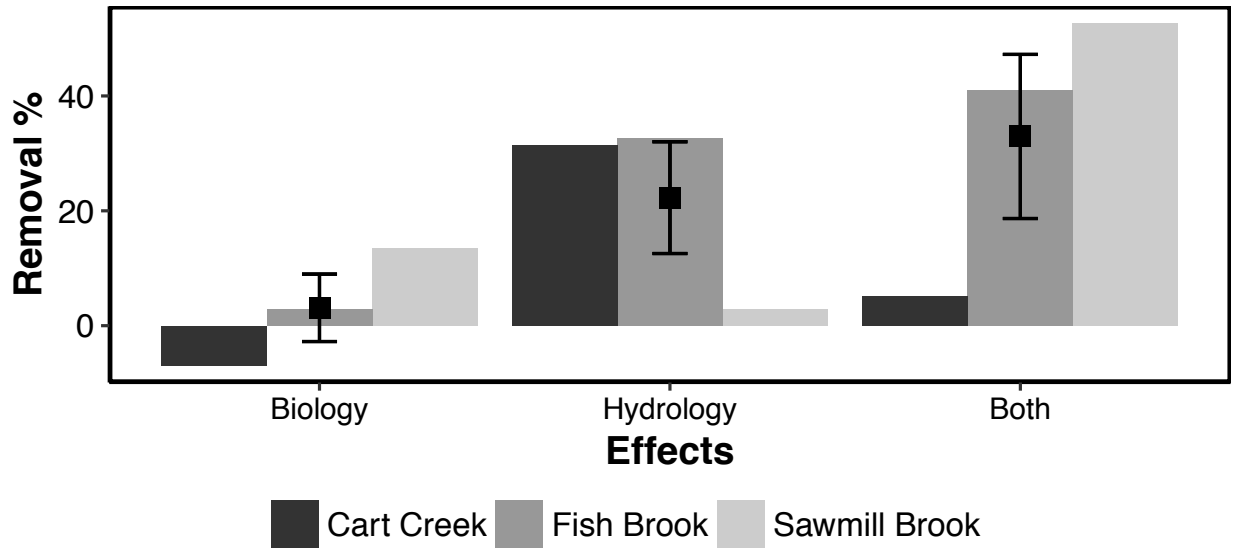
Figure 37. Effects of wetland biology, wetland hydrology, and both wetland biology with wetland hydrology on removal compared to the baseline scenario with channel biology and channel hydrology. Bars represent the difference in removal for each scenario for each stream with points representing the mean removal for each effect with error bars showing one standard error in either direction.

As urbanization continues in the coastal northeastern Massachusetts watersheds, nitrogen loading to the landscape will continue as well. However, North American beaver (*Castor canadensis*) have been making a resurgence in Massachusetts (Foster et al. 2002). Beaver modify the landscape to suit their needs by damming streams and flooding large patches of the landscape, increasing the amount of area covered by fluvial wetlands. With the resurrection of the beaver population in the watersheds draining suburban Boston, MA, it is possible that the resulting increase in beaver dams and impoundments may offset the increasing N loading associated with urbanization.

There is also a current trend involving removal of mainstem dams along the river continuum (O'Connor et al. 2015). Reservoirs, like smaller headwater fluvial wetlands, may also have conditions that are conducive to making them biogeochemical hotspots. Many of the dam removals taking place are being done to restore fish passage or because the dams are in disrepair and it would cost more money to restore them. However, the tradeoffs between dam removal and the ecosystem services that dams provide must be taken into consideration (Gold et al. 2016). With the tradeoffs between removal of dams on higher order streams and rivers along with the increase in beaver activity resulting in an increase in small headwater fluvial wetlands, a balance between anthropogenic nitrogen loading to the landscape and prevention of excess nitrogen loading to the coast may be possible.

Conclusions

We developed a novel approach for estimating nutrient spiraling metrics in fluvial wetlands using a method derived for use in channelized streams coupled with new in situ sensor technology. Using this approach, we were able to quantify nitrate uptake rates in fluvial wetlands across sites and seasons. We then compared these fluvial wetland uptake rates to those found for channelized streams and fluvial wetland surface transient storage patches. These uptake rates were also used to examine potential controls on nitrate uptake and removal. We found that nitrate uptake was generally greater in the fall compared to the spring but was also dependent on wetland inundation levels. Nitrate uptake rates were generally higher than those found for channelized stream reaches and within a similar range as those

found for fluvial wetland surface transient storage patches. Gross primary productivity and ecosystem respiration were not found to be highly related to nitrate uptake rates. However, a wider range of both uptake and metabolic rates may reveal an as yet unknown relationship between fluvial wetland nitrate uptake and aquatic metabolism. The greatest uptake generally occurred along the rising limb of the breakthrough curves but this was likely due to the timing and duration of nitrate addition experiments. The limb experiencing the greatest amount of sunlight typically exhibited the highest demand for nitrate. Detention time was the main control of bulk removal of nitrate with the greatest removal estimates generally coinciding with the longest detention times. Future work will examine a greater number of fluvial wetlands across a wider range of hydrological and biological independent variables. This is important as urbanization is increasing in northeastern Massachusetts which will further increase nitrogen loading to the landscape. With the increasing beaver population in northeastern Massachusetts as well as the rest of southern New England, the potential for nitrate removal is also increasing. More information on the drivers of fluvial wetland nitrogen removal as well as the abundance and distribution of beaver ponds is needed to understand how the human population will interact with the beaver population to ultimately control nitrogen exports to the coast.

List of References

Appling AP, Hall RO, Arroita M, Yackulic CB. 2017. streamMetabolizer: Models for Estimating Aquatic Photosynthesis and Respiration. R package version 0.10.8.

Beltaos S, Day TJ. 1978. A field study of longitudinal dispersion. Canadian Journal of Civil Engineering. 5(4):572-575.

Cirmo CP, Driscoll CT. 1993. Beaver pond biogeochemistry: Acid neutralizing capacity generation in a headwater wetland. Wetlands. 13(4):277:292.

Covino TP, McGlynn BL, McNamara RA. 2010. Tracer Additions for Spiraling Curve Characterization (TASCC): Quantifying stream nutrient uptake kinetics from ambient to saturation. Limnology and Oceanography: Methods. 8(9):484-498.

Davidson EA, David MB, Galloway JN, Goodale CL, Haeuber R, Harrison JA, Howarth RW, Jaynes DB, Lowrance RR, Nolan BT, Peel JL, Pinder RW, Porter E, Snyder CS, Townsend AR, Ward MH. 2012. Excess Nitrogen in the U.S.: Trends, Risks, and Solutions. Issues in Ecology. 15:1-16.

Day NK, Hall RO. 2017. Ammonium uptake kinetics and nitrification in mountain streams. Freshwater Science. 36(1):41-54.

Etheridge JR, Birgand F, Osborne JA, Osburn CL, Burchell MR, Irving J. 2014. Using in situ ultraviolet-visual spectroscopy to measure nitrogen, carbon, phosphorous, and suspended solids concentrations at a high frequency in a brackish tidal marsh. Limnology and Oceanography: Methods. 12(1):10-22.

Fisher J, Acreman MC. 2004. Wetland nutrient removal: a review of the evidence. Hydrology and Earth System Sciences. 8(4):673-685.

Forshay KJ, Stanley EH. 2005. Rapid nitrate loss and denitrification in a temperate river floodplain. Biogeochemistry. 75(1):43-64.

Foster DR, Motzkin G, Bernardos D, Cardoza J. 2002. Wildlife dynamics in the Changing New England Landscape. Journal of Biogeography. 29(10-11):1337-1357.

Galloway JN, Cowling EB. 2002. Reactive Nitrogen and the World: 200 Years of Change. Ambio. 31(2):64-71.

Galloway JN, Townsend AR, Erisman JW, Bekunda M, Cai Z, Freney JR, Martinelli LA, Seitzinger SP, Sutton MA. 2008. Transformation of the Nitrogen Cycle: Recent Trends, Questions, and Potential Solutions. Science. 320(5878):889-892.

Gibson CA, O'Reilly CM, Conine AL, Lipshutz SM. 2015. Nutrient uptake dynamics across a gradient of nutrient concentrations and ratios at the landscape scale. Journal of Geophysical Research: Biogeosciences. 120(2):326-340.

Gold AJ, Addy K, Morrison A, Simpson M. 2016. Will Dam Removal Increase Nitrogen Flux to Estuaries? Water. 8(11):1-16.

Grace MR, Imberger SJ. Stream Metabolism: Performing & Interpreting Measurements. New South Wales Department of Environmental Conservation Stream Metabolism Workshop. 204 pp.

Grace MR, Giling DP, Hladyz S, Caron V, Thompson RM, MacNally R. 2015. Fast processing of diel oxygen curves: Estimating stream metabolism with BASE (BAyesian Single-station Estimation). Limnology and Oceanography: Methods. 13(3):103-114.

Hall RO, Tank JL. 2003. Ecosystem metabolism controls nitrogen uptake in streams in Grand Teton National Park, Wyoming. Limnology and Oceanography. 48(3):1120-1128.

Hanafi S, Grace M, Webb JA, Hart B. 2007. Uncertainty in Nutrient Spiraling: Sensitivity of Spiraling Indices to Small Errors in Measured Nutrient Concentration. Ecosystems. 10(3):477-487.

Heffernan JB, Cohen MJ, Frazer TK, Thomas RG, Rayfield TJ, Gulley J, Martin JB, Delfinao JJ, Graham WD. 2010. Hydrologic and biotic influences on nitrate removal in a subtropical spring-fed river. Limnology and Oceanography. 55(1):249-263.

Howarth RW, Billen G, Swaney D, Townsend A, Jaworski N, Lajtha K, Downing JA, Elmgren R, Caraco N, Jordan T, Berendse F, Freney J, Kudeyarov V, Murdoch P, Zhao-Liang Z. 1996. Regional nitrogen budgets and riverine N & P fluxes for the drainages of the North Atlantic Ocean: Natural and human influences. Biogeochemistry. 35(1):75-139.

Johnston CA, Schubauer-Berigan JP, Bridgham SD. 1997. The role of riverine wetlands as buffer zones. In: Haycock NE, Burt TP, Goulding KWT, Pinay G, editors. Buffer Zones: Their Processes and Potential in Water Protection. Harpenden (UK): Quest Environmantal. p. 155-170.

Kilpatrick FA, Cobb ED. 1985. Measurement of discharge using tracers, in Book 3 Applications of Hydraulics, United States Geological Survey, Washington, D.C.

Lightbody AF, Avener ME, Nepf HM. 2008. Observations of short-circuiting flow paths within a free-surface wetland in Augusta, Georgia, U.S.A. Limnology and Oceanography. 53(3):1040-1053.

McClain ME, Boyer EW, Dent LC, Gergel SE, Grimm NB, Groffman PM, Hart SC, Harvey JW, Johnston CA, Mayorga E, McDowell WH, Pinay G. 2003. Biogeochemical Hot Spots and Hot Moments at the Interface of Terrestrial and Aquatic Ecosystems. Ecosystems. 6(4):301-312.

Mulholland PJ, Fellows CS, Tank JL, Grimm NB, Webster JR, Hamilton SK, Martí E, Ashkenas L, Bowden WB, Dodds WK, McDowell WH, Paul MJ, Peterson BJ. 2001. Inter-biome comparison of factors controlling stream metabolism. Freshwater Biology. 46(11):1503-1517.

Mulholland PJ, Helton AM, Poole GC, Hall RO, Hamilton SK, Peterson BJ, Tank JL, Ashkenas LR, Cooper LW, Dahm CN, Dodds WK, Findlay SEG, Gregory SV, Grimm NB, Johnson JL, McDowell WH, Meyer JL, Valett HM, Webster JR, Arango CP, Beaulieu JJ, Bernot MJ, Burgin AJ, Crenshaw CL, Johnson LT, Niederlehner BR, O'Brien JM, Potter JD, Sheibley RW, Sobota DJ, Thomas SM. 2008. Stream denitrification across biomes and its response to anthropogenic nitrate loading. Nature. 452(7184):202-205.

O'Brien JM, Dodds WK, Wilson KC, Murdock JN, Eichmiller J. 2007. The saturation of N cycling in Central Plains streams: [15]N experiments across a broad gradient of nitrate concentrations. Biogeochemistry. 84(1):31-49.

O'Brien JM, Hamilton SK, Kinsman-Costello LE, Lennon JT, Ostrom NE. 2012. Nitrogen transformations in a through-flow wetland revealed using whole-ecosystem pulsed ^{15}N additions. Limnology and Oceanography. 57(1):221-234.

O'Connor JE, Duda JJ, Grant GE. 2015. 1000 dams down and counting. Science. 346(6234):496 497.

Payn RA, Webster JR, Mulholland PJ, Valett HM, Dodds WK. 2005. Estimation of stream nutrient uptake from nutrient addition experiments. Limnology and Oceanography: Methods. 3(3):174-182.

Pellerin BA, Bergamaschi BA, Downing BD, Saraceno JF, Garrett JD, Olsen LD. 2013. Optical techniques for the determination of nitrate in environmental waters: Guidelines for instrument selection, operation, deployment, maintenance, quality assurance, and data reporting. United States Geological Survey Techniques and Methods 1-D5. 37 p.

Powers SM, Johnson RA, Stanley EH. 2012. Nutrient Retention and the Problem of Hydrologic Disconnection in Streams and Wetlands. Ecosystems. 15(3):435-449.

R Core Team. 2017. R: A language and environment for statistical computing. R Foundation for Statistical Computing. Vienna, Austria.

Rodríguez-Cardona B, Wymore AS, McDowell WH. 2016. DOC:NO_3^- ratios and NO_3^- uptake in forested headwater streams. Journal of Geophysical Research: Biogeosciences. 121(1):205-217.

Ruggiero A, Solimini AG, Anello M, Romano A, De Cicco M, Carchini G. 2006. Nitrogen and phosphorous retention in a human altered stream. Chemistry and Ecology. 22(Sup1):S1:S13.

Schlesinger WH. 2009. On the fate of anthropogenic nitrogen. Proceedings of the National Academy of Science. 106(1):203-208.

Seitzinger SA, Harrison JA, Böhlke JK, Bouwman AF, Lowrance R, Peterson B, Tobias C, Van Drecht G. 2006. Denitrification across Landscapes and Waterscapes: A Synthesis. Ecological Applications. 16(6):2064-2090.

Smith VH, Tilman GD, Nekola JC. 1999. Eutrophication: impacts of excess nutrient inputs on freshwater, marine, and terrestrial ecosystems. Environmental Pollution. 100(1):179-196.

Stewart RJ, Wollheim WM, Gooseff MN, Briggs MA, Jacobs JM, Peterson BJ, Hopkinson CS. 2011. Separation of river network-scale nitrogen removal among the main channel and two transient storage compartments. Water Resources Research. 47(10):1-19.

Stream Solute Workshop. 1990. Concepts and methods for assessing solute dynamics in stream ecosystems. Journal of the North American Benthological Society. 9(2):95-119.

Tank JL, Rosi-Marshall EJ, Baker MA, Hall RO. 2008. Are Rivers Just Big Streams? A Pulse Method to Quantify Nitrogen Demand in a Large River. Ecology. 89(10):2935-2945.

Taylor G. 1921. Diffusion by continuous movements. Proceedings of the London Mathematical Society. 2(1):196-212.

Taylor PG, Townsend AR. (2010). Stoichiometric control of organic carbon-nitrate relationships from soils to the sea. Nature. 464(7292):1178-1181.

Thouin JA, Wollheim WM, Vörösmarty CJ, Jacobs JM, McDowell WH. 2009. The biogeochemical influences of NO_3^-, dissolved O_2, and dissolved organic C on stream NO_3^- uptake. Journal of the North American Benthological Society. 28(4):894-907.

Trentman MT, Dodds WK, Fencl JS, Gerber K, Guarneri J, Hitchman SM, Peterson Z, Rüegg J. 2015. Quantifying ambient nitrogen uptake and functional relationships of uptake versus concentration in streams: a comparison of stable isotope, pulse, and plateau methods. Biogeochemistry. 125(1):65-79.

Van Breeman N, Boyer EW, Goodale CL, Jaworski NA, Paustian K, Seitzinger SP, Lajtha K, Mayer B, Van Dam D, Howarth RW, Nadelhoffer KJ, Eve N, Billen G. 2002. Where did all the nitrogen go? Fate of nitrogen inputs to large watersheds in the northeastern U.S.A. Biogeochemistry. 57(1):267-293.

Whitmer S, Baker L, Wass R. 2000. Loss of Bromide in a Wetland Tracer Experiment. Journal of Environmental Quality. 29(6):2043-2045.

Wilderotter S. 2015. Parameterization of transient storage and nutrient retention in coastal New England wetlands. University of New Hampshire. Master's Thesis.

Williams M, Hopkinson C, Rastetter E, Vallino J. 2004. N budgets and aquatic uptake in the Ipswich River basin, northeastern Massachusetts. Water Resources Research. 40(11):1-12.

Wlostowski AN, Gooseff MN, Bowden WB, Wollheim WM. 2016. Stream tracer breakthrough curve decomposition into mass fractions: A simple framework to analyze and compare conservative solute transport processes. Limnology and Oceanography: Methods. 15(2):140-153.

Wollheim WM, Peterson BJ, Thomas SM, Hopkinson CS, Vörösmarty CJ. 2008. Dynamics of N removal over annual time persiods in a suburban river network. Journal of Geophysical Research. 113(3):1-17.

Wollheim WM, Harms TK, Peterson BJ, Morkeski K, Hopkinson CS, Stewart RJ, Gooseff MN, Briggs MA. 2014. Nitrate uptake dynamics of surface transient storage in stream channels and fluvial wetlands. Biogeochemistry. 120(1-3):239-257.

Zeileis A, Grothendieck G. 2005. zoo: S3 Infrastructure for Regular and Irregular Time Series. Journal of Statistical Software. 14(6):1-27.